



Forschungszentrum Karlsruhe
in der Helmholtz-Gemeinschaft

Wissenschaftliche Berichte
FZKA 7256

Design and Analysis of the Superconducting Current Feeder System for the International Thermonuclear Experimental Reactor (ITER)

V. L. Tanna

Institut für Technische Physik

Oktober 2006

Forschungszentrum Karlsruhe

in der Helmholtz-Gemeinschaft

Wissenschaftliche Berichte

FZKA 7256

**Design and analysis of the superconducting
current feeder system for the International
Thermonuclear Experimental Reactor (ITER)**

Vipulkumar L. Tanna

Institut für Technische Physik

von der Fakultät für Elektrotechnik und Informationstechnik
der Universität Karlsruhe (TH) genehmigte Dissertation

Forschungszentrum Karlsruhe GmbH, Karlsruhe
2006

Für diesen Bericht behalten wir uns alle Rechte vor

Forschungszentrum Karlsruhe GmbH
Postfach 3640, 76021 Karlsruhe

Mitglied der Hermann von Helmholtz-Gemeinschaft
Deutscher Forschungszentren (HGF)

ISSN 0947-8620

urn:nbn:de:0005-072566

Design and analysis of the superconducting current feeder system for the International Thermonuclear Experimental Reactor (ITER)

Zur Erlangung des akademischen Grades eines

DOKTOR – INGENIEURS

von der Fakultät für Elektrotechnik und Informationstechnik
der Universität Karlsruhe (TH)

genehmigte

DISSERTATION

von

Vipulkumar L. Tanna (M. Sc.)

aus Ahmedabad (India)

Tag der mündlichen Prüfung:

27. Juli 2006

Hauptreferent:

Prof. Dr. techn. P. Komarek

Korreferent:

Prof. Dr. rer. nat. M. Siegel

Design and analysis of the superconducting current feeder system for the International Thermonuclear Experimental Reactor (ITER)

Abstract

The superconducting magnet system (SCMS) of the International Thermonuclear Experimental Reactor (ITER) consists of 18 D-shaped Toroidal field (TF) coils, 6 Poloidal field (PF) coils, one Central Solenoid (CS) coil and 18 Correction coils (CC). The TF coils will be operating with a conductor current of 68 kA; whereas the maximum current in the PF coils is 45 kA (back-up mode is 52 kA), in the CS coil 45 kA and in the Correction coils (CC) 10 kA respectively. In order to supply such high currents from the power supplies to the SCMS, a current feeder system is required. It mainly consists of the superconducting (sc) bus bars, the current leads, and the water-cooled aluminium bus bars. Each sc bus bar has a length of ~25 meters. It consists of 1800 NbTi/Cu strands embedded in a stainless steel jacket (so-called cable in conduit conductors, CICC) and is cooled by forced flow supercritical helium. The sc bus bars specifications, the feeder conceptual design and the electromagnetic, thermo-hydraulic and quench performances are evaluated.

The main consumers of cooling power in sc fusion magnet systems are the current leads. The current lead connects sc bus bar at low temperature side (4.5 K) to the water-cooled bus bar at the room temperature (RT) side. Because it is a solid connection between the RT and the 4.5 K level, the heat load to the low temperature region is associated with thermal conduction and Joule heating along the current lead system. An optimum, reliable and low loss current lead system is essential for large superconducting devices. Massive savings in capital investment as well as operation costs would be possible if replacing the actually planned conventional current leads by HTS current leads. In this context, a comparative study of the ITER design with conventional and with HTS current leads has been carried out.

An obvious but also challenging option is the substitution of a part of the water cooled aluminium bus bars by HTS feeders. The design and optimization study of HTS feeders for ITER are based on Bi-2223/Ag superconductors and a conceptual layout are discussed. The cooling aspects and thermo hydraulic analysis of the HTS feeders has been carried out. The design

parameters of the HTS feeder termination are summarized. Finally, a techno-economical comparison between the water-cooled aluminium bus bars and the HTS feeders has been carried out for ITER. It is shown that HTS materials have reached their maturity and efficient calculation tools are now available for better design and optimization of the superconductor current feeder system including current leads using HTS materials.

Zusammenfassung

Design und Analyse des supraleitenden Stromschienensystems für den Internationalen Thermonuklearen Experimentellen Reaktor (ITER)

Das supraleitende Magnetsystem des Internationalen Thermonuklearen Experimentellen Reaktor ITER besteht aus 18 D-förmigen Toroidalfeldspulen, 6 Poloidalfeldspulen, einem zentralen Solenoid und 18 Korrekturspulen. Die Toroidalfeldspulen werden mit einem elektrischen Leiterstrom von 68 kA betrieben, während der Maximalstrom der Poloidalfeldspulen 45 kA (Back-up Mode 52 kA), des zentralen Solenoids 45 kA und der Korrekturspulen 10 kA betragen. Um diese hohen Ströme von den Netzgeräten zum Magnetsystem zu bringen, ist ein Stromzuführungssystem notwendig. Es besteht hauptsächlich aus supraleitenden Stromschienen (innerhalb des Kryostaten), den Stromdurchführungen und den wassergekühlten Stromschienen aus Aluminium. Jede einzelne supraleitende Stromschiene ist etwa 25 m lang. Sie besteht aus 1800 NbTi/Cu Supraleiterdrähten, ist von einer Edelstahlhülle umgeben und wird mit überkritischem Helium zwangsgekühlt. Im ersten Teil dieser Arbeit werden die Spezifikationen der supraleitenden Stromschiene beschrieben, ein Designkonzept ausgearbeitet und elektromagnetische, thermohydraulische und Quenchausbreitungsrechnungen durchgeführt.

Die Hauptverbraucher der Kälteleistung eines supraleitenden Magnetsystems, wie es in einem Fusionsreaktor benötigt wird, sind die Stromdurchführungen. Die Stromdurchführung stellt die elektrische Verbindung zwischen der auf 4.5 K betriebenen supraleitenden Spule und dem auf Raumtemperaturniveau befindlichen Netzgerät dar. Da diese Verbindung elektrisch und thermisch leitend ist, ist die auf dem 4.5 K Niveau abzuführende Wärmelast mit der Wärmeleitung und der Wärmeproduktion entlang der Stromschiene verknüpft. Ein optimiertes, zuverlässiges und verlustarmes Stromschienensystem ist unabdingbar für einen optimalen Betrieb großer supraleitender Systeme. Massive Einsparungen sowohl in Investitionskosten als auch in Betriebskosten sind möglich, wenn die in ITER derzeit geplanten konventionellen metallischen Stromzuführungen durch Hochtemperatursupraleiter-Stromzuführungen ersetzt werden würden. Im zweiten Teil dieser Arbeit wird ein detaillierter Vergleich zwischen einem konventionellen Stromdurchführungssystem und einem System unter Verwendung von Hochtemperatursupraleitern durchgeführt.

Eine nahe liegende aber ebenso herausfordernde Option ist der Austausch eines Teils der wassergekühlten Aluminiumstromschienen durch Hochtemperatur-supraleiterstromschienen. Im letzten Teil der Arbeit werden die Auslegung und Optimierung einer Hochtemperatur-supraleiterstromschiene für ITER unter Verwendung von Bi-2223/Ag Supraleiter diskutiert. Das Auslegungskonzept wird beschrieben sowie die Kühlaspekte diskutiert und eine thermohydraulische Analyse der Stromschiene durchgeführt. Letztendlich werden die technischen und ökonomischen Gesichtspunkte des konventionellen wassergekühlten und des Hochtemperatursupraleiterstromschienensystems miteinander verglichen. Hochtemperatursupraleiter können inzwischen technisch eingesetzt werden und es existieren leistungsfähige Berechnungswerkzeuge für die Auslegung und Optimierung eines supraleitenden Hochtemperatursupraleiterstromschienensystems.

Contents

Chapter 1 – Introduction	1
1.1 General Introduction.....	1
1.2 Motivation and problem specifications.....	2
1.3 Organisation of the tasks.....	3
Chapter 2 – Low and high temperature superconductivity and its applications in fusion devices	6
2.1 Phenomenon of superconductivity.....	6
2.2 Types of superconductors.....	7
2.3 Characteristics of superconductors.....	10
2.3.1 Critical current characteristics.....	10
2.3.2 J-B-T characteristics.....	11
2.4 Technical usable superconductors.....	12
2.4.1 Low temperature superconductors (LTSs).....	12
2.4.2 High temperature superconductors (HTSs).....	14
2.5 Applications of superconductivity in fusion devices.....	15
Chapter 3 – The role of cryogenic systems in fusion devices	18
3.1 Introduction.....	18
3.2 Worldwide large-scale helium cryogenic systems.....	19
3.3 Design philosophy of large-scale helium cryogenic system.....	19
3.4 Description of a helium cryogenic cycle.....	21
3.5 Cryogenic system performance.....	22
3.6 Different cooling schemes for fusion devices.....	24
3.6.1 Pool boiling / Bath cooling.....	25
3.6.2 Forced flow cooling.....	25
3.6.3 Problems with Two-phase cooling.....	26

Chapter 4 – Description of the ITER machine, magnets and its auxiliary utility systems 27

4.1 Introduction to ITER.....27

 4.1.1 Brief summary.....27

 4.1.2 Machine parameters.....28

4.2 Description of the ITER superconductor magnet system.....29

4.3 Description of the ITER current feeder system.....31

 4.3.1 Review of worldwide current feeder systems for fusion devices.....31

 4.3.2 Description of the LTS current feeder system.....32

 4.3.3 Current leads requirements.....34

 4.3.4 Water-cooled aluminum bus bars.....35

4.4 Auxiliary utility systems.....34

 4.4.1 Magnets power supplies.....35

 4.4.2 Cryoplant.....36

 4.4.2.1 Summary of cryogenic requirements.....37

 4.4.2.2 Description of the cryogenic system.....37

 4.4.2.3 Economics of helium system.....37

Chapter 5 – Description of conventional and HTS current leads 39

5.1 Design Considerations of Current Leads for ITER.....39

5.2 Different Current Lead Design Options.....40

5.3 Discussions on Current Leads Design Options for ITER.....41

 5.3.1 Bath/Vapor cooled Conventional Current Leads.....41

 5.3.2 Forced flow cooled constant cross section and variable
 cross-section current leads.....42

 5.3.3 Overloaded conventional current leads.....42

 5.3.4 High Temperature Superconductor current leads.....43

 5.3.5 Worldwide survey of current leads used in
 Fusion devices and test facilities.....45

5.4 Present ITER design of current leads.....45

5.5 Review of a 70 kA HTS Current Lead as Demonstrator for ITER.....48

 5.5.1 70 kA HTS current lead design48

 5.5.2. Summary of Test results.....49

Chapter 6 – Design and analysis of a LTS current feeder system for ITER **53**

6.1	Conceptual design of a LTS current feeder system for ITER.....	53
6.1.1	Design drivers.....	53
6.1.2	Technical requirements and specifications of LTS current feeders.....	54
6.1.3	Design concept of a LTS feeder.....	55
6.2	Boundary conditions for the analysis of the LTS current feeder.....	57
6.2.1	Modeling of the TF feeder for ITER.....	57
6.2.1.1	Heat load calculations.....	57
6.2.1.2	Electromagnetic field calculations.....	58
6.2.1.3	Material properties data base.....	61
6.3	Steady state hydraulic analysis (single channel approach).....	62
6.3.1	Basic assumptions for steady state analysis.....	62
6.3.2	Thermo-hydraulics and helium mass flow rate optimization study.....	62
6.3.3	Cooling modes comparison study.....	66
6.4	One dimensional transient thermo-hydraulic analysis (Dual channel approach).....	68
6.4.1	Verification of the single channel steady state model.....	70
6.4.2	Analysis of quench initiation and propagation.....	72
6.4.3	Analysis of the loss of helium flow in the feeder.....	74
6.4.3.1	Analysis of a LOFA and a no safety discharge of the magnet.....	74
6.4.3.2	Analysis of a LOFA and a consecutive safety discharge of the magnet.....	75
6.4.4	Effect of higher heat loads: Experience from the TOSKA facility.....	76
6.5	Discussions on PF and CS LTS current feeder system.....	76
6.6	Quench detection and instrumentation.....	77

**Chapter 7 – Comparative study with ITER design with and
without HTS current leads** **80**

7.1	Introduction.....	80
7.2	Cost Analysis for the operation.....	81
7.2.1	Duty Cycle of the ITER magnet system.....	81
7.2.2	Calculations of the power consumption.....	82
7.2.2.1	Cooling power for forced flow conventional leads.....	84
7.2.2.2	Cooling power for HTS current leads.....	85
7.2.2.3	Liquid Nitrogen operation for HTS current leads.....	88

7.3 Capital Cost Analysis for HTS current leads for ITER.....	90
7.3.1 Basic Assumptions to the HTS current lead capital cost analysis.....	91
7.3.2 Results of the capital cost analysis for HTS current leads modules.....	92
7.4 Summary of ITER design with and without HTS current leads.....	94
Chapter 8 – Conceptual design of a HTS current feeder system for ITER	96
8.1 Introduction.....	96
8.2. Design concept of the HTS feeders for ITER.....	97
8.2.1 Design Drivers.....	97
8.2.2 HTS feeder design concept.....	98
8.3 Design optimization of the HTS feeders.....	100
8.3.1 50 K helium design.....	104
8.3.2 70 K sub-cooled LN ₂ design.....	107
8.3.3 Comments on 80 K helium design.....	109
8.4.4 Effect of external field and bending on HTS feeder.....	109
8.4 Description of the HTS feeders cooling schemes.....	111
8.4.1 Cooling scheme with 50 K Helium.....	112
8.4.2 Cooling scheme with sub-cooled LN ₂	113
8.5 Thermal analysis of the HTS feeders.....	113
8.5.1 Steady state and Pulsed heat losses analysis.....	113
8.5.2 Hydraulic analysis.....	116
8.6 Feeder termination (transition to room temperature).....	119
8.7 Techno-economical comparison to the conventional bus bars.....	120
Chapter 9 – Conclusions and future prospects	123
9.1 Conclusions.....	123
9.2 Future prospects.....	126
Appendix I – Current operation reference scenario in ITER	128
(Inductive operation, 15 MA)	
Bibliography	130

List of frequently used Abbreviations and Symbols

The abbreviations and symbols are usually explained within the text. In the consequence the frequently used abbreviations and the most important symbols are described here.

Abbreviations

1D	One Dimension
Al	Aluminium
AMSC	American Superconductor Corporation Limited
BB	Bus Bar
CC	Correction Coil
CF	Cryostat Feed through
CL	Current Lead
CRPP	Centre de Recherches en Physique des Plasmas, Lausanne (Switzerland)
CS	Central Solenoid
CTB	Coil Terminal Box
DDD	Design Description Document
EAS	European Advanced Superconductor GmbH
FZK	Forschungszentrum Karlsruhe, Karlsruhe (Germany)
HTS	High Temperature Superconductor
IF	In-cryostat Feeder
ITER	International Thermonuclear Experimental Reactor
ITP	Institute for Technical Physics
LHe	Liquid Helium
LN ₂	Liquid Nitrogen
LOFA	Loss of Flow Accident
LTS	Low Temperature Superconductor
MLI	Multilayer Insulation
PF	Poloidal Field
RT	Room Temperature
SCMS	Superconducting Magnet System
TF	Toroidal Field
VB	Vacuum Barrier

Symbols

B	Magnetic induction
B_c	Critical magnetic induction
B_{c2}	Upper critical magnetic induction
e	Thermodynamic efficiency
H_{irr}	Irreversible Magnetic field strength
H_r	Exergy parameter
I	Current
I_c	Critical current
J_c	Critical current density
U	Cooled perimeter
\dot{m}	Mass flow rate
η_c	Carnot efficiency
ΔP	Pressure drop
T	Temperature
T_C	Temperature of cold surface
T_W	Temperature of warm surface
T_c	Critical temperature
T_{cs}	Current sharing temperature

Chapter 1- Introduction

1.1 General Introduction

The construction and operation of ITER is the next step towards controlled nuclear fusion. The main goal of the ITER project is to demonstrate that power generation by nuclear fusion is feasible in an economically and environmentally acceptable way. In a fusion reactor the hot plasma is confined by the magnetic fields generated by the superconducting coils system and the plasma current [1]. Thus, the superconducting magnet system is an indispensable component. The superconducting magnet system is designed with the low temperature superconductors (LTSs) and needs to operate at liquid helium (LHe) temperature (~ 4.5 K). In order to charge the superconducting magnet system (at 4.5 K) from the power supply at room temperature (RT), a current feeder system is required. It consists of a superconducting feeder, a current lead and a water-cooled Aluminium bus bar. So, the current feeder system basically acts as current transmission line from 4.5 K to 300 K. In the present design, the ITER magnet system uses Nb_3Sn for the Toroidal Field (TF) and Central Solenoid (CS) coils and NbTi for the Poloidal Field (PF) and Correction Coil (CC) magnets respectively. For practical reasons the superconductor feeder will also be made of NbTi [2, 3]. The superconducting current feeder system requires higher stability and safety margin than the magnets because in any kind of operation or fault condition, the large amount of magnetic stored energy in the coils must be extracted safely via the current feeder paths [4, 5]. An extensive literature review of designs and performance tests of worldwide superconducting current feeder system for fusion devices is given in chapter 4. The preliminary design overview and requirements of the sc feeders for ITER are also discussed in chapter 4.

The current leads are used to conduct the electric current from the room temperature (RT) side, where the power supply is located, to the low temperature side (4.5 K) where the superconducting coils are operating. As they are solid connections between the RT and the 4.5 K level, heat is flowing to the cold region due to thermal conduction and Joule heating within the current lead system [6]. An optimized low loss and reliable current lead system is essential for large superconducting devices in order to save the precious cryogenic capacity of the system at 4.5 K [7]. Varieties of current lead design options are reported in the literature and specifically discussed in chapter 5. Finally, the connections of the current leads to the power supplies are done via water-cooled Aluminium bus bars. Since it is a metallic connection located at room temperature, much

more installation space compared to sc feeders is required and a large amount of resistive losses has to be removed efficiently with the help of a dedicated and reliable water cooling system. For the superconducting magnet system of ITER, total 60 units of current leads and superconducting feeders for a total current of 2568 kA are required.

Figure 1.1 shows a sketch of the current feeder system for ITER using a current lead and a water-cooled Aluminium bus bar.

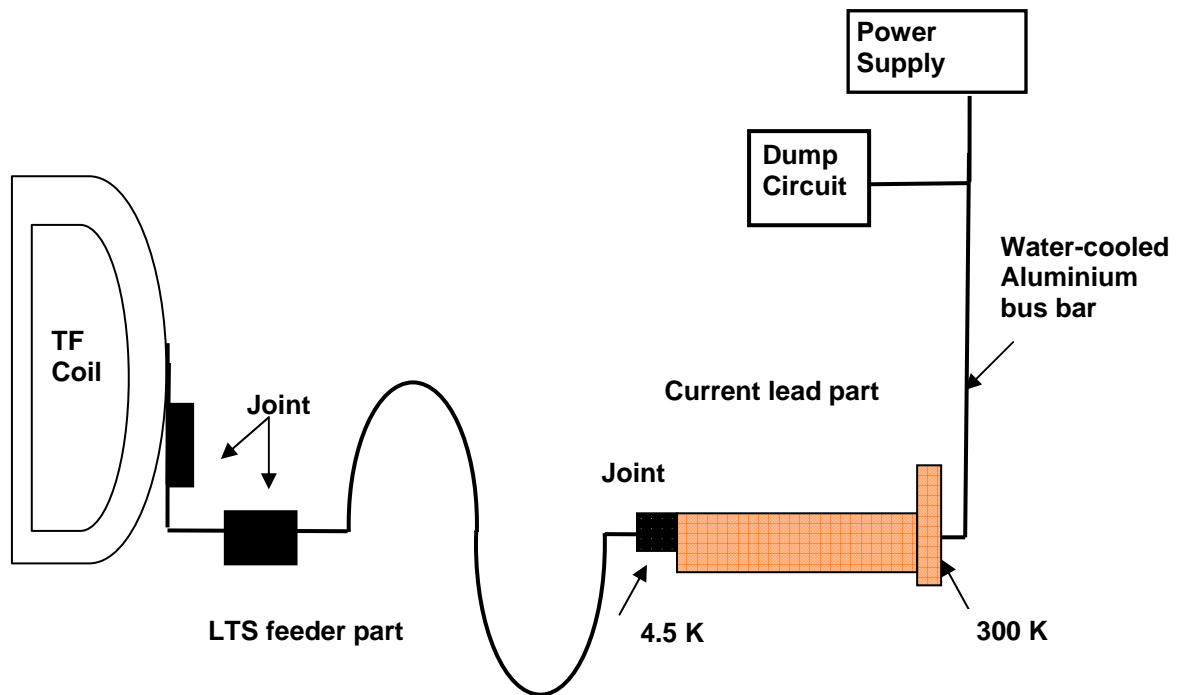


Figure 1.1 Schematic layout of the present design of current feeder system for ITER

1.2 Motivation and problem specifications

After an extensive review of the feeder system described in the ITER design description document (DDD) [2, 3], it is clear that the current feeder system uses a conventional concept of feeding the current to the superconductor magnets. The detailed conceptual design and thermo-hydraulic analysis of the feeders are not worked out so far.

In the first step, the problem was specified to carry out a conceptual design and a detailed thermo-hydraulic analysis of a LTS feeder to evaluate its performance parameters. These investigations are essential to design the LTS feeder for a safe and reliable operation of LTS feeders system.

In the next step, the introduction of high temperature superconducting (HTS) material between the NbTi feeder and the resistive heat exchanger was investigated because it

significantly reduces the heat load at the 4.5 K level, thereby saving costs of the cryogenic system considerably. The motivation is based on the successful completion of R & D programs launched in Japan [8] and in the EU [9] for construction and test of HTS current leads for ITER. So, the actual ITER design was compared to a design using HTS current leads. This study elaborates the differences in initial and operating costs and points out the implications with other ITER components and the required ITER design changes. Furthermore, the possible benefits of a third ITER design option which not only replaces the conventional current leads but also the water-cooled bus bars by HTS feeders are assessed.

1.3 Organization of the thesis

The main purpose of the thesis is to study the design aspects and relevant analyses of the ITER current feeder system including three main parts, the LTS feeder design and analysis, the comparative study of the ITER feeder design with and without HTS current leads, and finally the replacement of a part of the water-cooled Aluminium bus bars by HTS feeders. The main objective is to obtain a safe, reliable and economic operation of the ITER current feeder system and to work out its boundary conditions and critical parameters. In principle, the superconducting current feeder system has direct impact on the operation of any fusion device from the following points of view,

1. During the quench of the superconducting magnets, the large amount of stored magnetic energy in the order of MJ – GJ has to be extracted via the superconducting current feeders path, e.g. in case of ITER, it is of the order of ~ 50 GJ and needs to be extracted safely via the superconductor feeder path.
2. The superconducting magnets always require a cryogenic supply system and the capacity of the associated cryogenic plant is determined by the heat loads acting on the system. Experience shows that the current leads cause the major contribution to the total heat loads, e.g. in case of ITER 25% of the total cryogenic capacity is consumed by the conventional current leads. This will have a direct impact on the running cost of the machine. The use of high temperature superconductor (HTS) current leads provides a techno-economical solution as the HTS current leads have large advantages compared to conventional one.
3. At the room temperature side, the current leads are usually connected to Copper / Aluminum bus bars in order to perform the connection to the power supplies. For large current applications, bus bars demand high operating costs, more space for installation and extra electrical grids for supply. One possibility could

be the replacement of a part of these bus bars by HTS feeders in order to provide a better technical solution.

The thesis has been divided into nine chapters.

Chapter 1 starts with a brief introduction to the current feeder system. Motivation and problem specification and the organization of the thesis are presented.

In chapter 2, the phenomenon and properties of low and high temperature superconductivity is described and a discussion about technically usable superconductors is done. Finally, an application of superconductivity in fusion devices and their components like e.g. superconducting magnets and HTS current leads are briefly discussed.

Chapter 3 mainly focuses on the role of the cryogenic system in fusion devices. A brief review of worldwide large-scale helium refrigeration/liquefaction systems is presented. The design philosophy and performance of such cryo systems is discussed. The comparison of different cooling schemes used in a fusion machine is outlined. Finally, the economy of large-scale helium refrigeration system and industrial Liquid Nitrogen (LN₂) plants is summarized.

In chapter 4, a brief summary of the ITER machine with its main machine parameters is given. The description of the superconducting magnet system and current feeder system is carried out along with its auxiliary utility systems i.e. the power supply and the cryogenic system. In this chapter, the design requirement of each sub-system is discussed as a part of input to the thesis work.

In chapter 5, the main focus is given on the current leads. The design consideration of ITER current leads, different possible current lead design options for ITER and their performance study are discussed. A review of test results of the EU 70 kA HTS current lead as demonstrator for ITER is carried out.

Chapter 6 covers the design drivers and specifications of the LTS feeders. The conceptual design and related various analyses including electro-magnetic, steady state (using single channel approach) and one dimensional transient thermo-hydraulic analyses (using dual channel approach) are carried out for the TF feeder. This is required in order to estimate the critical parameters of the feeder under ITER normal and emergency operating conditions. Finally, the PF and CS feeder systems are briefly discussed.

In chapter 7, the implementation of a HTS module between the NbTi feeder and the resistive heat exchanger is discussed. It significantly reduces the heat load at the 4.5 K level and thereby a considerable amount of the cryogenic power costs can be saved. Using the test results of a 70 kA HTS current lead (developed at Forschungszentrum

Karlsruhe within the frame of EU fusion technology program) as input, a techno-economical comparative study has been carried out for an ITER design with and without HTS current leads. The impact of saving the cryogenic capacity using HTS current leads is outlined.

Chapter 8 deals with the possibility to replace a part of the high current water-cooled Aluminium bus bar by HTS feeders. The introduction of the HTS feeders would not only eliminate the Joule heating (except at the terminations) but also reduce the space for installation. A conceptual layout of a HTS feeder system for ITER is worked out. The design optimization, cooling schemes and thermal analysis have been studied taking into account the machine operating conditions. The design related critical issues are identified.

In the last chapter, the main results are concluded and the future prospects of the thesis work are presented.

Appendix-I summarizes the different current operation scenario of ITER.

Chapter 2 - Low and high temperature superconductivity and its applications in fusion devices

In this chapter, the phenomenon of low and high temperature superconductivity is described and a discussion about technically usable superconductors is done. Finally, applications of superconductivity in fusion devices and their components like e.g. superconducting magnets, LTS current feeders, and HTS current leads are briefly discussed.

2.1 Phenomenon of superconductivity

Superconductivity is a phenomenon occurring in certain materials at very low temperatures characterized by zero electrical resistance and in low external magnetic field the exclusion of an interior magnetic field (the Meissner effect) [10,11]. Many metallic elements and a large number of alloys transform into the state of superconductivity below a certain temperature, the so-called critical temperature (T_c). Figure 2.1 shows the behaviour of resistivity (ρ) at the superconducting phase transition, compared with the metallic conductor (e.g. copper, RRR ~ 100). Here, RRR is known as the residual resistivity ratio. It is a ratio of resistivity at 300 K to resistivity at 4.2 K for a specific material.

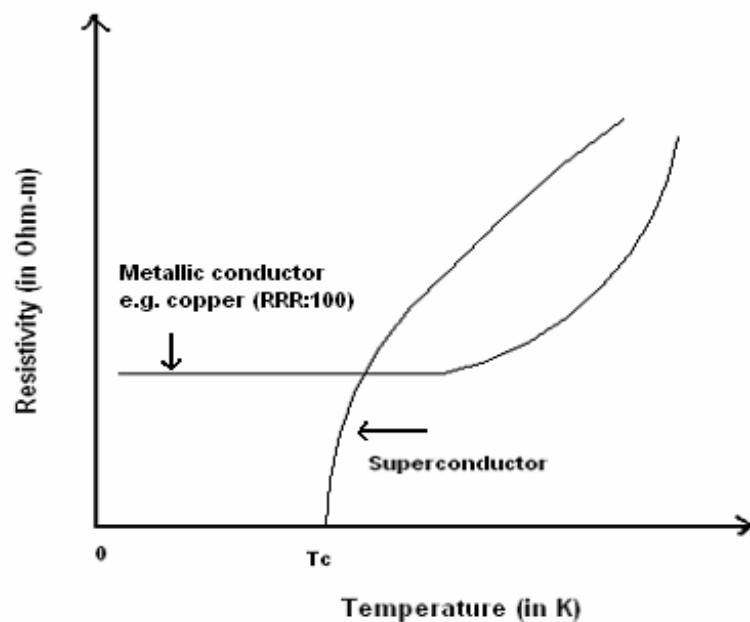


Figure 2.1 Superconducting transition and comparison to a metallic conducting material

In conventional superconductors, superconductivity is explained by the microscopic theory (BCS theory). From this theory, the supercurrent is not carried by single electrons but by pairs of electrons of opposite momenta and spins, the so-called Cooper-pairs. All pairs occupy a single quantum state and basically they are bosons. Thus, the superconductivity is caused by microscopic interaction between the electrons and phonons within the lattice, leading to the correlated behaviour of the electrons [12]. The transition from normal state to superconducting state is not abrupt but the density of Cooper pairs rises from zero to its maximum values smoothly over a length scale the so-called the coherence length ξ .

There also exists a class of materials, known as unconventional superconductors, which exhibit superconductivity but whose physical properties do not follow directly the classical theory of conventional superconductors. One class of these is the so-called high-temperature superconductors (HTS). The first time high temperature superconductivity in a lanthanum-based cuprate perovskite material was observed by J.G. Bednorz and K. A. Mueller in 1986 [13], which had a critical temperature of 35 K (Nobel Prize in Physics, 1987).

The value of the critical temperature is a characteristic parameter of a specific material. Conventional superconductors usually have critical temperatures ranging from less than 1 K to around 23 K (for Nb₃Ge). Solid mercury, for example, has a critical temperature of 4.2 K. In 2001, an applicable medium temperature range superconductor was discovered, namely magnesium diboride (MgB₂) with $T_c = 39$ K. Soon after the discovery of MgB₂, many experimental studies indicated that MgB₂ should be basically classified as a conventional phonon-mediated BCS superconductor. The cuprate superconductors like e.g. YBa₂Cu₃O₇, Bi₂Sr₂Ca₁Cu₂O_y (Bi-2212) and Bi_{2-x}Pb_xSr₂Ca₂Cu₃O_y (Bi-2223) can have much higher critical temperatures ≥ 85 K. This is important because liquid nitrogen (at 77 K, 1 bar) could be used as a refrigerant. In 1988, mercury-based cuprates have been found with critical temperatures of 138 K.

2.2 Types of superconductors

There exist mainly three types of superconductors with rather different response to magnetic fields.

Type I superconductors: The elements lead, mercury, tin, aluminium and others are called 'Type I' superconductors. They do not admit a magnetic field in the bulk material and show perfect diamagnetism the Meissner effect. The Type I superconductor can tolerate a magnetic field only in a thin surface layer, the thickness of the layer is known

as the London penetration depth λ_L . Type I superconductors are also referred to as 'soft superconductors'. Figure 2.2 (left side) shows the schematic magnetization behaviour of Type I superconductors. It shows that the Type I superconductors are in the Meissner state when the applied field is below the critical field (H_c) and they are in normal conducting state when the applied field is higher than the critical field (H_c). As their critical fields are too small (~ 0.1 T) they are ruled out for high field applications. The 'Type I' superconductors show a completely reversible response to an external applied field [14].

Type II superconductors: It was realized in the 1950s that most alloys and compound superconductors are belonging to a second class of superconductors' the so-called 'Type II' superconductors. In the magnetic field vs temperature space, the phase diagram of this class of superconductors is comprised of two distinct superconducting regions. There is an upper critical field line H_{c2} (T) above which the material is in its normal resistive state, and there is a lower critical field line H_{c1} (T) below which the material is in superconducting state with perfect diamagnetism as shown in Figure 2.2 (right side).

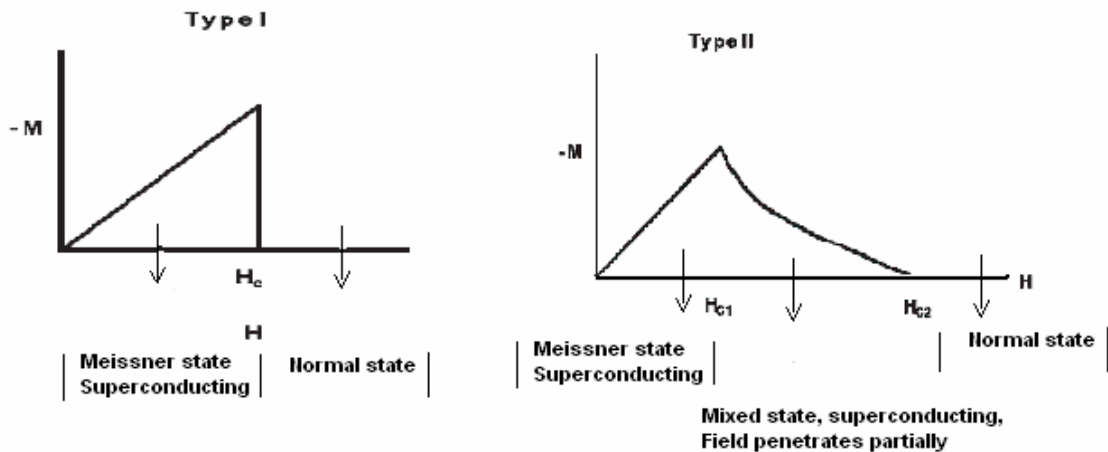


Figure 2.2 The schematic magnetization behaviour of the Type II superconductors [14]

The region between these two lines corresponds to the superconductor being in mixed state or so-called Shubnikov phase. In this state the material has zero resistance provided that the material has strong pinning but is not a perfect diamagnet [14]. In the mixed state, the magnetic flux penetrates the superconductor in the form of vortices, with each vortex carrying an identical quantum of flux, defined as $\Phi_0 = h/2e$. Where, $h = 6.625 \times 10^{-34}$ Js is the Planck's constant and $e = 1.6 \times 10^{-19}$ As the fundamental unit of electron charge. Figure 2.3 represents the mixed state, in which the normal cores and encircling supercurrent vortices are shown. The vertical lines represent the flux threading the cores. The surface current maintains the bulk diamagnetism.

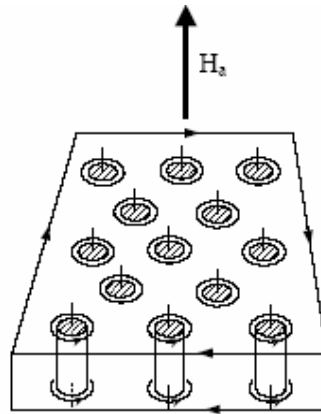


Figure 2.3 The mixed state in Type II superconductors

These vortices are normal regions in which Cooper pairs do not exist and thus they have higher free energy than that of surrounding superconducting region. The Type II superconductors remain superconducting up to much higher fields (10 T or even more) and at the first view they seem to be attractive for the applications of high-field magnet coils but they face a problem with flux flow resistance [15, 16].

When the current is passed through a Type II superconductor exposed to a magnetic field larger than H_{c1} , the current exerts a force on the magnetic flux lines and they will begin to move through the material and generate resistive heating. For useful applications, the flux flow should be prevented by means of providing impurities or defects in the material so-called pinning center. The pinning center prevents the flux flow.

Type III superconductors: A Type II superconductor with strong pinning is called a Type III superconductor, also referred as a hard superconductor. For a hard superconductor, not only the temperature and the magnetic field have to be specified but also the critical current density. The pinning force (F_p) prevents the flux flow until the Lorentz force (F_L) exceeds F_p . This defines a critical current density in hard superconductors ($J_c = f_p / F_0$), below which the transport current is carried without any resistance, and above which the flux-flow resistivity starts playing a role. Here, f_p is the pinning force per unit length. Hard superconductors are very well suited for high-field magnets; they permit current flow without dissipation in high magnetic fields. But there is a penalty; they exhibit a strong magnetic hysteresis as shown in Figure 2.4 [16, 17].

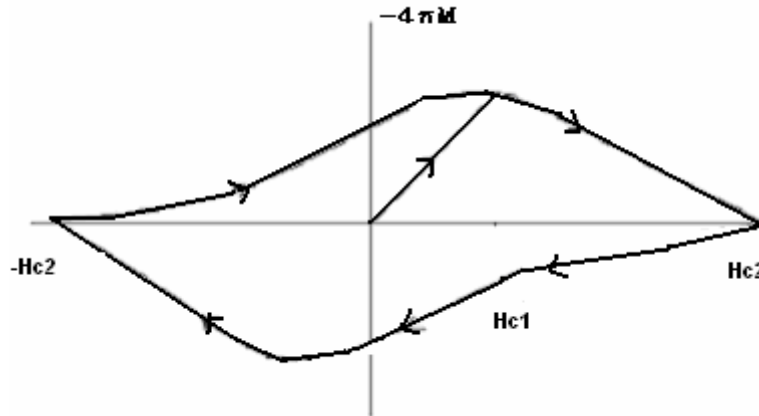


Figure 2.4 Magnetization – field characteristics in Type-III superconductors [16, 17]

2.3 Characteristics of superconductors

2.3.1 Critical current characteristics

For technical applications, it is important to introduce a criterion for the definition of the critical current. The voltage-current (U-I) characteristics of superconductors reveal how dissipation occurs as a result of current. To be able to compare different conductors and measurements, the voltage U is translated to the electric field E. It is necessary to define a criterion for the critical current I_c as the current measured at a certain electrical field E_c . For example, in case of low temperature superconductor (LTS) materials like e.g. NbTi or Nb₃Sn, $E_c = 0.1 \mu\text{V}/\text{cm}$ is used and for high temperature superconductor (HTS) materials like e.g. BSCCO or YBCO, $E_c = 1.0 \mu\text{V}/\text{cm}$ is widely used. The power-law characteristic of E – I can be expressed as follows [16],

$$E(I) = E_c \left(\frac{I}{I_c} \right)^n \quad (2.1)$$

The n – value is the power-law exponent for the “take off” of the E-I characteristic at the superconductor-normal transition. It characterizes the steepness of the transition into normal conductivity and represents thereby some quality factor of the wire. Figure 2.5 shows the principle E – I characteristics for technical superconductors.

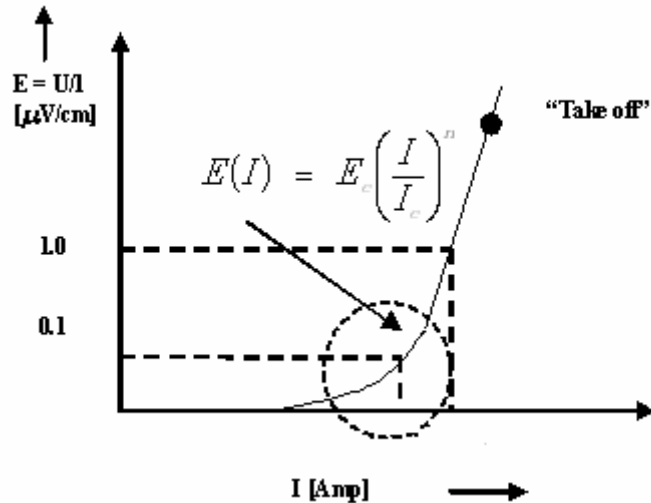


Figure 2.5 E – I characteristics for technical superconductors [16]

2.3.2 J-B-T characteristics

The superconducting state is defined by three very important parameters: critical temperature (T_c), critical magnetic flux density (B_{c2}), and critical current density (J_c). The J-B-T surface is the top limit for superconductivity. If one parameter value is varied, the values of the other two changes as well. For example, a higher operating temperature allows only a lower current and magnetic flux density. The J-B-T phase diagram is shown in Figure 2.6, which illustrates the relationship between T_c , B_{c2} , and J_c . Starting from this surface, and moving toward the origin, the material is superconducting. In regions outside this surface, the material is normal conducting.

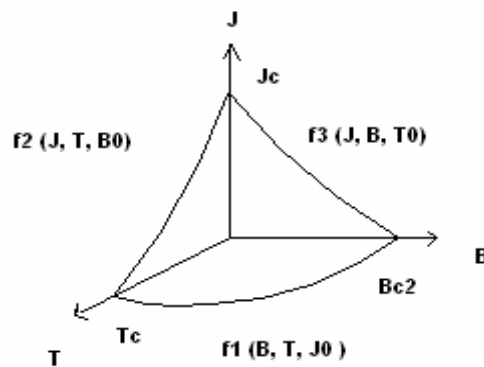


Figure 2.6 Phase diagram of superconductors

The following Table 2-1 summarizes the technical data for relevant LTS and HTS materials respectively [16]. Practical critical surfaces of superconductors are also reported in [18].

Table 2-1 Technical data for the LTS and HTS materials [16]

Material	T_{c0} (in K) at B =0	B_{c2} (in T) at T =	Applicable Tempe. (in K)	Available form in market	J_c (in kA/cm ²) (T, B)
NbTi	9.6	12 - 14 (0 K)	≤ 5	Wire	100 (1.8 K / 13 T)
Nb ₃ Sn	18	25 – 27 (0 K)	≤ 10	Wire	20 (4.2 K / 20 T)
Bi-2212 (Bi ₂ Sr ₂ CaCu ₂ O _y) (y = 8 – 10)	85	> 100 (4.2 K)	≤ 30	Wire / tape	500 (4.2 K / 0 T)
Bi-2223 (Bi ₂ Pb _x Sr ₂ Ca ₂ Cu ₃ O _y) (y = 8 – 10)	110	> 100 (4.2 K) > 0.5 (77 K)	≤ 77	Wire / tape	300 (4.2 K / 0 T) 25 – 30* (77 K / 0 T)
YBCO (YBa ₂ Cu ₃ O ₇)	90	8 – 9 (77 K)	≤ 77	Thin sect. with Ni /steel tape	3000** (77 K / 0 T)

* refers to samples value (< 1 km) and ** refers so far only to short sample (< 10 cm)

2.4 Technical usable superconductors

2.4.1 Low temperature superconductors (LTS)

The low temperature superconductor (LTS) typically refers to the Nb based alloys (most commonly NbTi, Nb₃Sn, and Nb₃Al. After the discovery of "high temperature" oxide superconductors in 1986, a classification was made from the temperature point of view. "Temperature" here refers to the temperature below which the superconductor must be cooled in order to become superconducting. For LTS this temperature is usually well below 20 K (-253 °C). NbTi has become the dominant commercial superconductor because it can be economically manufactured in a ductile form with the prerequisite nano-structure needed for high critical current. NbTi is used for field applications below 10 T. Multifilamentary composites of Nb₃Sn are used to produce superconducting magnets with field strength above 10 T and up to 21 T. They are very brittle and sensitive to bending and tensile stresses. All these conductors require cooling of about 4 K (Liquid He-I) or even at 1.8 K (He-II) as coolant. Figure 2.7 shows the critical current density vs magnetic field of the LTS materials at 4.2 K [18]. There are two approaches to form an A15 phase in Nb₃Sn, bronze process and internal tin process.

In the bronze process, the bronze matrix is formed when the conductor is already in its final stage. This method requires only a few subsequent steps in heat treatment; one

starts at 200°C, 100 hrs, continuous at 375°C for 24 hrs and finally 580°C for 50 hrs. Because of their good mechanical stability, bronze process strands are preferred in applications operated in high strain environments. Since bronze process strands do not have enough Sn for A15 reaction of the whole cross-section, the un-reacted Nb, which enhances the mechanical stability of the filaments, remains at the core part of the filament [19].

Several different routes are used to fabricate internal tin composites. One method uses Nb rod extrusions and a second method, the Jelly Roll method in a coiled expanded Nb mesh. The internal tin route requires a significant number of intermediate heat treatments at 700°C for 25 – 65 hrs to form the intermetallic A15 compound at the interlayer of the bronze to Niobium. However, internal tin route provides higher critical current density than the bronze route [19]. Under a highly stressed condition, Nb₃Sn strands degrade because of the tetragonal deformation of the cubic lattice. The critical current density of a Nb₃Sn strands depend on many factors, including number and design of the strand sub-elements, Nb filament size, amount of Sn and of Nb in the non-Cu section, Cu to non-Cu ratio and heat treatment cycle [20].

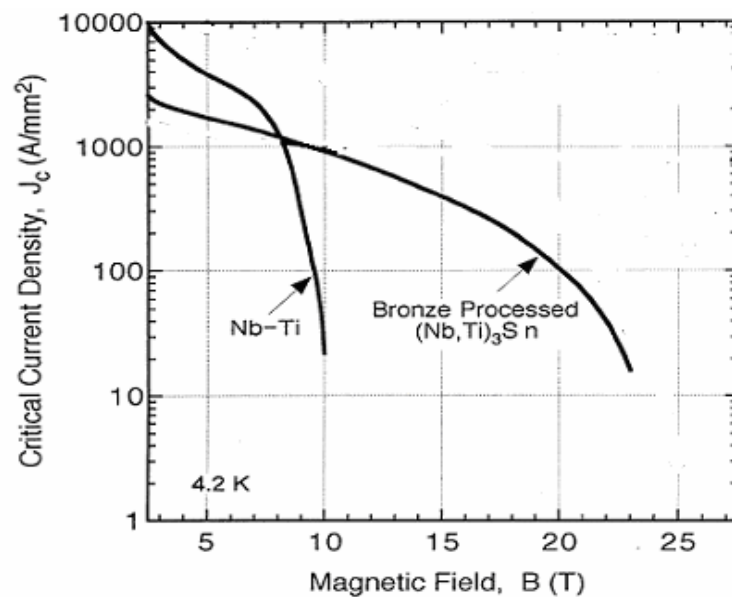


Figure 2.7 Non-Cu J_c (4.2 K) vs B curves for LTSs [18]

2.4.2 High temperature superconductors (HTS)

High temperature superconductors (HTS) are oxide superconductors, with perovskite crystal structure. After the discovery of superconductivity in $\text{La}_{2-x}\text{Ba}_x\text{CuO}_4$ with a transition temperature of about 35 K by Bednorz and Muller [13] in 1986, a substitution of Yttrium for Lanthanum led to the discovery of $\text{YBa}_2\text{Cu}_3\text{O}_{6+d}$ ($d \leq 1$) often referred as YBCO or Y-123 because of the ratio of Y: Ba: Cu in this material. This was the first superconductor discovered with a T_C of 90 K, well above the boiling point of liquid nitrogen. The discovery was followed in 1988 by the discovery of Bismuth ($\text{Bi}_2\text{Sr}_2\text{Ca}_2\text{Cu}_3\text{O}_{10+d}$) based superconductors with an even higher T_C . A large family of these superconductors with over 40 members is now known.

The BSCCO family of superconductors has also a perovskite type structure with copper oxide planes and chains and orthogonal unit cells. Two common members are $(\text{Bi}_2\text{Sr}_2\text{Ca}_1\text{Cu}_3\text{O}_{8+d})$ ($d < 1$) commonly known as Bi-2212 or 85 K phase, and $\text{Bi}_2\text{Ca}_2\text{Sr}_2\text{Cu}_3\text{O}_{10+d}$ commonly known as Bi-2223 or 110 K phase [21]. From the techno-commercial point of view, BSCCO based tapes and conductors are known as 1st generation conductors. Long lengths of Bi-2212 wires are possible to be drawn with a surface coating method whereas the powder-in-tube (PIT) method is applicable for Bi-2223 tapes. Unfortunately the high silver content of PIT BSCCO and the labor-intensive manufacturing process makes this HTS expensive for industrial applications in spite of the good performance. However, the BSCCO based tapes and conductors are used to demonstrate a variety of HTS power devices including power cables, fault current limiters, motors and generators. Figure 2.8 shows a cross-sectional view of a Bi-2223 /Ag/ AgMg tape produced by European Advanced Superconductors (EAS) [22].

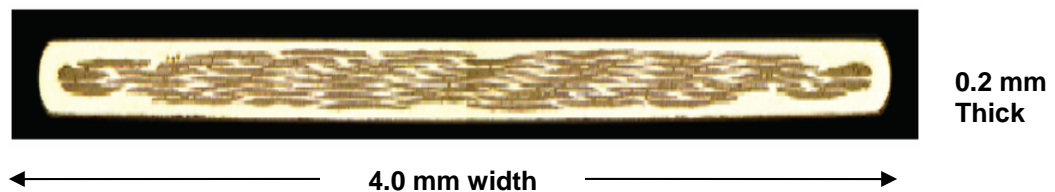


Figure 2.8 A cross-section view of typical Bi-2223/Ag/AgMg tape produced by EAS

More recently, large progress in Yttrium-based surface coated HTS conductors (YBCO) has been achieved. This 2nd generation coated conductor (2G HTS) offers operation at high magnetic fields close to 77 K and in a way for manufacturing next generation HTS electric power devices and components. Nevertheless, YBCO production is much more complex than BSCCO. Figure 2.9 shows the architecture of an YBCO based coated

conductor. Thin film deposition techniques are used to produce surface-coated conductors on bi-axially textured substrates with the following process steps [23],

- Electro polishing the metal substrate “tape” to a high degree of smoothness
- Deposition of a buffer layer
- Deposition of the superconductor (YBCO)
- Sputtering process to add a thin cover layer

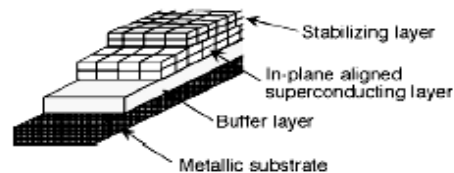


Figure 2.9 Architecture of YBCO coated conductor from [24]

Today there are mainly two processes used to fabricate the basic substrate for YBCO coated conductors as mentioned below,

- RABITS (Rolling Assisted Bi-axially Textured Process)
- IBAD (Ion beam Assisted Deposition Process)

2.5 Applications of superconductivity in fusion devices

Applications of superconductivity exist in wide areas of interest for researchers, starting from small-scale to large-scale applications. Here, the main focus is given on fusion devices (tokamaks and stellarators) related applications. Particularly, this applications fall into the large-scale applications. While discussing the large-scale applications of superconductivity, a distinction has been made between low temperature (LTS) and high temperature superconductor (HTS) use.

- **Superconducting magnets**

During 1968-78, the first superconducting T-7 tokamak was built in Russia and operated during the 80's with $B_{max} = 4.5$ T using NbTi type monolithic electro-polished conductors cooled by forced flow helium at 4.5 K. Later, this tokamak was transferred to China during 1991-1994 and renamed afterwards to HT-7. The more advanced step after T-7 was T-15 which was built during 1977-1988. Here, the Nb₃Sn monolithic electro-polished conductors operated with forced-flow helium was used to reach a higher field level of 6.6 T [25].

The first bath cooled tokamak, the so-called Tore Supra was constructed in France during 1978 operating with He-II (at 1.8 K). It uses a NbTi monolithic conductor for a

maximum field of 8.8 T. Similarly, in Japan during 1982-1986, TRAIM-1M was built with a maximum field of 11 T with a bath cooled Nb₃Sn monolithic conductors.

A new conductor concept, the so-called cable-in-conduit conductor (CICC) was designed and developed at MIT (Hoenig, Montgomery) [26]. It provides compactness to the superconducting strands, act as a narrow helium cryostat for the conductor and particularly, the conduit provides mechanical protection to the superconductor wires in it. For the "IEA-Large Coil Task" in the early 1980s, one coil was made with CICC. Following this new development, worldwide several countries have started developing magnets for their tokamak devices including SST-1 India, EAST China, KSTAR Korea, and JT-60U in Japan. Finally the ITER magnet system uses Nb₃Sn for the Toroidal Field (TF) and Central Solenoid (CS) coils and NbTi for the Poloidal Field (PF) and Correction Coil (CC) magnets respectively.

The stellarator LHD in Japan was built with superconducting helical field coils (using NbTi-Cu /Al monolithic conductors, pool boiling LHe-I at 4.4 K, B_{max}= 6.9 T) and poloidal field coils (using NbTi-Cu CICC, forced flow supercritical helium at 4.5 K, B_{max} = 5.0 T) [27].

Similarly, Wendelstein-7X which is under construction in Germany uses NbTi CICC for its magnets, cooling with supercritical helium at 4.5 K, B_{max} = 3 T). Here, B_{max} is the magnetic field at the plasma center.

- **LTS current feeder system**

In order to charge the superconducting magnet system (at 4.5 K) of any superconducting fusion device by the power supply at room temperature (RT), a current feeder system is required. As the magnetic self field of the feeder is much lower than that of the main magnet coils and as they are quite away from the magnet system, it is possible to use NbTi conductors in the low temperature part. Worldwide several fusion devices use the NbTi/Cu CICC concept in a compact rigid duct for their LTS feeders like e.g. SST-1 India and so far even ITER. The stellarator device LHD in Japan uses the NbTi/Cu/Al monolithic conductors for its LTS feeder design [27].

- **HTS current leads**

HTS current leads for high current have become a reliable commercial product for accelerators. The large-scale LHC project at CERN is installing 64 units of 13 kA current leads. The current leads consume a significant capacity of the whole cryogenic system of the particular devices. Using Bi-2223 materials, HTS current leads are now also under development and are already successfully tested at various places e.g. 60 kA

HTS test current lead developed by JAERI, Japan [28], and 70 kA EU HTS current lead as a part of R & D developed by the Forschungszentrum Karlsruhe collaboration with CRPP, Switzerland. With the specialized joining techniques and main advantage of low thermal conductivity of HTS materials in the temperature range of 4 K – 65 K, it is possible to save on overall refrigeration power by a factor of 3 – 4 compared to conventional current leads [9] [29] depending on the cooling modes as described in more details in Chapter 7. This enormous savings in the cryogenic power would lead to economical solution in terms of operational costs for a long time.

Chapter 3 - The role of cryogenic systems in fusion devices

Here the role of the cryogenic system in fusion devices is discussed. A significant part of the total electrical power of the whole machine is consumed by the cryogenic system alone. It is an indispensable and challenging technology for long duration plasma confinement devices with a superconducting magnets system. The design philosophy, system performance and pros and cons of different cooling schemes are discussed.

3.1 Introduction

The word *cryogenics* means the production of icy cold as a synonym used for low temperatures. The cryogenic engineering deals with the operation temperatures below -150° C (123 K). The requirement of a cryogenic system for fusion device is indispensable because they use superconducting magnets which operate at cryogenic temperatures (~4.5 K). Economic considerations are continuously required to increase the performance of the large-scale superconducting magnet and cryogenic systems [30]. High efficiency (e.g. 30% of Carnot), reduced operation costs, reliability and availability are the key issues in design and development of a large-scale cryogenic system. The main tasks of the large-scale cryogenic systems are the following [31],

- (i) Production of low temperatures by means of refrigeration power (which includes a network of compressors, refrigerators/liquefiers etc.).
- (ii) Storage and distribution of cryogens by means of dewars, cryostats, transfer lines, cryogenic valves boxes.
- (iii) Handling of purifiers, cooling components and warm gas management systems including gas balloons, high pressure storage, and medium pressure storage of helium inventory.
- (iv) Variability, flexibility and stability of the system are obtained during different modes of operation like e.g. cool down, warm up, stable operation, transient or fault event like a quench etc. via powerful and reliable process control, instrumentation and monitoring and data acquisition systems.
- (v) Finally, to train the manpower for obey the standards and safety regulations in all aspects at the design, operation and maintenance levels.

3.2 Worldwide large-scale helium cryogenic systems

The following Table 3-1 summarizes worldwide large-scale cryogenic systems used for various fusion and accelerator machines.

Table 3-1 Summary of worldwide helium cryogenic systems [32]

System	Country	Capacity	Cold mass	Type of cooling scheme for magnets
Tokamak				
SST-1	India	1.3 kW at 4.5 K	35 t at 4.5 K	Forced flow
HT-7U (EAST)	China	2.0 kW at 4.5 K	14 t at 4.5 K	Forced flow
TORE SUPRA	France	2.5 kW at 1.8 K	165 t at 1.8 K	Pool boiling
KSTAR	Korea	9.0 kW at 4.5 K	180 t at 4.5 K	Forced flow
ITER	IT	18 kW at 4.5 K (such 4 units)	3500 t at 4.5 K	Forced flow
Stellarator				
LHD	Japan	10 kW at 4.5 K	786 t at 4.5 K	Pool boiling (helical coils) Forced flow (PF coils)
W-7X (construction)	Germany	10 kW at 4.5 K (expected to change)	400 t at 4.5 K	Forced flow
Accelerator				
HERA	DESY, Germany	6.5 kW at 4.3 K	34,00 t at 4.3 K	Pool boiling
LHC	CERN, Switzerland	18 kW at 4.5 K (8 such units)	40,000 t at 1.9 K	Pool boiling

3.3 Design philosophy of large-scale helium cryogenic system

Usually, a helium refrigeration system is designed for either refrigeration cycles or liquefaction cycles depending upon the type of loads needed to be cooled at 4.5 K. The helium cryogenic system of any fusion device or accelerator is based on custom requirements because it has both, refrigeration as well as liquefaction demands. The capacity of the helium cryogenic system should be designed to meet following requirements,

- (i) Specified steady state heat loads on the system
- (ii) Average pulsed losses
- (iii) Specified cool-down time of a system

Particularly in tokamaks, different sources of steady state heat loads are acting which include radiation, residual gas conduction, thermal conduction, and joule heating. Other than these, there will be additional losses from the cold support structure, cryogenic transfer piping, distribution boxes, valves and manifolds.

During the plasma start-up, ramp down, and plasma disruptions, fast and slow discharges produce large eddy currents in the cold metallic structures. An abrupt change in the magnetic fields will cause a pulse loss so called AC loss within the superconducting magnets system. Other than these, particularly for a thermonuclear reactor like ITER, additional losses by nuclear heating will occur.

Apart from the losses related to the magnets system, there are other losses which need to be considered, e.g. cryopump load, cold circulator load, and thermal shield load etc. The overall size of cryogenic cooling system should be fixed in order to remove above heat loads at the operating temperature.

In general, the steady state cryogenic plant capacity at the operating temperature (T_{op}) is defined as 1.5 times average steady state heat loads plus the average over a day contribution from the pulsed heat loads. The basis for the factor 1.5 is from the assumption on the cool-down efficiency of 50% [33].

As the initial cool-down process is limited by thermal stress problems, a rather long cool-down time is needed for large systems depending upon their mass need to be cooled down to T_{op} . Typically, for small devices (with cold mass of ~ 1 ton) to large cold mass devices (with cold mass of ≥ 35 tons), the duration of the cool-down process may take 7 days to 30 days limited by the thermal stress in the cold mass. In general, 0.5 K/hr – 1.5 K/hr cool-down velocity is required to maintain the temperature difference of < 50 K between the highest temperature of the cold mass and the inlet temperature of the coolant.

Thus, the maximum refrigeration capacity of the cryogenic system should be determined from the required capacity in steady state and cool-down operation.

In spite of the refrigeration requirements mentioned above, the current leads, consume a significant amount of cryogenic plant capacity in terms of pure liquefaction load. As an example, in the SST-1 tokamak, the vapor cooled current leads consume 55% of the total cryogenic capacity [34] whereas in ITER, the present design of the forced flow conventional current leads would consume almost 25% of the total cryogenic capacity depending upon the machine operational duty cycle [2]. Here, the duty cycle means the operation time of the machine with respect to zero current mode so called stand-by mode. The net liquefaction consumption or coolant mass flow rate is given by l/hr or g/s. As this consumption varies with respect to duty cycle an average load over a duty cycle should be considered while sizing the liquefaction requirements but it requires a large

helium reservoir as additional storage. Again some margin on these numbers should be considered in the design as a factor of safety (around 20 – 30% more). The conversion factor for refrigeration power to liquefaction power varies from machine to machine cold-box process. In general, as a rule of thumb, the following conversion factors are applied as an example,

- 3 Watts of refrigeration power = 1 l/hr of liquefaction
(For SST-1 cryo plant with COP of 466) [35]
- 6 Watts of refrigeration power = 1 l/hr of liquefaction [36]

(The ITER cryo plant will have COP of 233, as same as the LHC 18 kW cryo plant [37])

The efficiency of any refrigerator is defined with the COP, is known as the coefficient of performance, The Coefficient of Performance for a refrigerator is defined as the ratio of the heat removed from the cold reservoir (in terms of cooling) to the mechanical work added to the system (in terms of energy consumption). Thus, it is the ratio of the useful energy output (Q) of a system to the mechanical work (W) required to operate it i.e. $COP = Q_c / W$.

For a heat engine, the first law of thermodynamics states as the following,

$$Q_c + W = Q_h \quad (3.1)$$

From the second law of thermodynamics one can also define COP value as following,

$$COP = \left(\frac{Q_c}{Q_h - Q_c} \right) \quad (3.2)$$

Here the subscripts, h and c are corresponds to the hot and cold temperatures. It is desirable to have the value of COP is always less than 1 for any refrigerator.

3.4 Description of a helium cryogenic cycle

There exist different variety of helium cryogenic cycles exists [30], among them the large-scale system uses a modified Claude cycle which is a combination of a Joule Thomson (J-T) cycle and a Brayghton cycle as shown in Figure 3.1. Since for helium the J-T effect sets in below its inversion temperature at ~ 40 K effective cooling by isentropic expansion through a throttle valve starts only below 10 K and 20 bar and that is why it is useful in a cryogenic cycle. The cooling is produced by the extraction of mechanical work during an adiabatic expansion in an expansion machine [31]. In case of LHC and ITER, by cascading many standard unit modules of 18 kW at 4.5 K with the modified Claude cycle are used [38] and discussed in section 4.4.2 of Chapter 4.

3.5 Cryogenic system performance

The second-law of thermodynamics states that a penalty of operation at low temperatures can be much worsened by the presence of internal irreversibility. This has an impact on the overall efficiency of the refrigerator, and hence on its capacity and energy consumption.

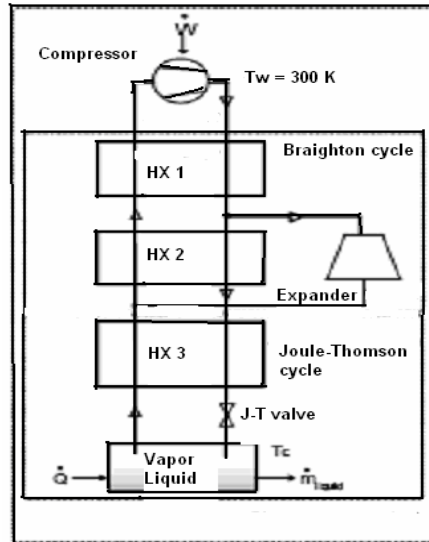


Figure 3.1 Claude cycle for helium systems [31]

In large-scale cryogenic systems, the main driving factors are the optimization of the refrigeration cycles and the choice of efficient and reliable machine components like e.g. compressors, heat exchangers, turbo-expanders, valves. Nowadays, the large-scale helium refrigeration systems operate with 30% of the reversible Carnot cycle as exergy efficiency and provide an excellent performance in the temperature range of 4.5 K to 300 K. These machines operate continuously for more than 9 months per year without any problems. The overall efficiency of such cryogenic machine is defined in terms of Carnot efficiency (η_c) and exergy efficiency (e) as follows,

$$\text{COP} = (\eta_c e) \quad (3.3)$$

$$P_{300K} = \left(\frac{E}{e} \right) \quad (3.4)$$

Where, the Carnot efficiency is given by,

$$\eta_c = \left(\frac{T_c}{T_w - T_c} \right) \quad (3.5)$$

$$E = \dot{m} [T_0 (S_w - S_c) - (h_w - h_c)] \quad (3.6)$$

Here, E is known as Exergy flow, e is known as exergy efficiency. Loads at different temperatures are converted into exergy with reference at 300 K and then it is converted to an equivalent load at 4.5 K through Carnot efficiency. Here, T_c and T_w are referred as cold and warm temperatures respectively,

Table 3-2 summarizes the capacity, the COP and thermodynamic efficiency values for several kW class helium refrigeration systems worldwide.

Table 3-2 Summary of several kW class helium refrigerators at 4.3 – 4.5 K [39]

Device	Cryogenic capacity [kW]	Operating Temperature [K]	Electrical Power [MW]	COP ⁻¹ [$W_{300K} / W_{4.5K}$]	e
SST-1	1.35	4.5	0.63	466	0.1409
FZK	2.0	4.4	0.88	440	0.1526
HERA	6.5	4.3	2.7	415	0.1655
KSTAR	9.0	4.5	3.0	333	0.1973
W-7X	7.0	4.5	1.6	230	0.2856
LHD	10	4.5	3.5	350	0.1877
LEP	12	4.5	2.7	225	0.2919
LHC	18	4.5	4.2	233	0.2815

The COP variation and efficiency data are explained by different expansion techniques present in large helium refrigeration systems, for example starting from the isenthalpic expansion (simple J-T expansion) to isentropic expansions in different stages using turbo-expanders, one can improve COP of the particular helium refrigerator [40 – 41].

The temperature dependency of the exergy efficiency can be explained as follows, above 120 K, the efficiencies of heat exchanger and turbine are rather low compared to 80 K. This is the reason, why Claude systems are practically never used above 120 K. It slowly becomes more efficient, when one comes closer to 80 K. Because efficiency depends on the pressure drop of the coolant as well as efficiency of the main heat exchanger.

The efficiency gets clearly better when one goes from 80 K to 20 K supposing the load matches the temperature of the turbines in the cycles. So in general, around 20 K the maximum of the efficiency is reached. Below 20 K the JT-region is present, where the low pressure and high pressure streams have different heat capacities. It causes the spreading of the temperature differences. Here, adding one or more turbines in the J-T region would prevent the spreading of the temperature differences in heat exchanger. In case of a turbine added Joule -Thomson region, the drop of efficiency from 20 to 4.4 K is rather small. If one reaches temperatures below 4.4 K, the efficiency is further reduced because of the pressure drop in the low pressure branches. At 1.8 K it may be 30% lower than at 4.4 K dependent on the efficiency of the cold compressors. The

temperature dependence of the thermodynamic efficiency for some of the systems is plotted in Figure 3.2 [31] [40 - 42].

V. Keilin as well as T. Ando have given an empirical formula for the exergy efficiency of the modified Claude cycle with a COP of 305 in the temperature range of 3 – 20 K as follows [43 - 44],

$$e = 0.0014T_{in} + 0.24 \quad (3.7)$$

Nevertheless one can see from the above discussion, there are so many parameters, which may have an influence on the overall performance of the refrigerator, so it is rather difficult to state a general formula for a complex system.

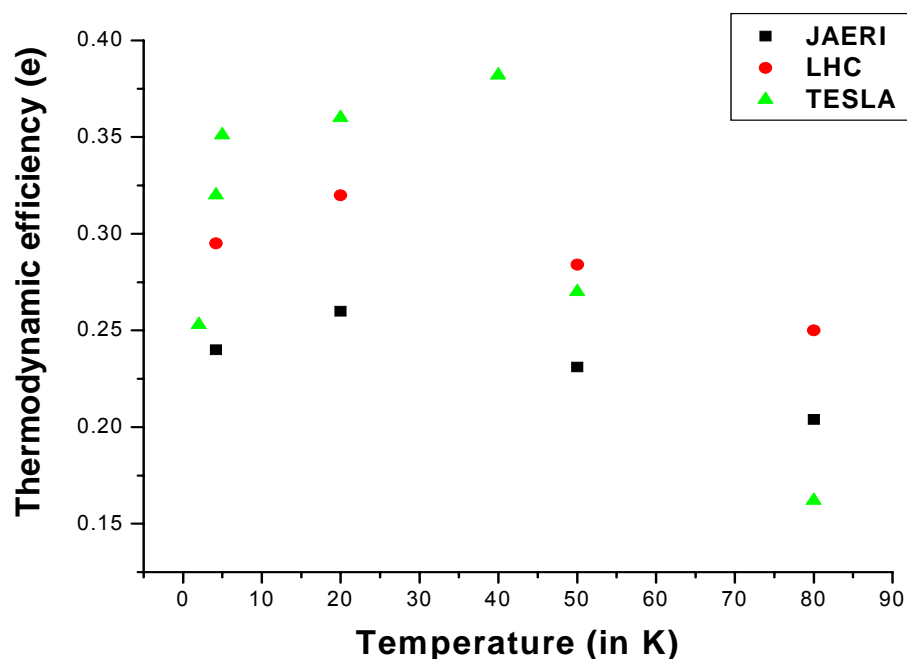


Figure 3.2 Temperature versus thermodynamic efficiency of the helium plant

3.6 Different cooling schemes for fusion devices

The phase-diagram of helium (P-T diagram as shown in Figure 3.3) [31] offers flexibility in order to cool the system with different cooling schemes and cooling principles like e.g. bath cooling so-called pool-boiling, single phase cooling, two-phase cooling, forced flow cooling with helium-I, and pool-boiling as well as forced flow with helium-II which is also known as super fluid helium.

The cooling scheme for superconducting magnets is selected based on magnet design, system layout and operating needs. Efficiency of the cryogenic system, hardware, cost

and reliability are considered in the design phase. In fusion devices, there are two cooling schemes popular in the community as mentioned below,

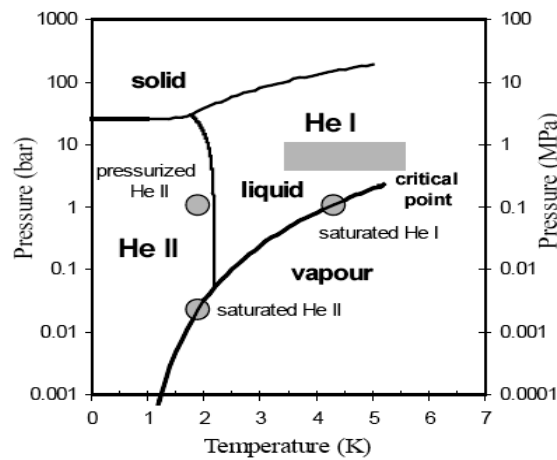


Figure 3.3 Phase diagram of helium (P-T diagram) [31]

3.6.1 Pool boiling / Bath cooling

Monolithic superconductors are cooled with the pool-boiling scheme using the saturated liquid helium to cool the magnets. The latent heat as well as sensible heat is used to remove the heat loads efficiently. In the Tore Supra tokamak at France, 160 tons of the sc magnet mass was cooled with pool-boiling 1.8 K super fluid helium. As well, the helical coils system of LHD, Japan was cooled with pool-boiling 4.2 K helium. The pool-cooled conductors offer a number of attractive advantages, including cryostability, low-risk manufacturing and joining techniques, and effective use of the superconductor material i.e. cost effectiveness. However, the size and stored magnetic energy of future fusion magnets with large mechanical as well as electromagnetic loads in the winding pack and high-voltage operation call in the case of quench for fast discharge conditions. Thus, the forced flow conductors with potted winding packs and high voltage insulation are the only option for large fusion magnets with a stored energy of > 1 GJ [32].

3.6.2 Forced flow cooling

The forced-flow conductors offer a variety of layouts, among them cable-in-conduit-conductors (CICCs) are the best choice for GJ energy magnets. The CICC act as narrow cryogenic channel cryostat, where the better coolant heat transfer is possible and the conduit provides also better mechanical strength to the conductor and minimizes the eddy current loss [45]. In forced-flow scheme, a superconducting magnet

is cooled by supercritical helium using cold circulating pumps or cold compressors as a pumping device through a heat exchanger cooled slightly below the magnet temperature in a helium bath. The efficiency of the supercritical helium system depends on the magnitude of the pump work and the temperature difference.

3.6.3 Problems with Two-phase cooling

Two-phase system offers many advantages compared to forced flow supercritical helium systems reported in [46]. This is true because the cryogen has latent heat of vaporization as well as sensible heat. But it is applicable only to small experimental laboratory scale systems like e.g. solenoid magnets, short length cryogenic transfer lines etc. As discussed earlier the fusion devices face large heat fluxes. They have long and complicated flow paths due to its complex cable design which in turn gives a higher value of the vapor fraction with respect to the liquid phase, so-called the quality factor (x). Depending upon the quality factor and mass flow rates, there is a possibility to form different two-phase flow patterns [30]. Among different flow patterns, the two-phase flow instability occurs particularly due to slug and plug flow regions leading to flow chocking phenomenon. That is why it is not desirable to use a two-phase flow system in fusion devices.

Chapter 4 - Description of the ITER machine, magnets and its auxiliary utility systems

Here, a brief summary of the ITER machine is given with defining the main machine parameters. The superconducting magnets system is described along with the current feeder system and its auxiliary utility systems like the power supply and cryogenic system.

4.1 Introduction to ITER

The construction and operation of the International Thermonuclear Experimental Reactor (ITER) is the next step towards the controlled nuclear fusion with costs of ~10 B€ and will be built in Cadarache, France in the frame of an international collaboration, including EU, Japan, Korea, China, India, USA, and Russia. The first plasma operation is expected in 2013. The main goal of the ITER project is to demonstrate that power generation by nuclear fusion is feasible in an economically and environmentally acceptable way.

4.1.1 Brief summary

In a fusion reactor the hot plasma is confined by the magnetic fields generated by the superconducting toroidal field coil system and the plasma current. Thus, the superconducting coil system is an indispensable component. Experimental ways for the magnetic confinement in a toroidal arrangement are called tokamak and helical arrangements are known as stellarator. The working principle of a tokamak is shown in Figure 4.1 and more details may be found in [47]. The International Thermonuclear Experimental Reactor (ITER) is also planned according to this principle.

For the first time, the plasma will be generated in ITER with power reactor-like properties over a longer time period (some 300 seconds). The investigations on plasma physics will concentrate on all aspects of burning plasma which essentially is maintained by alpha particle-heating. Alpha particle-heating means the transfer of kinetic energy of alpha particles originating from the fusion reaction to the plasma particles (electrons and ions).

Furthermore key technologies for a fusion power station, i.e., plasma heating, superconducting magnets, plasma facing components, fuel cycle, blanket concept and remote handling will be tested under power reactor-like conditions. Figure 4.2 shows a bird view of ITER [48].

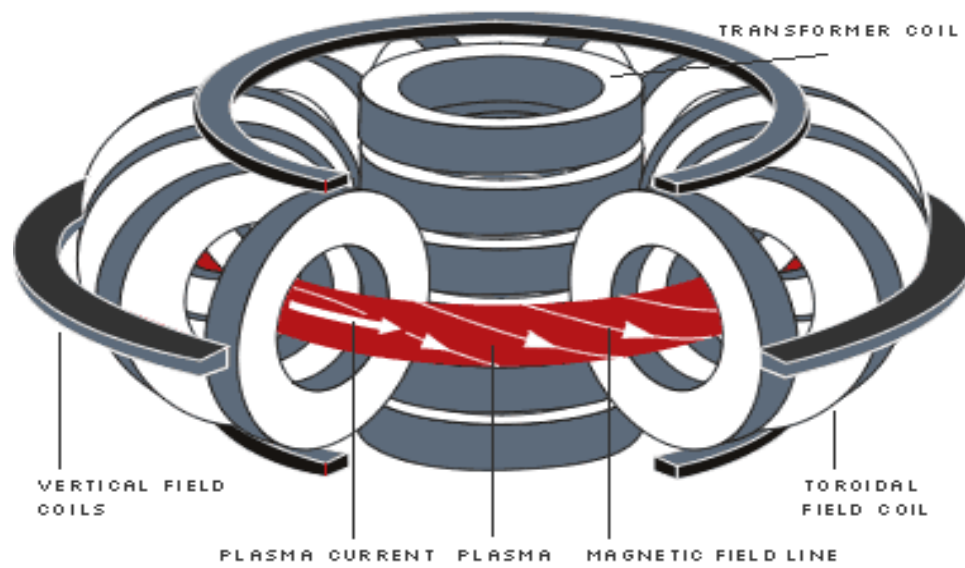


Figure 4.1 Tokamak principle

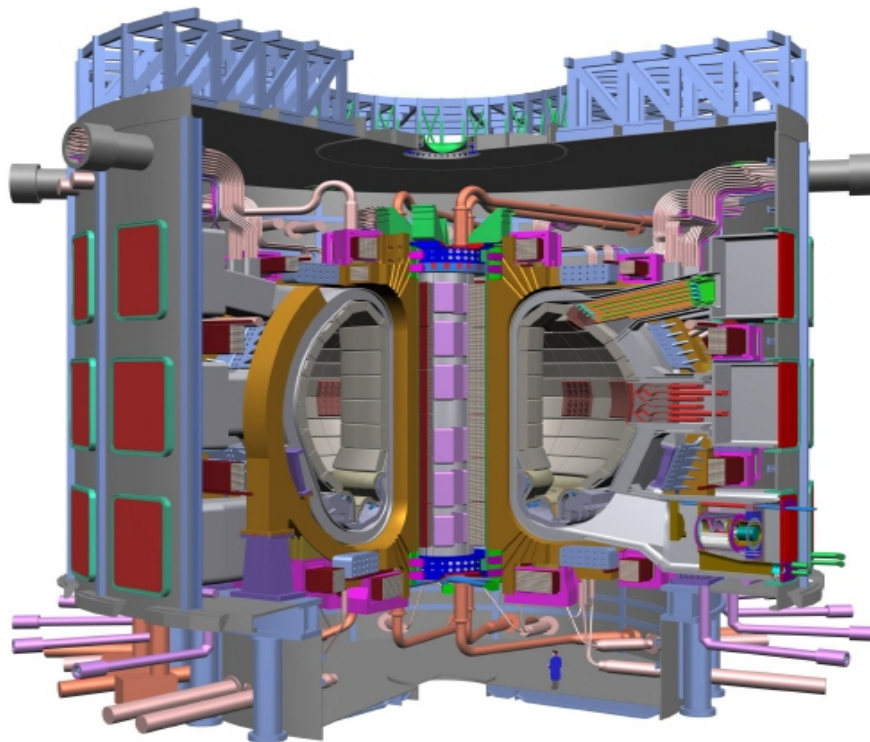


Figure 4.2 A bird view of ITER

4.1.2 Machine parameters

The ITER machine is a tokamak with nominal plasma major radius of 6.2 m and plasma minor radius of 2 m. The nominal plasma current is 15 MA and the toroidal field (TF) at the major radius is 5.3 T.

The main parameters of ITER machine are summarized in Table 4-1 [49].

Table 4-1 Main parameters of ITER

Total fusion power (in MW)	500
Q- Fusion power/Auxiliary heating power	10
Average (1 MeV) neutron wall loading (MW/m ²)	0.57
Plasma major radius (in m)	6.2
Plasma minor radius (in m)	2.0
Plasma current (in MA)	15
Toroidal magnetic field at 6.2 m radius (in T)	5.3
Plasma volume (in m ³)	837
Installed auxiliary heating/current drive power (in MW)	73

4.2 Description of the ITER superconductor magnet system

A three-dimensional view of the ITER magnet system is shown in Figure 4.3. The magnet system consists of 18 TF coils, a central solenoid (CS), six PF coils and three sets of correction coils (CCs) [2] [50]. The CCs are used to correct error fields due to toroidal asymmetry and to stabilize the so called 'plasma resistive wall modes'. All ITER coils are superconducting. The CS and TF coils operate at high field and use Nb₃Sn superconductors. The PF coils and CCs operate at lower field and use NbTi superconductors. All conductors are of the cable-in-conduit (CICC) type where a bundle of strands is enclosed in a metal jacket, which contains the helium coolant as well as, and contributes to the structural integrity of the coils. All coils are cooled with forced flow supercritical helium in the range of 4.4 – 4.7 K.

Particularly, the TF coil winding packs are enclosed in casings which constitute the main structural components of the magnet system. These winding packs are using the concept of a conductor with a circular cross-section contained in grooves of so-called 'radial plates' which provide mechanical support for the conductor and protection for the conductor insulation. This concept has been selected due to the greater insulation reliability despite cost and radial build penalties.

The CS assembly consists of a vertical stack of six electrically independent modules but they are hydraulically connected to each other.

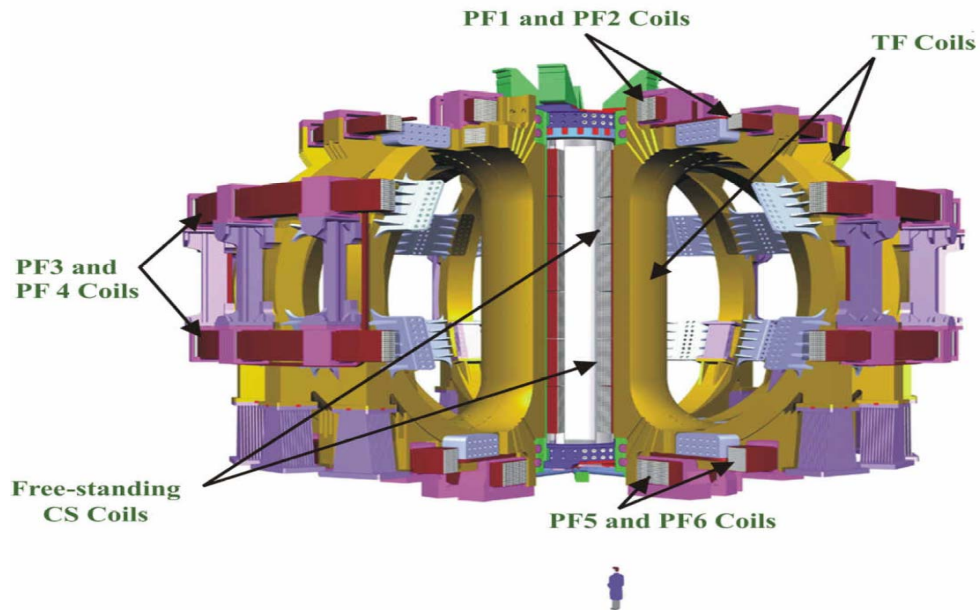


Figure 4.3 A 3-D view of the ITER main magnet system

The six PF coils are mechanically attached to the TF coil cases through flexible plates allowing radial displacements.

The three sets of CCs are located above, at, and below the equatorial plane of the machine. Table 4-2 lists some of the important magnet parameters. A typical cross-sectional view of the central solenoid model coil (CSMC) conductor ($51 \times 51 \text{ mm}^2$) (left) and an exploded cross-section of toroidal field model coil (TFMC) conductor (right) are shown in Figure 4.4.



Figure 4.4 Cross-sectional view of the CSMC conductor (left) and TFMC conductor (right)

Table 4-2 Main parameters of the ITER magnet system

Number of TF coils	18
Magnetic energy in TF coils (in GJ)	~ 40
TF coil current (in kA)	68
Maximum field in TF coils (in T)	11.8
CS current (initial magnetization / end-of-burn) (in kA)	41.5/ 45.2
CS peak field (initial magnetization / end-of-burn) (in T)	13.5 / 12.8
PF coil current (normal operation / back up mode) (in kA)	45 / 52
Correction coil current (in kA)	10
Weight of TF coils including structures (in tons)	5621
Weight of CS including clamps (in tons)	926
Weight of PF including clamps (in tons)	2835
Weight of CCs including clamps (in tons)	80
Total weight of magnet system (in tons)	~ 10135

4.3 Description of the ITER current feeder system

In order to charge the superconducting magnet system (at 4.5 K) from the power supply at room temperature (RT), a current feeder system is required. It consists of a low temperature superconducting feeder, a current lead and a water-cooled Aluminium bus bar. So, the current feeder system basically acts as current transmission line from 4.5 K to 300 K. The schematic layout of the present design of the current feeder system for ITER is already shown in Chapter 1 (refer Figure 1.1). As the maximum field acting on the sc feeder is lower than that of the main coil system and due to its complex cable structure, it has been envisaged to use similar kind of CICC's for all the TF, PF and CS sc feeders systems made from NbTi / Cu. These sc feeders will also be cooled with forced flow supercritical helium at 6 bar and 4.5 K as for the magnets for ITER [3].

4.3.1. Review of worldwide current feeder systems for fusion devices

The worldwide superconducting fusion devices like tokamaks and stellarators require superconducting current feeder systems in order to charge their magnets at 4.5 K. In this line, several designs, development and tests of existing superconductor current feeder systems are reviewed exemplarily as mentioned below.

A conceptual design of the sc bus line for the Large Helical Device (LHD) has been described in 1991 [51, 52]. The challenging issue was the development of a flexible sc

bus line together with industry. It was the first time in the world that a 120 m long flexible sc bus line was developed with a rated current of 13 kA by using monolithic NbTi / Cu / Al conductor. A (+/-) pair of such bus bars were inserted in a flexible steel cryostat envelop with vacuum and superinsulation for ease of assembly and installation.

In 1996, an internal report described a conceptual design of a sc bus duct and other auxiliary sub-systems for the TPX tokamak which was planned to be constructed at Princeton but later on cancelled [53]. It was a rigid and compact bus duct concept in which a (+/-) pair of NbTi /Cu based conductors were housed in a rigid cryostat with a vacuum, 80 K thermal shield, and superinsulation with low thermal conductivity glass fiber supports. This bus duct was designed for a rated current of 30 kA.

A description of the sc current feeder system for the KSTAR device was given in 2002 [5] [54]. It uses the same concept as the LHD sc bus line but the rated current is 35.2 kA for the TF feeders and 20 – 25 kA for the PF and CS feeders. All the LTS feeders are cooled with forced flow supercritical helium at 4.5 K.

The conceptual design and development of the sc bus lines for the SST-1 tokamak was described in 1997, the same design concept like TPX bus duct was used. It was designed for a maximum current of 10 kA [55]. The test results along with of a pair of 10 kA vapor cooled leads were presented in 2003 [56]. The sc feeders of SST-1 are planned to be cooled with the forced flow supercritical helium at 4.0 bar and 4.5 K.

4.3.2. Description of the LTS current feeder system

Each pair of the horizontal mounted current leads will be installed in the coil terminal box (CTB). The CTBs provides the interface to utility systems like power supply and cryogenic plant. In order to connect the LTS feeders with the power supply via current leads, a 25-m long LTS current feeder is required and is made of three parts, the in-cryostat feeders, the Cryostat Feedthrough (CF) and the CTB. An elevation view of magnets and feeders is shown in Figure 4.5. Figure 4.6 shows the part wise view of the current feeder system including the Cryostat Feedthrough (CF) and the CTB. It has been decided to use the same type of conductors as used in the coils, i.e., dual channel cable-in-conduit-conductors (CICCs). As the maximum field acting on the sc bus bar is small (< 1.5 T) compared to the coils, the conductors are made of NbTi / Cu strands. They are cooled with forced-flow supercritical helium at 6 bar and 4.5 K as used for the magnets. The current design outline of the feeder's layout is given in the Design Description Document [3] and technical requirements and specifications are discussed in Chapter 6 of section 6.1.2.

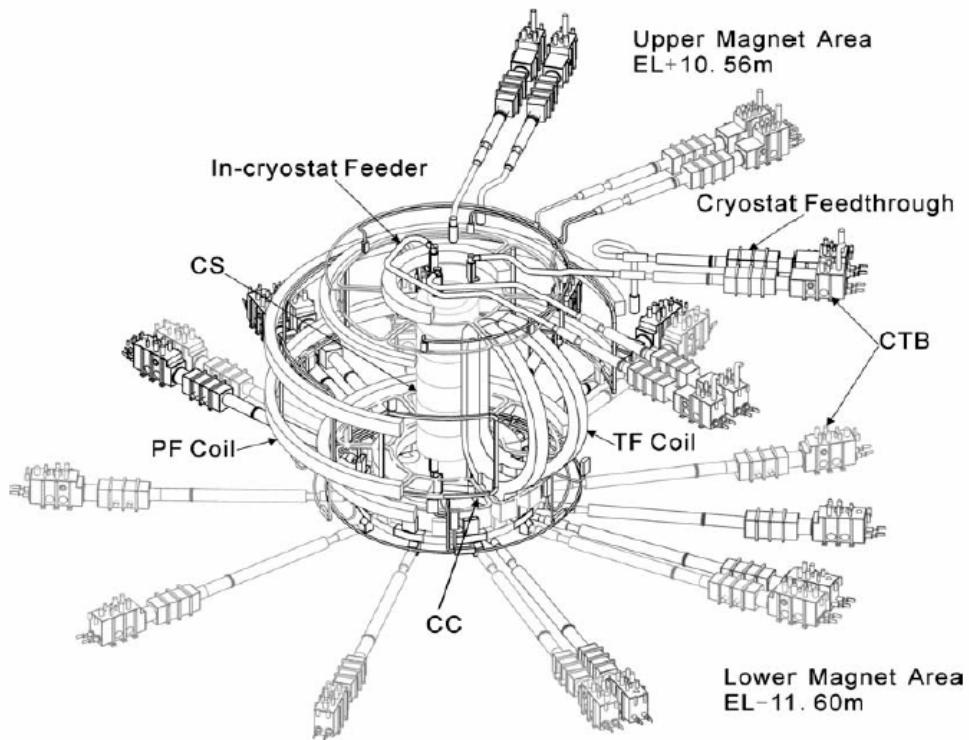


Figure 4.5 An elevation view of the magnets and feeders in ITER [2]

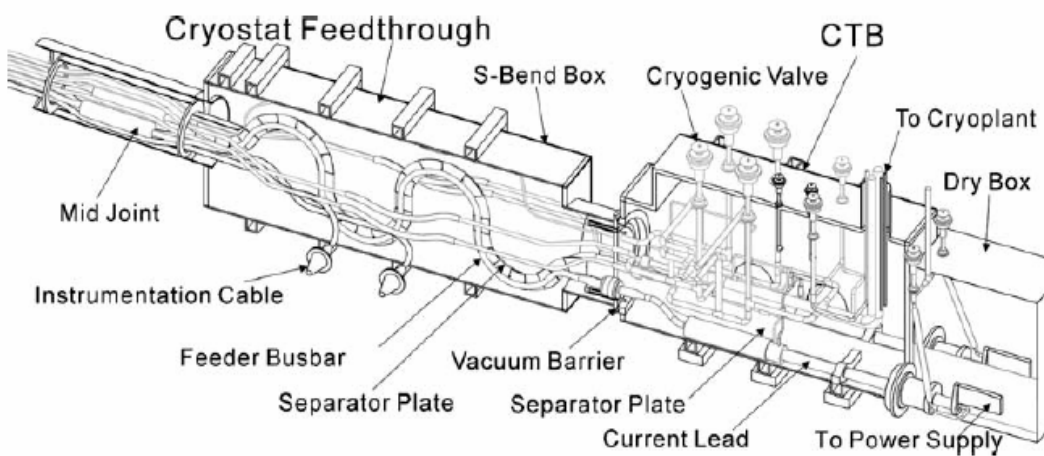


Figure 4.6 Cryostat feed through and CTB with valves and current leads [2]

Each In-cryostat feeder (IF) is a sub-assembly, which is connecting a coil to the end of a Cryostat Feed through (CF) and it is located just inside the cryostat. The IF consists of the feed and returns current supply bus bars, the supply and return helium lines and the instrumentation lines [2, 3] as shown in Figure 4.7 below.

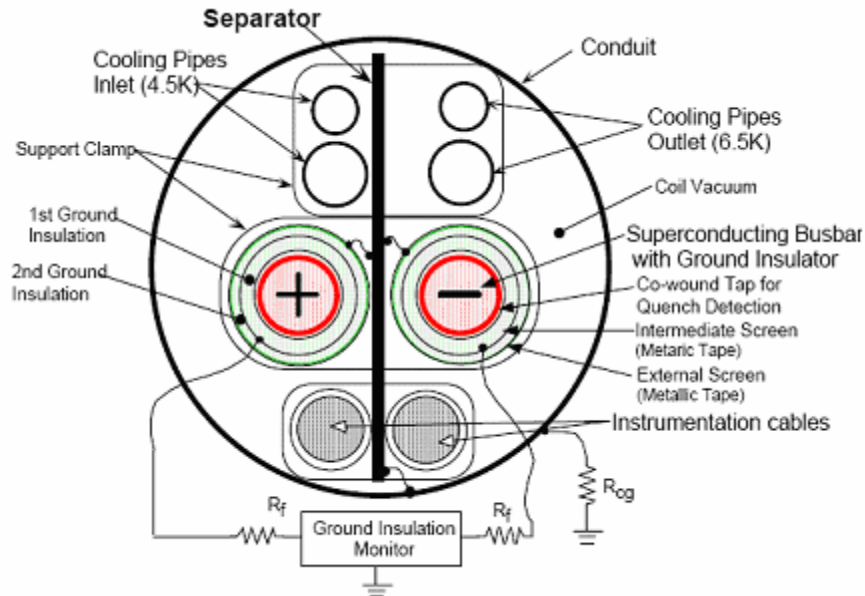


Figure 4.7 Cross-section of the In-cryostat feed through with cooling piping and instrumentation cables (courtesy from ITER DDD report [2])

Each feeder contains a pair of superconducting bus bars which are separated by a steel plate, four pipes for coolant supply and return and two pipes for high and low-voltage instrumentation cables. The steel separator plate separates the bus bars and piping for their ground insulation monitoring. It extends along the entire length of the conduit, as additional protection against a short circuit between the bus bars. The cooling pipes and the external conducting screens on the bus bars are electrically connected to the separator, the separator is connected to the conduit, and the conduit is connected through its cryostat feed through to the grounded cryostat wall. The vacuum inside the conduit is part of the cryostat vacuum for all coils.

The Cryostat Feed through (CF) includes a straight length from the cryostat wall to a S-Bend Box, this bend accommodate the movements of the in-cryostat feeders and the coils, relative to the fixed S-bend box and Coil Terminal Boxes (CTB), due to differential thermal contraction and expansion during cool down and warm up, due to electromagnetic forces.

4.3.3. Current lead requirements

The current leads are the solid connection between the sc feeders at 4.5 K and the room temperature bus bars to the power supply. In any fusion devices with superconducting magnets, the current leads are the major cryogenic load. As they are metallic connections from the temperature of 4.5 K – 300 K, the losses due to Joule

heating and thermal conduction are significant for higher operating currents as well as during the off-current operation (zero current) so called stand-by modes. Since the cryogenic loads due to the current leads vary in case of normal operating condition and during the stand-by mode, depending upon the machine duty cycle an optimum design of the current leads is essential [57].

In ITER, each CTB contains one pair of copper current leads; those for the CC contain 2 pairs. The forced flow helium cooled current leads provide the electrical connection between the room temperature bus bars from the power supply to the LTS feeder at 4.5 K inside the CTB. The present ITER design of the current leads is of forced flow helium cooled conventional type. The technical requirements of ITER current leads are discussed in Chapter 5.

4.3.4 Water-cooled aluminum bus bars

The main design data on the water-cooled DC bus bars are given in Table 4-3 [58].

Table 4-3 Design data of the water-cooled bus bars

Device / Parameter	Unit	TF	CS & PF	CC
Rated current	kA	68	45	10
Rated voltage (between poles and to ground)	kV AC	17.5	17.5	3.3
Short circuit current	kA	300	200	40
Cross-section	mm ²	41000	20000	4500
Total length *	m	100	1300	1000
Total number of flexible joints *		4	50	40
Total number of bends *		3	60	50
Joule heating	kW/m	3.4	3.0	0.66

* refers to two-polarity bus bars

4.4 Auxiliary utility systems

4.4.1 Magnets power supplies

The water-cooled bus bars finally connect to the power supply at the room temperature. There are two physical interfaces between power supplies and the magnets at the coil terminal boxes (CTBs) [58].

i) The current supplies and discharge circuits for the coils: They consist of one supply for the 18 TF coils plus 9 discharge resistors connected between each coil pair. Each PF coil and CS coil module has its own supply and discharge resistor.

ii) The magnet structure grounding scheme: The magnet structures are all connected to ground through the bus bar containment pipes to the cryostat wall. The connection of the cryostat to the overall machine grounding scheme is part of the power supplies.

The coil power supplies include the following 9 systems supplying controlled dc current to the TF and PF coils and the CS modules.

- 1 common power supply unit for the 18 TF coils
- 5 units for the CS module, in which 4 for CS 2 and CS 3 upper and lower modules and 1 for CS 1 upper and lower modules.
- 2 units for individual supply of the PF1 and PF6.
- 1 unit common for the PF2 – PF5 outer coils (4 coils).

In addition, there are 9 units of relatively smaller power supply systems with identical configuration for supply of the 9 correction coils (CC) [58, 59].

The TF coils are combined in 9 groups, each containing two coils which are connected in series inside the cryostat. These groups are connected to one 12-pulse, 2 – quadrant thyristor-converter rated for 68 kA, 900 V no load voltage. When the TF system is charged and the current has reached the requested value, the primary transformer is switched from the 69 kV - to - 22 kV. This would give a reactive power with constant current for few weeks / months. In case of a quench, the maximum stored magnetic energy of ~ 41 GJ has to be removed safely. There are 9 Fast Discharge Units (FDU) which need to be activated. These units consist of two circuit breakers and discharge resistors. The circuit breakers for FDU's are located in the tokamak building gallery, near to the CTBs. The discharge resistors and counter-pulse capacitors (to make the zero current) are located in the diagnostic building, which is adjacent to the tokamak building. Two circuit breakers are connected in series with each of the FDU's. The first, called the current commutation unit (CMU), is designed for multiple operations and will open when a quench is detected. In case of failure in one of the CMU, the second circuit breaker so-called the pyrobreaker will be operational and will stop the current. But repetitive operations of pyrobreaker are not desirable nevertheless they are very reliable.

4.4.2 Cryoplant

The ITER machine requires the largest cryogenic system built so far with cold mass of 18000 tons and a total helium plant capacity of 72 kW at 4.5 K. Using cascading technique, 4 numbers of 18 kW at 4.5 K modules will be envisaged to meet the ITER cryogenic requirements. The total refrigeration capacity of the helium refrigeration system is defined as 1.5 times of the total steady state heat loads as already discussed

in Chapter 3. This is a kind of safety factor usually taken for sizing the plant capacity of large-scale cryo systems.

4.4.2.1 Summary of the cryogenic requirements

The break up of the cryogenic demand is summarized in Table 4-5 below [38].

Table 4-5 ITER cryogenic requirements at 4.5 K

Static heat loads	11.9 kW
Average pulsed loss	10.7 kW
Heat load due to cold circulator	11.4 kW
Heat load due to cold compressors	6.5 kW
Cryogenic distribution loss	1.5 kW
Liquefaction to cool all the conventional current leads	130 g/s
Cryo pumps and small cryogenic users	6 kW + 30 g/s
Total heat load	~ 48 kW + 160 g/s

From above mentioned heat loads and cool-down requirements, the cryoplant for the ITER machine is sized for capacity of 72 kW at 4.5 K. In order to meet these requirements, 4 nos. of 18 kW of standard modules will be used.

4.4.2.2 Description of cryogenic system

The basic cryogenic system is structured into many components and sub systems starting from warm gas management systems include high pressure helium gas storage, medium pressure helium gas storage, recovery compressors and warm gas balloons for helium gas recovery during emergency, LN₂ storage and distribution system for pre-cooling of LHe plant [60], main helium screw compressors, purifier unit, cold-box system mainly consists of efficient heat exchangers, turbines or turbo-expanders, and J-T valve and sub-cooler assembly. The ITER cryo plant process discussed in [38] is shown in Figure 4.8.

4.4.2.3 Economics of helium systems

Based on the experience with the CERN helium cryogenic system, a detailed cost analysis for large 18 kW helium systems at 4.5 K has been worked out for an economic exchange index of the year 1998. The actual capital cost of the CERN 18 kW plant has been given by the following relationship [37]:

$$\text{Cost [1998 M€]} = 1.68 \times [\text{Capacity in kW at 4.5K}]^{0.7} \quad (4.1)$$

A best practical fit has also been worked out as following:

$$\text{Cost [1998 M€]} = 1.42 \times [\text{Capacity in kW at 4.5K}]^{0.6} \quad (4.2)$$

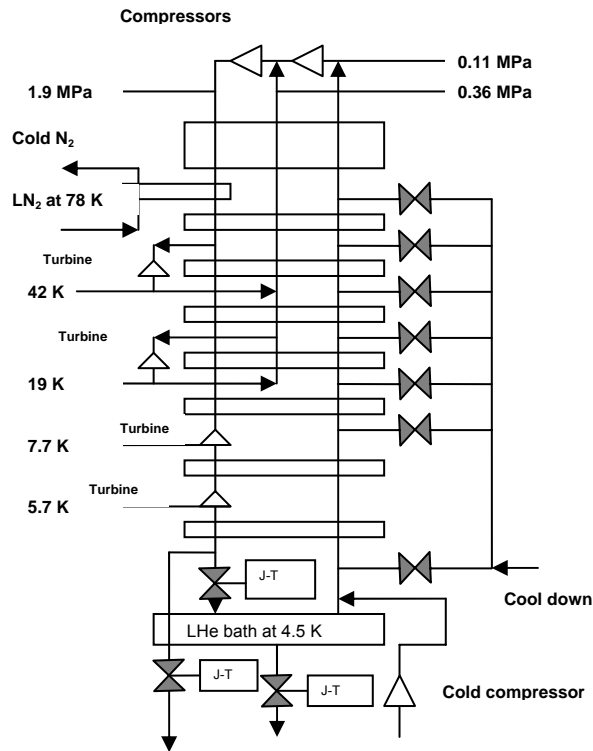


Figure 4.8 Typical helium cryogenic plant process for ITER [38]

From the above equations, the cost estimation for the kW class helium refrigeration systems is shown in Figure 4.9.

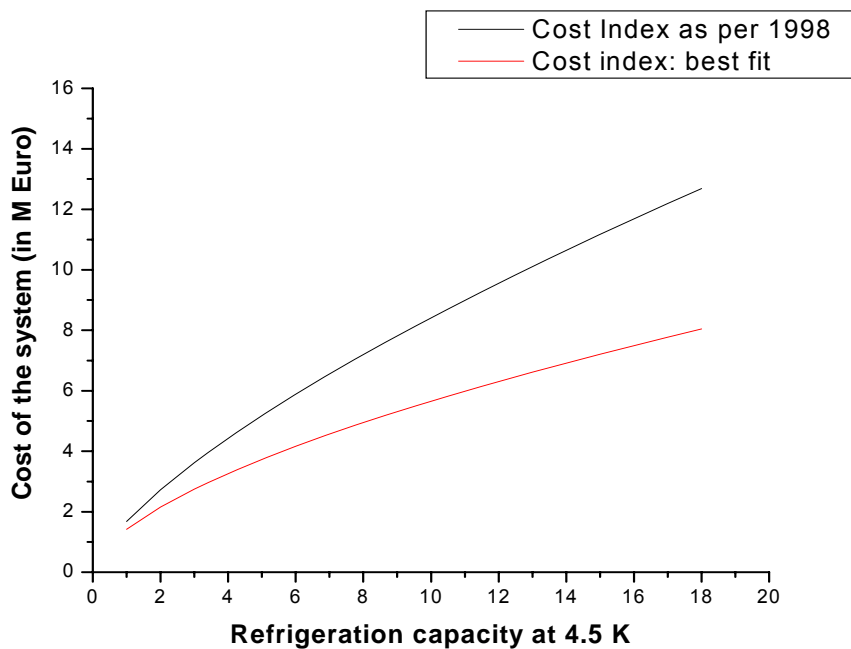


Figure 4.9 Cost estimates for several kW helium refrigeration systems

Chapter 5 - Description of conventional and HTS current leads

In chapter 5, the main focus is given on the current leads. The design consideration of ITER current leads, different possible current leads design options for ITER and their performance study are discussed. A short summary of the EU 70 kA HTS current lead and the test results is carried out.

5.1 Design Considerations of Current Leads for ITER

The following design drivers have to be considered for the ITER current leads [3],

1. The steady state operation for the TF coil current leads have to be designed for a maximum rated current of 68 kA.
2. The PF coil, CS coil and CC current leads have to be designed for pulsed operation with a maximum rated current of 52 kA (back up mode for the PF), 45 kA (CS) and 10 kA (CC) respectively.
3. All current leads should be mounted in horizontal position.
4. All current leads will be cooled by forced flow supercritical helium of an inlet pressure of 4 bar and inlet temperature of ~ 4.5 K.
5. The maximum test voltage of the current lead systems is not yet completely defined but has to be consistent with the requirements for the coils. For the TF coil system, a maximum discharge voltage of 10 kV is required; the test voltage needs to be higher.
6. All current leads have to be Paschen tight.
7. The current leads should be able to support the fast discharge as well as the slow discharge of the magnet system. In case of a loss of coolant flow they have to carry the full current for at least for 540 s without any drawback to the electric system.

The loss of flow accident (LOFA) is the most serious condition for the current leads. In case of ITER current leads, two conditions are adopted for a complete loss of flow in the ITER DDD 1.1 [2] but need to be commented:

- a. The time taken for the temperature of the room temperature end to rise by 100 K is > 300 s (to give time for detection). It is not clear why 300 s will be needed for

detection. A loss of flow can easily be detected by measuring the flow of helium from the heat exchanger.

- b. The heat load at the cold end to the conductor increases by less than a factor of 3 in 600 s. This is a quite big challenge for a forced-flow cooled conventional lead because no liquid helium reservoir is available.

In general, the requirement to carry the full current for a safety time of 540 seconds, i.e., 9 minutes, is very ambitious for a current lead design. For vapour cooled leads the safety time depends on the storage volume of liquid helium whereas for forced flow cooled leads, this depends on the lead design itself. Till today, there exists no current lead cooled by supercritical helium which would fulfil the ITER requirements especially condition (b) is impossible to realize because of the temperature increase along the lead which naturally leads to an increase of the heat load towards the cold end. Recently a loss of helium mass flow experiment was performed for the 80 kA conventional current lead at Forschungszentrum Karlsruhe. The result was that even by making use of the heat capacity of the copper rod surrounding the Nb₃Sn inserts, there was a safety discharge after more than 3 minutes [61].

5.2 Different Current Lead Design Options

In general, different types of current lead designs are possible:

- (i) Bath cooled conventional current lead
- (ii) Vapor cooled conventional current lead (constant and variable cross section of current carrying part)
- (iii) Forced flow cooled conventional current leads (constant and variable cross section of current carrying part)
- (iv) Forced flow cooled binary HTS type current leads (with 50 - 80 K helium as coolant for the heat exchanger)
- (v) Forced flow cooled binary HTS current leads (LN₂ as coolant for the heat exchanger)

The following different types of lead design are compared in both operational modes, i.e., steady state for TF coil current leads and pulsed mode for PF-coils, CS-coils and CC current leads.

- I. Steady state (For ITER TF system)
 1. Horizontal, forced flow supercritical helium cooled conventional leads (Constant cross section)
 2. Horizontal, forced flow supercritical helium cooled HTS current leads (Constant cross section)
- II. Pulsed mode (For ITER PF, CS and CC system)
 1. Horizontal, forced flow supercritical helium cooled conventional leads (heat exchanger made of SF-Copper) (Constant cross section)
 2. Horizontal, forced flow supercritical helium cooled conventional leads (heat exchanger made of SF-Cooper, variable cross section)
 3. Horizontal, forced flow helium cooled HTS current leads (HTS material: Bi2223, heat exchanger made of OFHC, constant cross section)

5.3 Discussions on Current Leads Design Options for ITER

5.3.1 Bath/Vapor cooled Conventional Current Leads

Bath/vapor cooled conventional current leads cannot be used in ITER because of following reasons:

- (i) ITER current leads have to be horizontally installed in the coil-terminal box. As it has space constrains, only a small volume of current lead is allowed.
- (ii) As the ITER magnets are cooled by forced flow supercritical helium and in order to make the cooling scheme as simple as for the magnets, the current leads should also be cooled with forced flow supercritical helium.
- (iii) The forced flow supercritical helium cooling of the current lead is more stable because no pressure and liquid level oscillations are present.
- (iv) The heat leak at the cold end of the forced flow cooled current lead is 70-75% lower than that of bath/vapor cooled leads at a mass flow rate of 0.058 g/s-kA per lead. This is because the specific heat of vapor is lower than that of supercritical helium especially at lower temperature and excellent heat exchange between the metal and helium cold gas [62].

5.3.2 Forced flow cooled constant cross section and variable cross-section current leads

Several years of R & D experience on current leads at the Forschungszentrum Karlsruhe as well as at JAERI have shown that in order to provide a good current lead performance, especially for higher currents, an efficient and optimized design of the heat exchanger part is required. For steady state operation, it can be made with a constant cross-section along the length of the current carrying conductor part [62 - 64]. For pulsed current mode, the variable cross section type is still an option for current leads. On the other hand, different kind of current lead designs for one machine will enhance the overall investment costs (requires new fabrication tools and complex manufacturing techniques). So, it is desirable to use constant cross section type current leads even in pulsed operation mode and moreover, the operational costs of the pulsed leads with a variable cross-section is higher during the operation time compared to the fixed cross section leads.

5.3.3 Overloaded conventional current leads

If the stand by operation time is drastically longer than the current operation time, so-called overloaded current leads may be an option. Those current leads consist of a low RRR brass alloy and are optimized for zero or low current. During maximum current operation, the leads will not be able to work in a thermally stabilized condition but the overload factor for brass is much larger than e.g. for copper [65]. Although it is not desirable to use such over-loaded leads for steady state operation with large currents, they may be useful for pulsed operation for a shorter time. The current overload factor (OF) depends on the duty cycle of the particular machine and the maximum acceptable temperature [65].

It was so far only used in a low current (~460 A) pulsed 6 T wiggler magnet device under vapor cooled configuration but no experimental results exist so far for large current applications. Recently, the KSTAR tokamak project has also proposed to use overloaded current leads at 20-30 kA for their poloidal field coils with a overloading factor of ~ 2.5 [66]. For the pre-qualification test of these current leads, a test was conducted for a lower current up to 400 A in pulsed modes [54] but no real experiment so far exists with high current pulsed overloaded leads cooled by forced flow helium.

5.3.4 High Temperature Superconductor current leads

A very attractive alternative option is to use so-called binary HTS current leads. Although the investment costs are considerably higher than for conventional current leads, the operational costs will be reduced drastically leading to an amortization after a few years.

HTS current leads may or may not need active cooling of the HTS part (which covers the temperature range between 4.5 K and an intermediate temperature, T_{int}) because it may be cooled by heat conduction from the low temperature sc feeder. The conventional heat exchanger which covers the temperature range from T_{int} up to room temperature needs to be actively cooled either by helium gas at a temperature range of 50 – 80 K or by sub-cooled LN_2 . The qualitative description of advantages of using HTS materials in current feeder systems is discussed here.

The fundamentals of cryogenic benefits can be understood from the following Figure 5.1. The cold enthalpy of the cryogenic fluid is used to balance the Joule heating and the loss due to thermal conduction within the lead. As there is significant variation of thermal and electrical properties of the material within the temperature range of 4.5 K – 77 K, the HTS based binary leads would be the better solution for ITER because it allows operation with low thermal conductivity and smaller cross section area in comparison to a conventional copper lead in the temperature range from 4 K to 77 K [29]. The upper part can be fabricated as an optimized heat exchanger made of copper working in the temperature range of 77 K – 300 K. The result is a reduction of the heat load and consequently of the electric power of the cooling system and therefore the operational costs. Experiences show that using HTS current leads, the power consumption could be reduced by a factor of 3 – 5 depending upon the cooling modes [9][29].

Two HTS current lead projects were carried out within the fusion programs by different laboratories in conjunction with industry:

- a 60 kA HTS current lead with the heat exchanger cooled by 20 K helium (JAERI [43])
- a 70 kA HTS current lead with the heat exchanger cooled by 50 K / 80 K helium and even with LN_2 (FZK/CRPP, [67 – 70]),

Although the JAERI project was rather comprehensive, the EU project covered a very extensive testing including tests at different operating temperature, steady state as well as pulsed operation, evaluation of the current sharing temperature and loss of helium mass flow simulation studies.

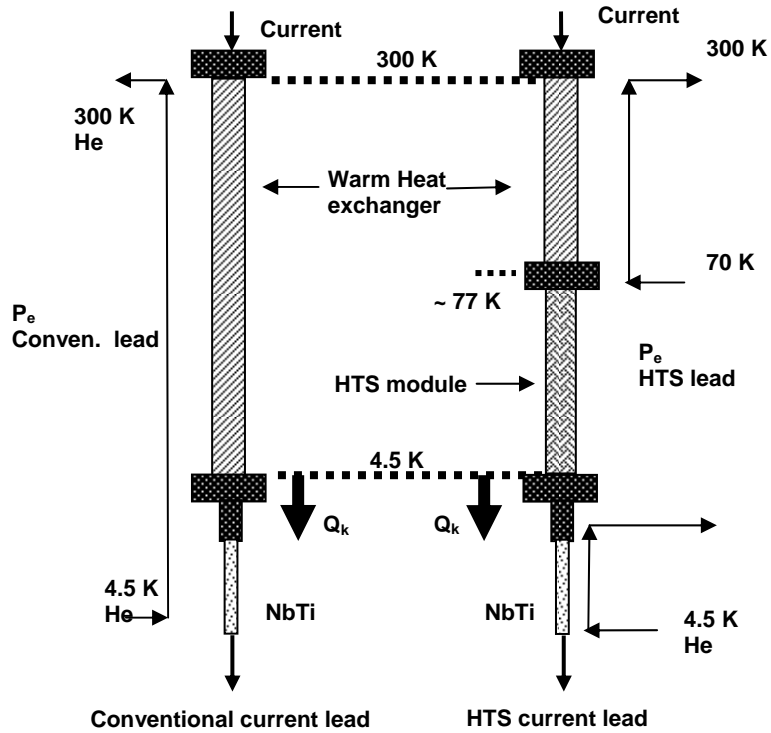


Figure 5.1 Working principles of conventional and HTS current leads

Figure 5.2 shows the photograph of the 70 kA HTS current lead as demonstrator for ITER.

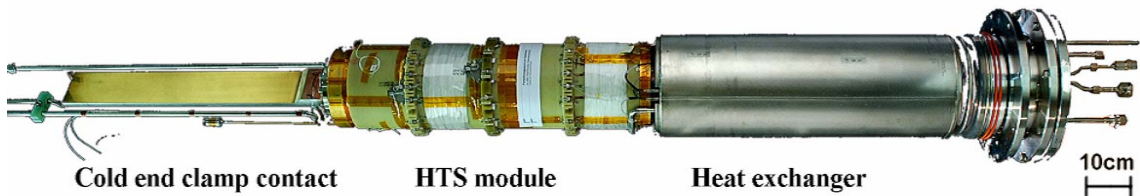


Figure 5.2 Photograph of the 70 kA HTS current lead developed at FZK within the EU fusion program as demonstrator for ITER

The EU 70 kA HTS current lead was successfully tested even with LN₂ [69,70]. Some of the main results will be summarized in section 5.5.

So, from the above discussion it is desirable to use either conventional leads or HTS based binary current leads for ITER. The choice for the particular option for ITER current leads will depend upon the techno-economical study.

5.3.5 Worldwide survey of current leads used in Fusion devices and test facilities

In Table 5-1, various current lead designs for plasma experiments and Fusion test facilities are collected and compared.

Table 5-1 Current lead design survey summary

	Type of Leads	Maximum current	Cooling
Tokamak			
KSTAR	Vapor cooled Brass alloys leads	35 kA for TF 20-30 kA for PF	Vapor cooled
TPX (only concept)	Forced flow cooled conventional leads	~45 kA for TF 0-31 KA for PF	Forced flow cooled
SST-1	Vapor cooled Copper alloys leads	10 kA for TF and PF	Vapor cooled
EAST	HTS Binary leads	20 kA	Binary lead cooling concept
Stellarator			
LHD	Vapor cooled copper alloys leads	20-30 kA	Vapor cooled
W-7X	Forced flow cooled conventional leads or as an option HTS current leads	~18 kA	Forced flow cooled
Test facility for Fusion development			
TOSKA	- Vapor cooled - Conventional forced flow type - HTS binary type	0 – 80 kA (conv.) 10 - 70 kA (HTS)	forced flow
JAERI	Forced flow cooled conventional leads	~15 kA - 50 kA (conv. forced flow) - 60 kA (HTS)	Vapor cooled

5.4 Present ITER design of the current leads

The following description has been taken from the ITER-DDD 1.1 [3]. Each CTB contains one pair of copper current leads; those for the CC contain 2 pairs. The helium cooled current leads provide electrical connection between the room temperature bus bars from the power supply and the superconducting bus bars at 4.5 K inside the CTB.

The base cryoplant load and space requirements for the current leads have been calculated assuming cooling with forced flow supercritical helium at 4.5 K inlet temperature, and without the use of either low temperature or high temperature superconducting inserts along the thermal gradient part of the lead. The number and capacity of the current leads are shown in Table 5-2, and a conceptual design of the conventional forced-flow current lead is shown in Figure 5.3.

Table 5-2 Current leads requirement for ITER

Coil type	No. of Coils	No. of current lead pairs	Max. current	Operation
TF	18	9	68 kA	Steady state
PF	6	6	52 kA	Pulsed
CS	6	6	45 kA	Pulsed
CC	6/6/6	9	10 kA	Pulsed

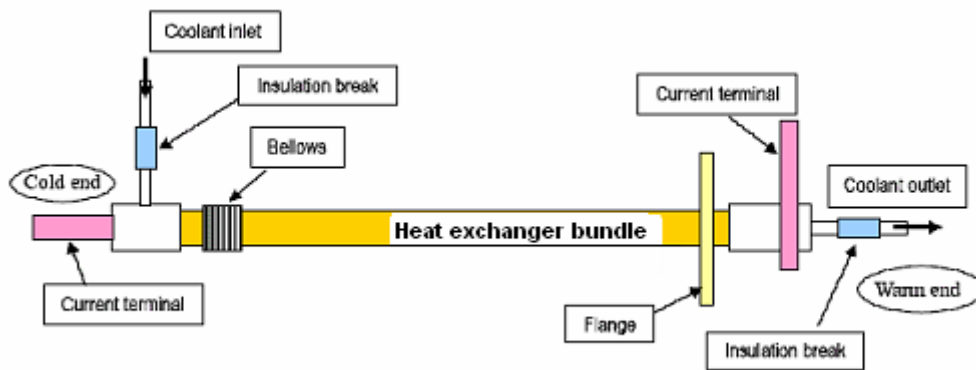


Figure 5.3 Schematic diagram of the forced flow conventional current lead design [3]

The most critical component driving the design is the heat exchanger bundle. This may be a cable matrix (as tested by JAERI [62]), or a series of disks (as tested by the Forschungszentrum Karlsruhe within the TFMC project [63]). At the cold end, between the heat transfer bundle and the current terminal, there is a length of superconducting cable (cooled by the He flow) that insulates the cold current terminal from heat conducted from the current lead. For a particular concept, the dimensions of the lead and the helium consumption are determined by the operating current and the length and cross-section of the copper in the heat transfer bundle. There are two sorts of layouts that have been analyzed here:

- i) The bundle is considered to consist of 2 mm diameter copper strands, RRR=100, constant cross-section, with a void fraction of 20%
- ii) The bundle has a variable cross-section and (for the purpose of the analysis) the strands have a variable diameter (the manufacturability of this concept is uncertain and a tapered bar with fins may be required). The variation in the cross-section must be substantial in order to be effective (the cold end has approximately one third the area of the hot end).

In each case, the helium inlet pressure is 4 bar and there is vacuum thermal insulation around the bundle.

The current scenarios for the CS, PF and CC are pulsed, and in some plasma scenarios the coils are operating well below their maximum design values for most of the time (i.e. during the dwell and burn phases). A current lead designed to work efficiently at maximum current will generally not work at optimum performance at lower currents (generally, the extra copper needed to reduce the resistive heating at high current produces extra heat conduction from the warm end at lower currents). At present this has not been included in the design considerations but could be a factor in later optimization. The current leads are sized for optimum performance when carrying the coil maximum design current. The helium flow to the leads is not adjusted to follow the operating current through a pulse scenario (although it could be reduced for the PF, CC and CS for periods when there is no plasma operation). It could be set too low for the peak operating current, so that the lead operates in a transient condition, with a slow (time scale many hundreds of seconds) when the current exceeds the design current, and a slow recovery when it is less.

Performance test experiments on forced flow cooled conventional current leads for fusion application by FZK have shown good performance [62].

Similar experiences exist from JAERI [63] for conventional constant cross section copper (RRR 100) forced flow current leads.

From the above discussions, the following parameters are set as a reasonable design basis for the current lead design (in addition to the loss of flow requirements) [63]:

- Cold end heat load <math><0.1\text{W/kA}</math> (current defined by I_{max})
- Maximum length of heat exchanger (TF, CS and PF): 2.0 m
- Maximum length of heat exchanger (CC): 1.2 m
- Minimum copper current density at the hot end 11 A/mm²
 - Specific mass flow under operating condition 0.06 g/s/kA
 - Specific mass flow under stand-by conditions 0.04 g/s/kA
- For variable cross section and particularly applied for pulsed leads,
 - Specific mass flow under operating condition 0.1 g/s/kA
 - Specific mass flow under stand-by conditions 0.01 g/s/kA

The results of the analysis mentioned in [2] clearly show that the helium budget for the operation is quite higher in case of variable cross section leads compared to constant

cross-section ones. In addition, the manufacturing procedure for variable cross section is more difficult especially for higher currents. So, it is desirable to design all current leads for ITER with constant cross section only.

The performance of the FZK-type forced flow conventional current leads was found to be better than the JAERI leads because of using the benefits of long Nb₃Sn insert at the bottom region of the leads which has to be paid by the complicated HX design [64].

5.5 Review of a 70 kA HTS Current Lead as Demonstrator for ITER

The Forschungszentrum Karlsruhe (FZK) and CRPP were responsible for a development program to construct and test a 70 kA HTS current lead which is more or less a demonstrator for the ITER current leads using Ag/Au stabilized Bi-2223 HTS tapes. The HTS current lead was designed to meet the ITER requirements and should be able to withstand minimum 3 minutes during the loss of flow accident condition in a horizontal installation.

5.5.1 70 kA HTS current lead design

The HTS current lead consists of three parts as shown in Figure 5.2. A copper heat exchanger (HEX) covers the temperature from RT to 65 K which is the design value at 68 kA when the HEX is cooled with 50 K helium from the low temperature side. At the cold side of the HEX the HTS module is attached. The other end of the HTS module is connected to a special designed Cu transfer piece with Nb₃Sn inserts. This cold end is clamped to a bus bar that is used for current transfer. The bus bar is actively cooled by 4.5 K helium providing a cooling to the HTS CL from the low temperature side via heat conduction. As a consequence of this design the HTS module between HEX and cold end is only conduction cooled with 4.5 K at the cold end and 65 K at the warm end of the HEX. The HTS module was built by American Superconductor (AMSC) using Bi-2223/AgAu tapes.

The HTS current lead was installed in the B300 vacuum vessel of the TOSKA facility that has been used for the TFMC test [63]. In that test two conventional 80 kA current leads have been used to connect the TFMC. One of these vertical current leads was now replaced by the much smaller horizontal HTS CL. Both current leads were directly connected by a NbTi bus bar (BBIII). Figure 5.4 shows the B300 with the two current leads and BBIII. Figure 5.5 shows the installation of the HTS CL in the B300 in more detail.

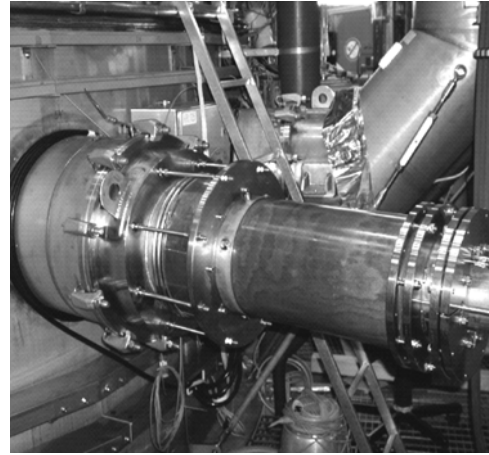
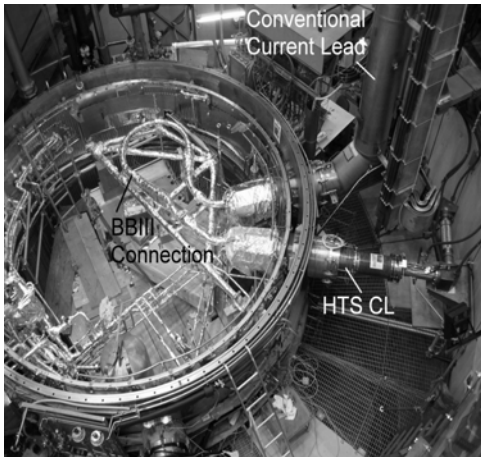


Figure 5.4 HTS CL installation in the TOSKA Figure 5.5 Horizontal installation of HTS CL

5.5.2. Summary of Test results

The 70 kA HTS current lead was successfully tested in very robust experimental conditions with different cooling modes like e.g. 50 K helium, 80 K helium and even with LN₂ at atmospheric and sub-atmospheric conditions. The whole test experiments were divided into 4 phases [67-70].

- **Experiments with helium cooling**

The first phase of the experiment took place from April to June 2004 focused on the operation of the current lead at standard conditions with $T_{\text{He, in}}=50$ K He at the inlet of the HEX. As visible in Figure 5.6 such an operation could be performed without problems and was even extended to 80 kA. The temperature of the HTS module warm end was approx. 65 K during these experiments. Also in the first phase, a bad performance of the screw contact was found due to the higher contact resistance ($\sim 60 - 70$ nOhm at 65 K) at the intermediate region between the HTS module and Cu-HEX which in turn gave a significant higher heat loads and mass flow requirements in the Cu-HEX to maintain the top end of the HTS module at ~ 65 K. Despite of this problem, the performance of the lead during operation was excellent.

After these results the current lead was retested in a second phase during December 2004 with modification of the screw contact by the silver soldered filled joint (with contact resistance ~ 10 nOhm). Using the better performance of this contact, the HTS current lead was tested with an inlet temperature $T_{\text{He, in}}=80$ K, neglecting that the CL was optimized for 50 K. With a temperature of 85 K at the warm end of the HTS module the current lead was really at the edge but a stable operation at 68 kA was possible as

can be seen in Figure 5.7 The temperature variation along the current lead was as calculated during the design.

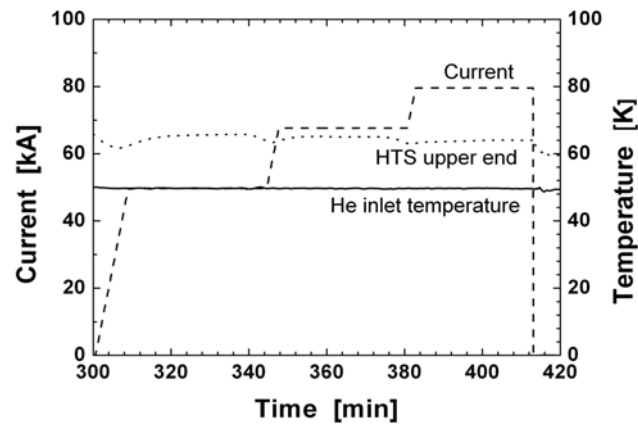


Figure 5.6 HTS CL operation with $T_{\text{He,in}}=50$ K. The temperature of the HTS module upper end was at approx. 65K [68]

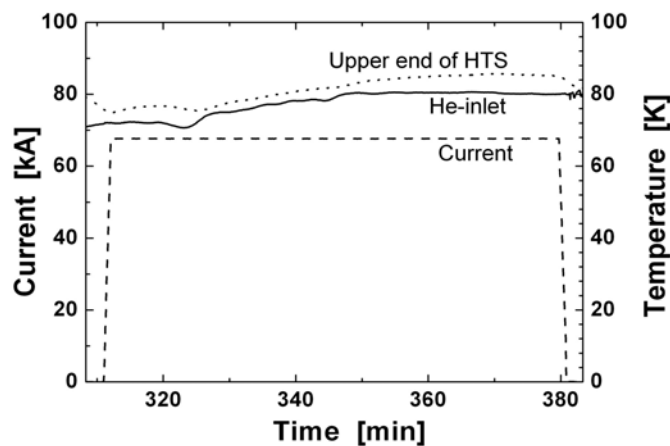


Figure 5.7 HTS CL operation at 68 kA with $T_{\text{He,in}}=80$ K. The temperature of the HTS module upper end was at approx. 85 K [68].

If operating the current lead with 80 K helium and a temperature difference of only 5 K between the upper end of the HTS module and the He inlet temperature, the Joule heating of the un-cooled resistive region between the HTS module and the heat exchanger is very critical. Both the soldered conical contact and the copper part of the lower heat exchanger end have an electrical resistance of about 25 nΩ at 85 K leading to 115 W which have to be removed by the helium mass flow [69].

The test was done as follows: the current was ramped to 68 kA with 1 kA/s at a He inlet temperature of 70 K. Next the He inlet temperature was stepwise increased to 80±0.5 K.

Both the helium mass flow rate and the inlet pressure were also increased step by step in parallel to the temperature increase. At 80 K and 68 kA the current lead could be operated successfully for more than 25 min until the current was ramped down with 1 kA/s.

- **Experiments with LN₂ cooling**

Due to the very successful results from the previous test campaigns of the 70 kA HTS current lead, the next proposal was to test this current lead also with LN₂ cooling at atmospheric and sub-atmospheric pressure. Such an operation with LN₂ cooling would be also very interesting for ITER because LN₂ is available at the ITER site in any case. The distribution is much simpler and the available time for discharging the coils after a LOFA is not critical because it depends only on the dimensions of the LN₂ reservoir in the HEX. The reliability of vacuum pump is essential in case of sub-cooled LN₂ operation. A large amount of cooling power can be saved if HTS current leads are cooled with LN₂. Typical HTS CL operation at 68 kA with atmospheric LN₂ is shown in Figure 5.8.

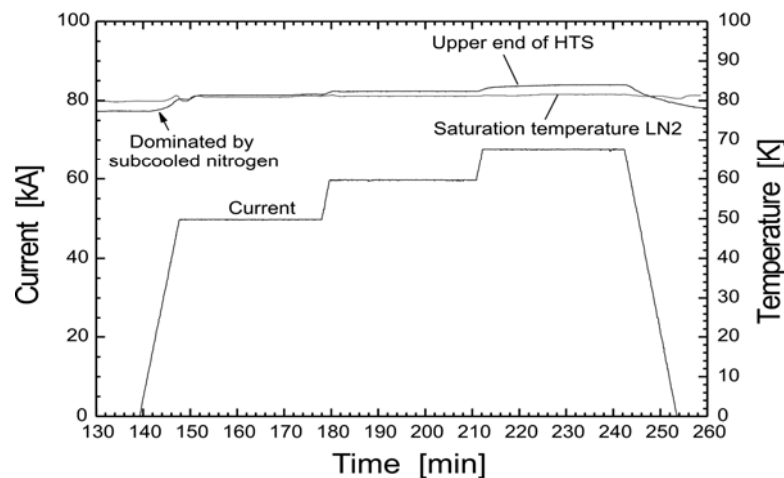


Figure 5.8 HTS CL operations at 68 kA with atmospheric LN₂ cooling [68]

The 70 kA HTS current lead performance in LOFA event is compared for 50 K helium 80 K helium, and LN₂ cooling as shown in Figure 5.9.

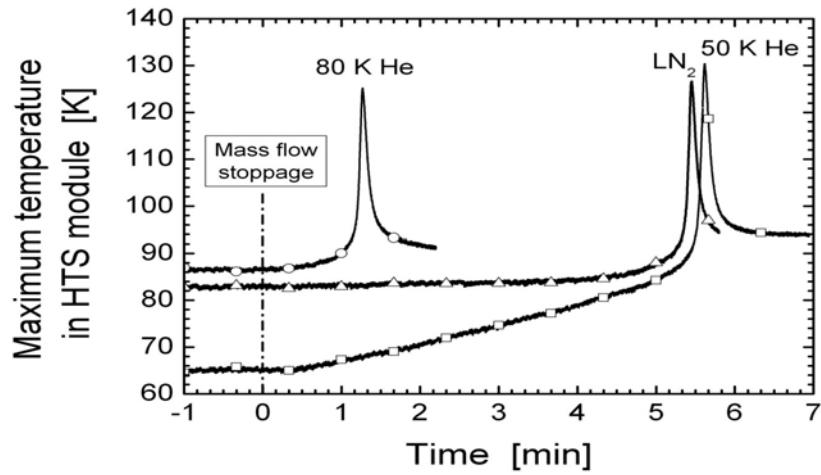


Figure 5.9 LOFA tests of 70 kA HTS CL with helium and LN₂ cooling [69, 70]

Finally, Table 5-3 summarizes the test results of a 70 kA HTS CL with helium and LN₂.

Table 5-3 Summary of the test results of a 70 kA HTS CL

Operation		I_{coil}	\dot{m}	T_{Inlet}	p_{Inlet}	$T_{\text{Warm end}}$	T_{Outlet}	\dot{Q}	t
Unit		kA	HEX g/s	HEX K	HEX bar	HTS K	HEX K	at 4.5 K W	LOFA min.
He Cooling	Standby	-	0.9	50	5.4	102	277	23	-
		-	1.9	50	5.4	67	264	14	-
		-	1.0	4.5	5.0	75	271	16	-
	Rated	68	4.7	50	5.4	65	260	14	5.5
		68	2.7	4.5	5.0	66	312	14	-
	68	16	80	7.6	85	175	20	-	-
	Extended	80	5.8	50	3.0	65	260	15	1.5
LN ₂ cooling	Standby _{at}	-	5	77	1.2	77	265	17	-
	Standby _{sub}	-	3.5	77	0.35	70	285	15	-
	Rated _{at}	68	11	77	1.6	83	265	20	5.5
	Rated _{sub}	68	13	77	1.1	80	288	19	-
	Extended _{sub}	75	13	77	1.2	82	288	19	-
Con , CL _D	Standby	-	1.0	4.5	-	-	-	6.8	-
	Rated	68	4.1	4.5	-	-	-	13.2	-

Chapter 6 - Design and analysis of a LTS current feeder system for ITER

In this chapter, the conceptual design and critical parameter analysis of a LTS feeder for ITER have been carried out. The detailed TF sc feeder model has been worked out considering the electromagnetic and thermo-hydraulic aspects. Forced-flow supercritical helium is used for cooling the sc feeders. In particular, the thermo-hydraulic performance of the sc feeder for two possible cooling scenarios is compared in a one-dimensional (1-D) single channel steady state approach. Afterwards, the model is extended to a real dual-channel model and one dimensional (1-D) transient thermo-hydraulic problem taking into account the transient heat transfer and quench propagation. The helium mass flow rate has been optimized under the ITER machine duty cycle condition to provide a safe and reliable operation of the feeder. Finally, the operation of the PF and CS sc feeders are discussed with respect to the TF feeders. The quench detection and instrumentation of the LTS feeder system are summarized.

6.1 Conceptual design of a LTS current feeder system for ITER

6.1.1 Design drivers

The sc current feeder system for ITER has to fulfill the following design requirements [3] [55]:

- (i) Higher stability margin compared to the coils because the large amount of stored magnet energy must be dissipated through the current feeder path.
- (ii) Higher copper amount in the conductor than in the coils as a stabilizer in order to control the temperature rise during the quench.
- (iii) The LTS feeder system should be designed with double insulation scheme in order to provide the Paschen tight condition.
- (iv) The conduit thickness should be designed to withstand the pressure rise during the quench.
- (v) The proper flexibility in the design should be provided in order to prevent thermal stress problems. A sharp bending within the feeder's route must be avoided to prevent arc problems.
- (vi) As the typical length of each sc feeder is small compared to the conductor length in a coil, i.e., about ~ 25 m, it is more economic to use the same conductor for all the TF, PF and CS feeders which means that they should be designed for the maximum current of 68 kA.

6.1.2 Technical requirements and specifications of LTS current feeders

The LTS feeder requirements for ITER are summarized in Tables 6-1 and 6-2 respectively; Figure 6.1 shows the cross-sectional view of a dual-channel cable in conduit conductor as it can be used for the sc feeder of ITER [3].

Table 6-1 Current leads and sc feeders' requirements

Coil type	No. of feeder pairs	Max. current	Operation	Inlet. Temp.
TF	9	68 kA	Steady state	4.5 K
PF	6	45 (52) kA	Pulsed	4.5 K
CS	6	45 kA	Pulsed	4.5 K

Table 6-2 Technical specifications of LTS feeders for ITER

Parameters	TF, PF and CS feeders	CC feeders
Type of strand	NbTi	NbTi
Operating current (kA)	68	10
Nominal peak field (T)	4	4
Operating temperature (K) (maximum)	5.0	5.0
Equivalent discharge time constant (s)	26	26
Cable diameter (mm)	41	16.2
Central spiral outer / inner diameter (mm)	8x6	0
Conductor outer diameter (mm)	47	20.2
Jacket material	SS316LN	SS316LN
Strand diameter (mm)	0.73	0.73
Cu to Non-Cu ratio in strand	6.9	6.9
Cabling pattern	3x4x5x5x6	3x4x5x5
Number of SC strands	1800	300
Local void fraction (%) in strand bundle	~34.0	~34.0
SC strand weight per conductor length (kg/m)	6.1	1.0

Internally cooled, cabled superconductors are made of transposed multi-stage twisted cables. The multifilamentary nature of the strands and the twist reduces coupling and eddy current losses. By increasing the surface area of the helium, the heat removal is increased. The twist is also important to make the cable mechanically stiff as well as to reduce the movement of strands / wires and cable itself because this movement within the cable space is prone to generate the heat and thus a quench. The ITER cable has as a base unit strand triplets and as the final stage a sextuplet twisted around a perforated central spiral channel [71]. In the present design of the ITER feeder, 1800 strands with a Cu: non-Cu ratio of 6.9 are used, which is an expensive layout. It would

be cheaper to use a sc strand with lower Cu: non-Cu ratio and add pure copper strands as it is done for the coils.

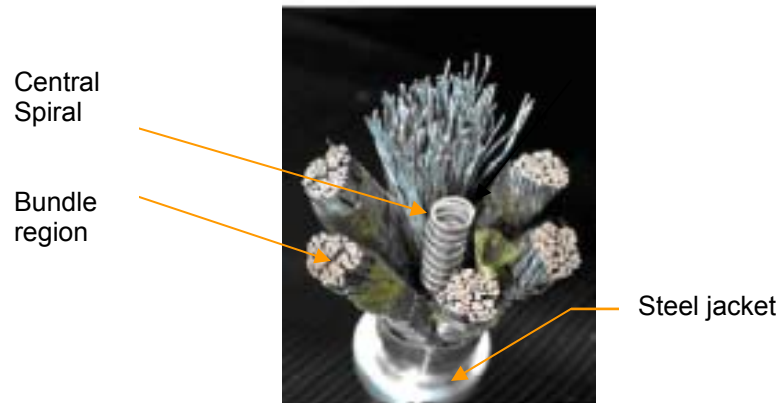


Figure 6.1 Cross-sectional view of dual channel CICC for the ITER LTS feeder

6.1.3 Design concept of a LTS feeder

The detailed conceptual design of the TF sc feeder systems has been worked out as part of a case study. In order to study the performance of the feeder, an optimized conceptual design scheme is needed, which is based on ITER technical requirements mentioned before. The proposed layout of the LTS feeder is shown in Figure 6.2.

There, a (+/-) pair of sc feeders is assembled inside a radiation shield (cooled at 80 K) and an outer vacuum jacket (at room temperature) with double insulation scheme. The support structure is made of a low thermal conductivity GFRP material (G-10 CR/ G-11 CR) [72]. The vacuum level of 10^{-5} to 10^{-6} mbar will be maintained in each sc feeder duct in order to minimize the residual gas conduction loss [30]. The support structure has to be designed with a simply supported cantilever beam case. The span length and numbers of GFRP supports should be optimized in order to obtain a maximum allowable deflection of $\sim 2-3$ mm. A similar type of the bus-duct concept was adopted for TPX [53] and SST-1 tokamaks [55].

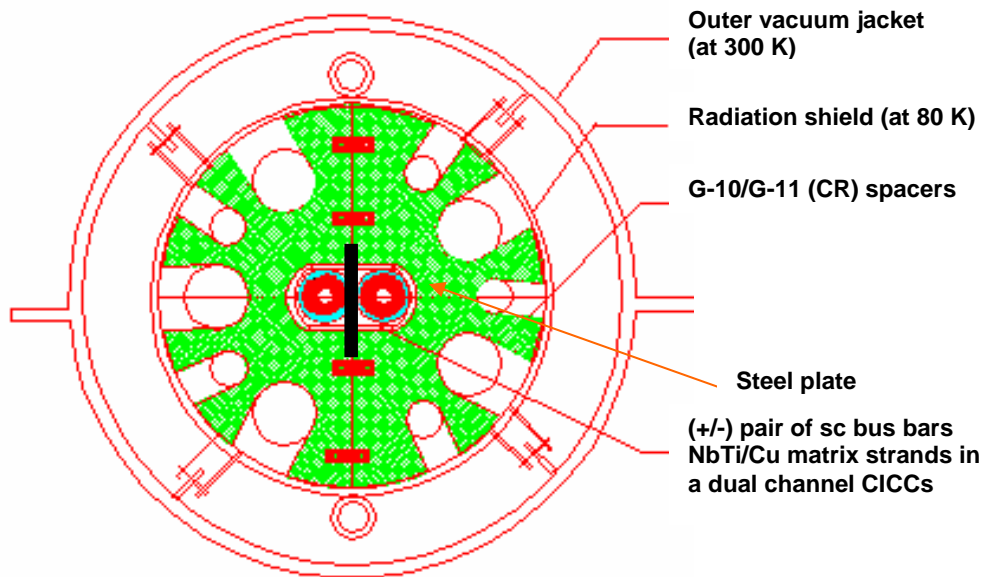


Figure 6.2 Cross-sectional view of a LTS feeder for ITER

- **Double insulation scheme**

Each bus bar has a double electrical insulation system that will allow the detection of a developing bus bar-to-ground short circuit and to stop the current before the short occurs, providing protection against further damage. The scheme consists of a double layer of insulation with a metallic shield as shown in Figure 6.3.

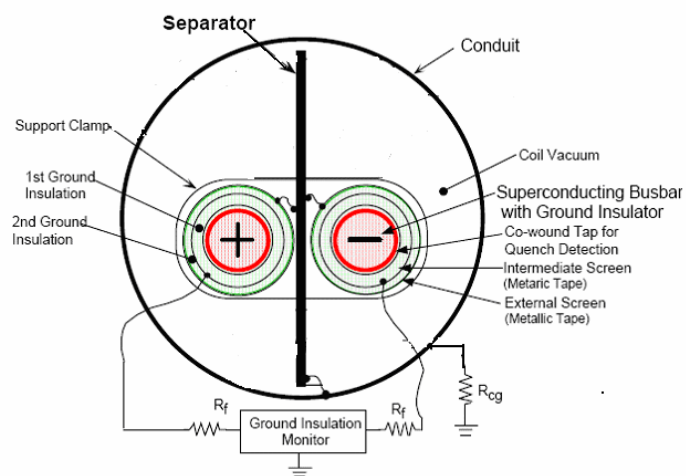


Figure 6.3 Double insulation scheme and ground insulator monitor for a (+/-) pair of sc bus bars

The insulation will be several half-layered layers of glass/polyimide, followed by one or two layers of metallic tape with glass in between (to prevent eddy currents), and finally several layers of half-layered glass/polyimide to complete the turn insulation. An over-wrap of steel tape will be applied for mechanical protection. This screen serves as extra protection against a short circuit between the coil terminals in addition to the steel separator plate. Here, the cooling pipes and instrumentation cables are not shown.

- **Cooling scheme**

It has been envisaged that a forced flow supercritical helium system will be used for all sc feeders operating at an inlet pressure of 6 bar and inlet temperature of 4.5 K [3]. There are two cooling scenarios possible as mentioned below,

1. Cooling of the sc feeders from the CTB side i.e. the helium inlet will be at the current lead side and the outlet at the coil side (ITER design option).
2. Cooling of the sc feeders from the coil side i.e. the helium inlet will be at the coil side and the outlet at the CTB side.

Detailed parametric studies have been carried out in order to evaluate the available margin for both cooling scenarios using a steady state single annular channel approach and to select the optimum one.

6.2 Boundary conditions for the analysis of the LTS current feeder

The modeling of the TF feeder has been carried out as per ITER sub systems layout plan including the steady state heat loads, the layout of the TF feeder, calculation of the magnetic field of the TF feeder in presence of the magnets system and crucial plasma case so-called End-of-Burn (EOB) [2]. Also the material data base needed for the steady state as well as transient analysis is obtained as a part of input boundary conditions.

6.2.1 Modeling of the TF feeder for ITER

6.2.1.1 Heat load calculations

The detailed steady state heat loads including radiation, residual gas conduction and thermal conduction are estimated for the TF sc feeder system. The heat loads due to the vacuum barrier at the Cryostat feed through (CF) and the Coil-Terminal Box (CTB) interface, the resistive joints at the magnet side, near the S-Bend and at the current lead side are also be included in order to estimate the total steady state heat flux acting on the whole sc feeder. The radiation loss has been estimated using the emissivity values

of ~ 0.12 at 4.5 K and 0.21 at 80 K for a steel surface. The use of superinsulation is considered as additional margin for the uncertainty in the estimation, while estimation of residual gas conduction losses for the base pressure of 10^{-5} mbar is considered. The standard thermal conductivity integral value of steel (from 80 K to 4.5 K) is used to estimate the conduction loss due to the vacuum barrier. A joint resistance of 1.5 nOhm is possible to be achieved near the magnet terminal side and 3 nOhm at the lead side because of a clamp contact. The steady state heat loads and the heat flux acting on the TF feeder are summarized in Table 6-3.

Table 6-3 Steady state heat loads and heat flux for the TF feeder

Source	Heat load at 4.5 K (in W)	Heat flux at 4.5 K (in W/m)
Joint loss at the magnet terminal (R = 1.5 nOhm)	7.0	14
Loss due to radiation, residual gas conduction and thermal conduction due to spacers	7.0	0.29
Loss due to the intermediate joint near the S-bend (R = 1.5 nOhm)	7.0	14
Conduction loss due to the vacuum barrier at the end of cryostat feed through	4.2	14
Joint loss towards current lead side (R = 3 nOhm)	13.8	43
Total losses	39	

6.2.1.2 Electromagnetic field calculations

The modeling of the TF feeder is carried out with the self field of the feeder and the stray field of the ITER magnets and the plasma using the EFFI code [73]. The EFFI code calculates the electromagnetic fields, forces and inductances for ironless magnet systems of arbitrary geometry. Any kind of complex geometry can be possible to model with EFFI by means of arcs and bar segments. In order to model different geometries in one file, input generators are desirable. For example, TOKEF is such generator for coils belonging to Tokamaks (TF and PF systems). The EFFI input consists of a title card, a unit data set, a geometry data set and an output data set.

In EFFI all current carrying parts of the ITER magnets (TF, PF and CS magnets) and the TF feeder has been modeled by means of arcs and bars. In case of each TF winding pack, an average current density for a given winding pack cross-section has been used.

An average has been considered for three current carrying regions as shown in Figure 6.4.

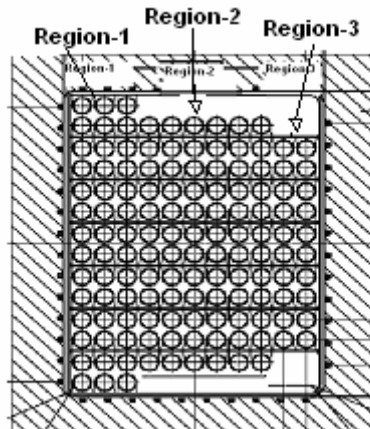


Figure 6.4 Cross-sectional view of the TF winding pack

Number of the TF coils: 18, Total current of one TF coils: 9.112 MA

Each turn carries current: 68 kA, Total no. of turns in each coil:

Region 1: 3 x 14 turns, Current in Region 1: 2.856 MA

Region 2: 6 x 12 turns, Current in Region 2: 4.896 MA

Region 3: 2 x 10 turns, Current in Region 3: 1.36 MA

Also the plasma was modeled as a spherical element of rectangular cross section. The geometrical parameters were taken from the ITER DDD report [2].

The various ITER current operating scenarios were studied to find out the most severe scenario where the magnetic stray field is the highest. At the end, the End of Burn (EOB) case was assigned to be the most crucial one and has been considered in the following analysis. The magnetic field distribution is shown in Figure 6.5.

As the TF feeder is operating at a maximum current of 68 kA, the field calculation is carried out for that case. Calculations show that the maximum magnetic field acting on the TF sc feeder system in presence of the ITER SCMS and the EOB case is ~ 1.6 Tesla.

Figure 6.6 shows the comparison of the maximum field in presence and absence of the ITER stray field. A little pick in the self field profile near the magnet terminal is consequence of an L - bend of the feeder (bending radius of 0.7 m) and afterwards the self field remains more or less constant with respect to length of the feeder even though it has the S-bend. This is because of smooth bending with a bending radius of 1.3 m

which means as we are going far from the magnets and the plasma, only self field effect dominates.

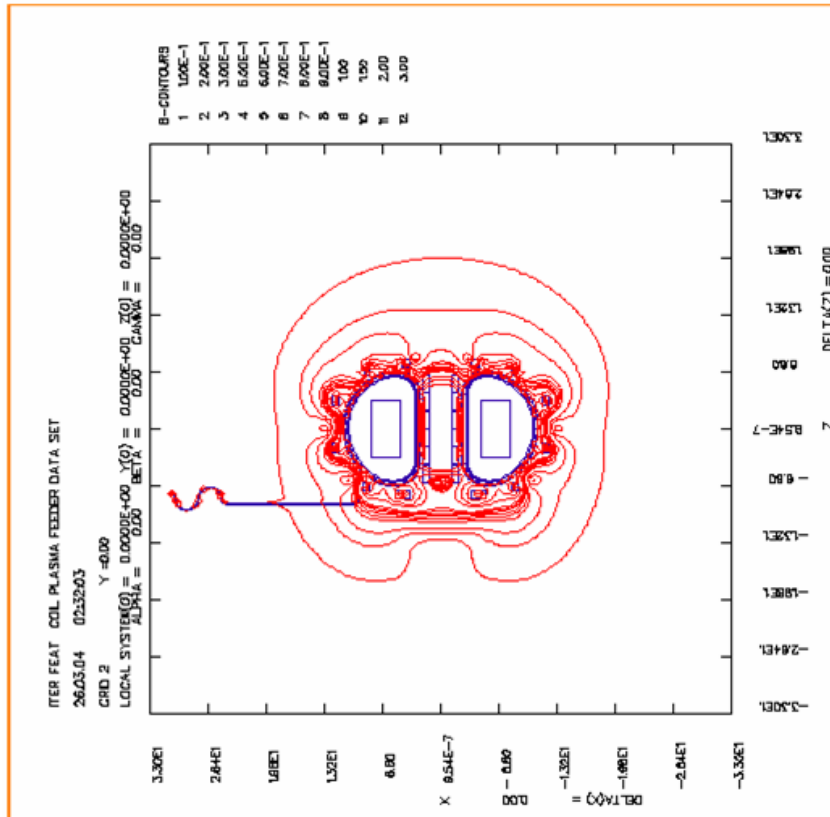


Figure 6.5 Contour lines of the magnetic field of one of the TF feeders together with the ITER magnets and the EOB plasma

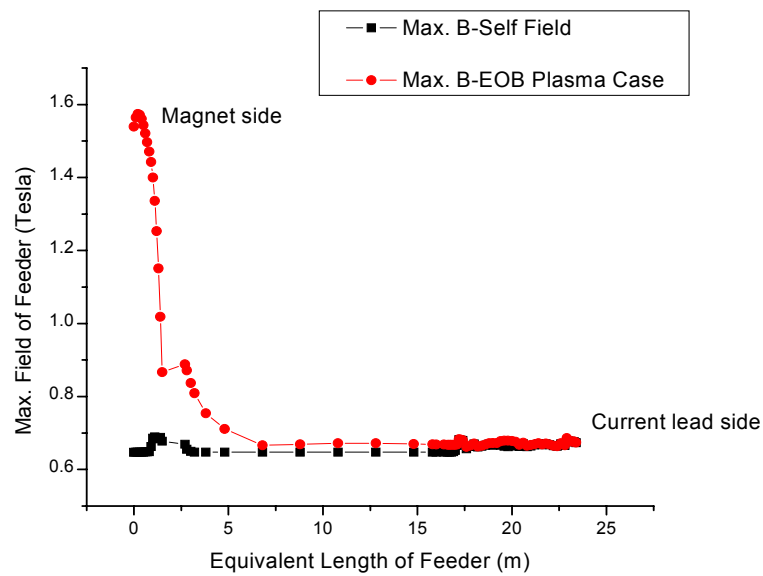


Figure 6.6 Comparison of the magnetic field profile along the TF feeder

Furthermore, a study was carried out in order to investigate the field effect of the neighboring conductor. Considering a (+/-) pair of conductors at 165 mm distance, only 3-5% field change was found compared to a single feeder as shown in Figure 6.7. That is why for the modeling of the TF feeder; only a single feeder approach is used.

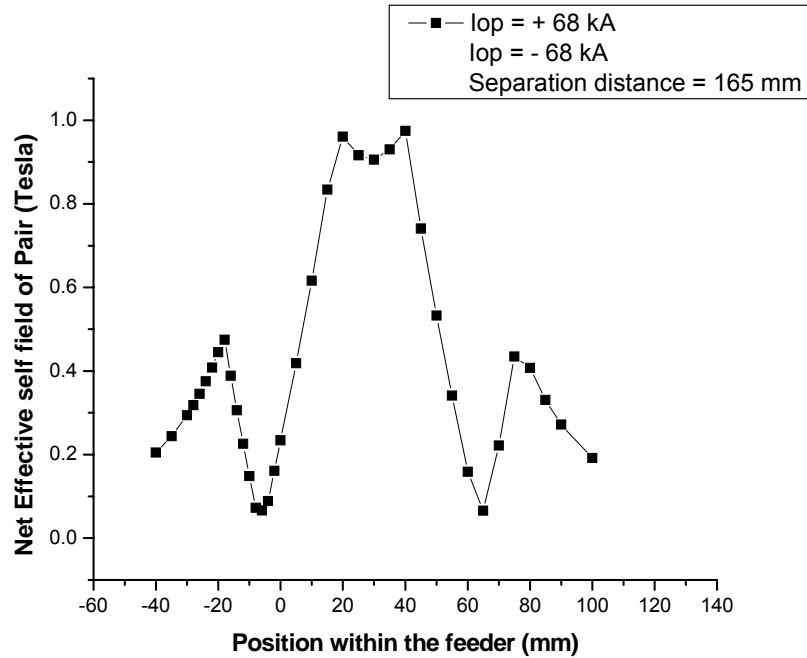


Figure 6.7 Self-field and stray field of a (+/-) pair of feeders at 68 kA

6.2.1.3 Material properties data base

Originally, an expression of the critical current density dependence on the magnetic field and the temperature for NbTi conductor was given by M.S. Lubell [74]. Especially in case of the ITER NbTi conductors, Ni-coating is used to reduce the coupling losses. Here, the NbTi critical current density is slightly modified by the following expression mentioned in the ITER DDD [71]) from the Lubell scaling parameters.

$$J_c(B, T) = \left(\frac{C_0}{B(x)} \right) \left(\frac{B(x)}{B_{c2}(T)} \right)^\alpha \left(1 - \frac{B(x)}{B_{c2}(T)} \right)^\beta \left(1 - \left(\frac{T(x)}{T_{c0}} \right)^n \right)^\gamma \quad (6.1)$$

Where, $C_0 = 8.03 \times 10^{10} \text{ A-T/mm}^2$, $\alpha = 0.57$, $b= 0.90$, $g=2.32$ and $n = 1.7$

For example, using above equation, a J_c value of NbTi $\sim 2900 \text{ A/mm}^2$ is obtained at 5 T and 4.2 K. All the properties of solid materials used are as per ITER DDD guideline report [71].

6.3 Steady state hydraulic analysis (single channel approach)

A detailed steady state hydraulic analysis has been carried out using the HE-SS code (which was developed by L. Bottura at the NET team) [75]. The analysis includes mass flow, friction factor and total pressure drop calculations for the TF sc feeder system with supercritical helium operating at 6 bar and 4.5 K.

6.3.1 Basic assumptions for steady state analysis

The following basic assumptions have been considered for a steady state analysis of the TF feeder.

- (i) The forced flow, supercritical helium cooling at 6 bar and 4.5 K for the TF feeder.
- (ii) The ITER CICC has two channels (i) annular bundle with void of ~ 34% (ii) central spiral channel, the steady state analysis assumes that the helium flows only in the bundle region.
- (iii) The parameterizations of NbTi and solid material properties are used as per ITER design guideline report [71].
- (iv) The temperature margin ~ 1.5 K should be maintained for NbTi.

The detailed parametric studies have been carried out in order to compare the available temperature margin for both cooling modes as mentioned in section 6.1.

The following strategy is used to evaluate the different parameters.

- Step-1: 1-D steady state thermal hydraulic analysis to obtain He mass flow rate, temperature profile and pressure drop.
- Step-2: Modeling of the TF feeder for the electromagnetic analysis without and with stray field contribution of the ITER magnet and maximum influence of plasma.
- Step-3: Evaluation of temperature margin taking into account the steady state heat flux and the magnetic field profile for the two different cooling modes.

6.3.2 Thermo-hydraulics and helium mass flow rate optimization study

The cable-in-conduit-conductor (CICC) concept allows the magnets to meet performance requirements such as high currents, high voltages, and low AC losses. In order to circulate large helium mass flow rates while keeping the level of pressure drop within acceptable levels, a specially designed dual channel CICC was developed for ITER. As discussed earlier, it has two flow regions (i) a central hole confined by a spiral

and (ii) the cable bundle region around the central hole. More details about the geometry of the specific spiral can be found in [76]. In the analysis, only the bundle region has been investigated because the central spiral channel and the bundle are hydraulically coupled. In the steady state the contribution of the friction and heat transfer process is rather high in the bundle compared to the hole. All external steady state heat loads are imposed on the jacket. Since the jacket has a good contact with the cable and via cable to the helium in the bundle, a good heat transfer process can be established. The cross-section of such a conductor has shown in Figure 6.1.

The steady state thermo-hydraulic properties can be described by the equations for the transport, heat transfer and friction losses and fluid flow. The essential fluid flow equations are given below,

$$v = \frac{\dot{m}}{(\rho A)} \quad (6.2)$$

$$Re = \frac{4\dot{m}}{\mu U} \quad (6.3)$$

$$\Delta P = \frac{f \dot{m}^2}{\rho} \frac{UL}{8A_f^3} \quad (6.4)$$

Where, v = velocity, \dot{m} = mass flow rate, A_f = flow area (in m^2), μ = dynamic viscosity (in Pa-s), Re = Reynolds number, f = friction factor for the bundle, U = cooled perimeter, L = total length and ΔP = pressure drop. The friction factor also called Darcy friction factor, is a dimensionless number and used in the fluid flow calculation. It basically expresses the linear relationship between the fluid mean velocity and pressure gradient. It is a function of the type of flows means Reynolds number (Re). For example, in case of a smooth tube with laminar flow the friction factor is given by following formula,

$$f = 64/Re \quad (\text{Laminar flow } Re < 2000) \quad (6.5)$$

The friction factor of the bundle region for CICC has a lot of uncertainties due to its complex geometrical structure. In order to find out the accurate value of the friction factor, the Katheder type friction factor valid in the range of Reynolds number of 1000-6000 [77].

$$f_{EU} = \left(\frac{1}{\text{void}} \right)^{0.742} \left(0.0231 + \frac{19.5}{Re_b^{0.7953}} \right) \quad (6.6)$$

Later it was modified especially for the ITER conductor [76] as mentioned below; the following expression for the friction factor is used in the analysis.

$$f_{EU,ITER} = \left(\frac{1}{\text{void}} \right)^{0.72} \left(0.051 + \frac{19.5}{\text{Re}_b^{0.88}} \right) \quad (6.7)$$

By using the value of steady state heat flux and pressure drop analysis along the length, the temperature of the feeder at the outlet was obtained by equation for the single phase helium heat removal as follows [78],

$$Q = \dot{m}(h_o - h_i) \quad (6.8)$$

Where, Q is the total steady state heat load, h_o and h_i are the enthalpies of the fluid at the outlet and inlet, respectively. Here, friction losses are not considered because they are not part of the external heat load but generated within the cable.

The temperature of the superconductor strands in the cable was obtained by using steady state heat transfer estimations (HESS code) in case of the helium. In order to find out the temperature margin ($T_{\text{margin}} = T_{cs} - T_{op}$), the estimation of current sharing temperature (T_{cs}) is needed following a $J_c(B, T)$ calculation. The current sharing temperature is defined as,

$$T_{cs} = T_{op} + (T_c - T_{op}) \left(1 - \left(\frac{I_t}{I_{cop}} \right) \right) \quad (6.9)$$

Where, T_{op} is the operating temperature, T_c is the critical temperature, I_t is the transport current and I_{cop} is the critical current at operating temperature. The helium properties are taken from the standard helium property code HEPAK [79].

Using equations (6.2 – 6.4), the pressure drop was calculated as a function of the helium mass flow rate for an inlet pressure of 6 bar and an inlet temperature of 4.5 K, as shown in Figure 6.8. The calculated pressure drop is of ~1mbar/m for a helium mass flow rate of 4.2 g/s.

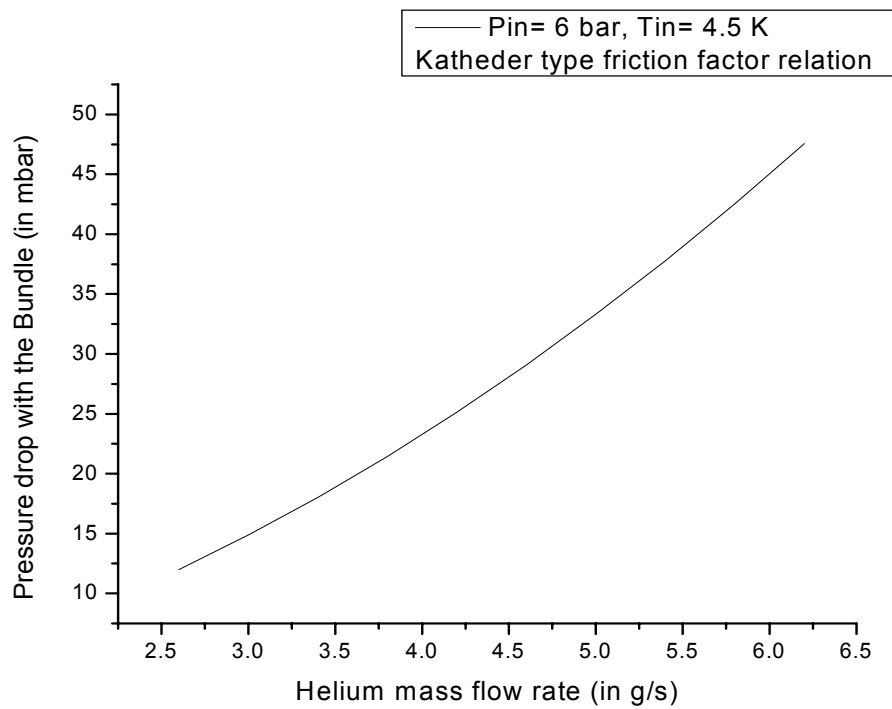


Figure 6.8 Pressure drop vs. mass flow rate characteristic for the TF feeder

The temperature profile of the TF feeder for different helium mass flow rates has been estimated in case of both the cooling modes, i.e. cooling inlet from magnet side and cooling inlet from current leads side as shown in Figure 6.9 and 6.10 respectively,

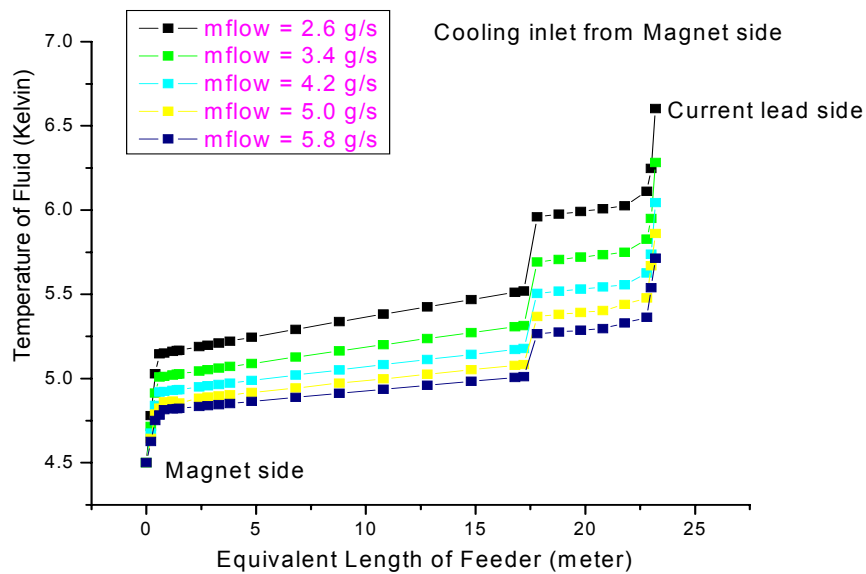


Figure 6.9 Temperature profile of the TF feeder for different helium mass flow rate

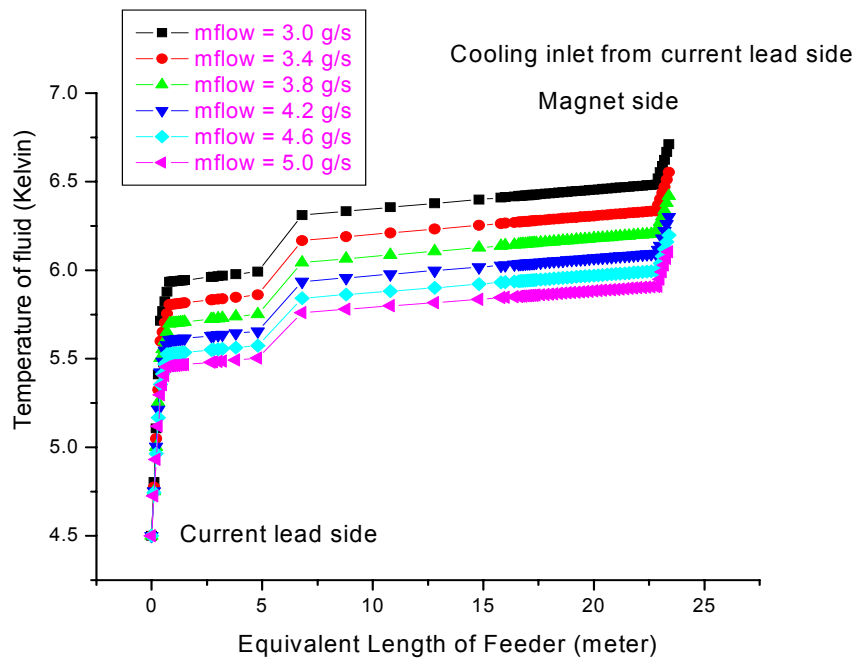


Figure 6.10 Temperature profile of the TF feeder for different helium mass flow rates

It is clear from the steady state analysis that for particular value of the helium mass flow rate, the temperature at the outlet of the TF feeder is higher in case of cooling from the current leads side compared to magnet side.

6.3.3 Cooling modes comparison study

The temperature margin along the length of the TF feeder is plotted for both possible cooling modes as shown in Figure 6.11 (a). It is clear that in any case the outlet of the feeder is the weakest location and prone to quench. In Figure 6.11 (a), the left side describes the cooling inlet from the current lead side and outlet at the magnet side. The right side describes the cooling inlet from the magnet side and outlet at the current leads side. In other words: to obtain the same temperature margin, a lower helium mass flow rate is required if the cooling inlet is at the magnet side than at the current lead side. A minimum helium mass flow rate of 3.4 g/s in the bundle is required to maintain the temperature margin of 1.5 K in case of cooling inlet from the magnet side, whereas 4.0 g/s is required in case of cooling inlet from the current leads side. Thus, the cooling from the magnet side is more efficient compared to the cooling from the CTB side.

Figure 6.11 (b) shows the temperature at the outlet of the TF feeder in presence and absence of the steady state heat loads. The friction losses would cause an increase in the temperature when the helium mass flow rate is increased. As the helium mass flow

rate increases for a given steady state heat load, the temperature at outlet of the feeder will decrease.

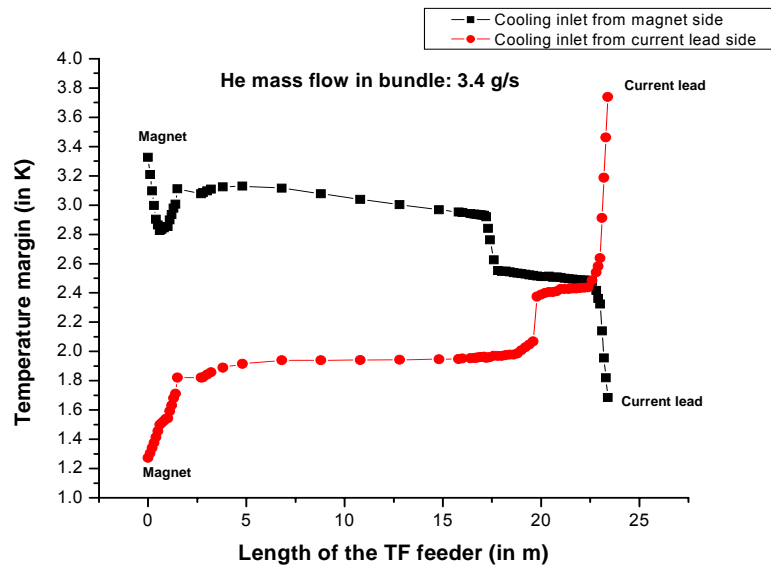


Figure 6.11 (a) Cooling modes comparison study for the TF feeder

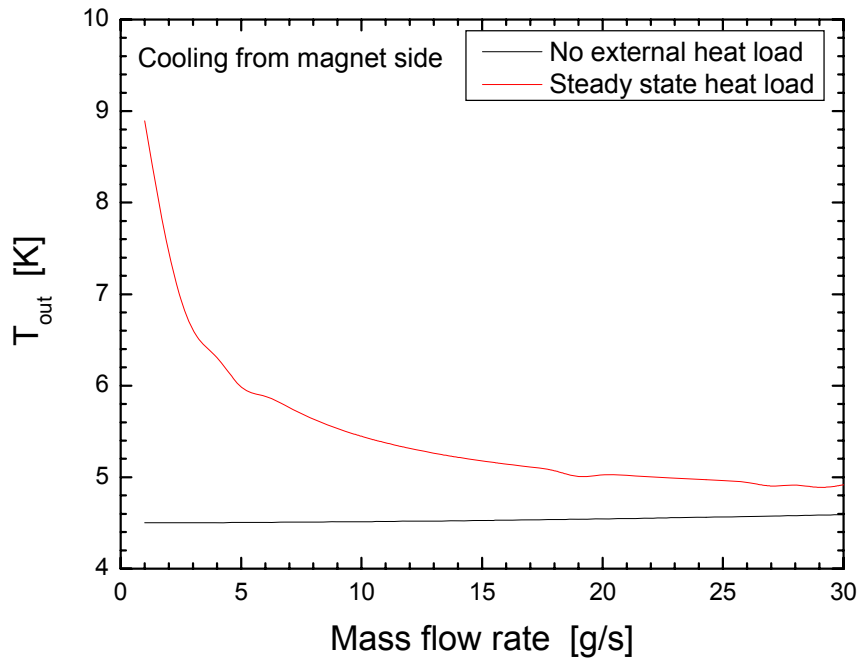


Figure 6.11 (b) Temperature at the outlet with mass flow rates

Finally, the temperature margin is plotted with respect to different helium mass flow rates in case of a preferred cooling mode i.e. cooling inlet from the magnet side (see Figure 6.11 (c)).

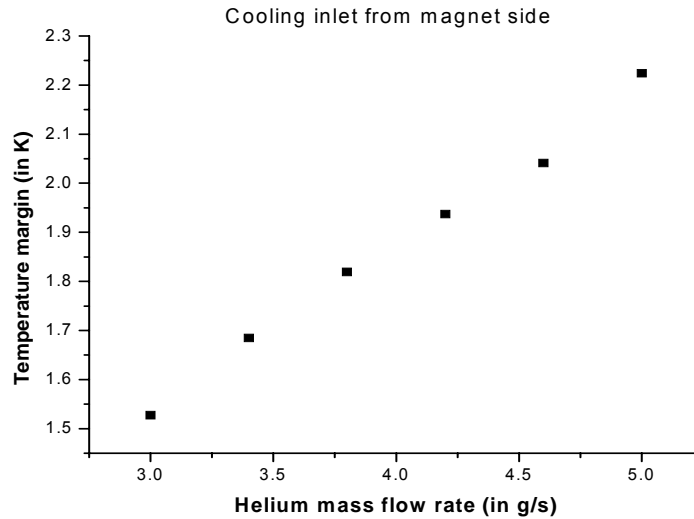


Figure 6.11 (c) Temperature margin with helium mass flow rate

The results of the single channel steady state analysis are as follows,

- (i) The critical current density is function of (B, T), has a stronger dependence of the temperature than of the magnetic field because the magnetic field of the feeder is higher towards the magnet side than the current leads side but always the outlet of the feeder is weak in both cooling modes.
- (ii) The lowest temperature margin is at the outlet of the feeder, independent of the cooling direction. This means that for cooling the feeder from the current lead side, the lowest margin is at the magnet side.
- (iii) To have the higher temperature margin at the magnet side, the preferred cooling is to provide the helium inlet there.
- (iv) The safe and reliable operation of the TF feeder demands a minimum helium mass flow rate in the bundle region of 3.4 g/s.

6.4 One dimensional transient thermo-hydraulic analysis (Dual channel approach)

A quench is the occurrence of a normal zone in the superconductor provoked by an internal or external disturbance which deposits energy. If the amount of energy is smaller than necessary to initiate a quench, the superconductor recovers. Otherwise it will lead to a thermal runaway and to a quench. The limit between recovery and quench is called electric stability limit and depends on the disturbance amplitude, time duration and wave form. For the design of the conductor its performance on the quench initiation and the quench propagation has to be known. In this context, the central channel plays

a role in the heat transfer process because it can absorb energy. The ability of energy deposition in the central channel depends on the time scale of the disturbance in the cable space because of the time required to transfer the energy from the bundle to the central channel region.

The one dimensional (1-D) thermo-hydraulic model of the TF feeders has been generated as an input for the finite element code Gandalf developed by L. Bottura [80]. Gandalf has been used to simulate the quench initiation and quench propagation in a dual channel CICC. The 1-D physical model consists of four independent components at different thermodynamic states as follows,

- the strands, consisting of the stabilizer and superconductor materials,
- the conduit, grouping the jacket and the insulation,
- the helium in the bundle, surrounding the strands within the cable, and
- the helium in the hole, flowing in an independent cooling passage.

The temperatures of these components are treated separately and the energy balances are coupled via heat transfer coefficients at the contact (wetted) surfaces. There is also a direct coupling between the helium in the cable and the jacket and between the helium in the bundle and the central channel (hole) by adjusting the parameter so-called 'porosity', in this way the bundle and the spiral channel is hydraulically coupled. Figure 6.12 shows the basic finite element used in Gandalf, showing degrees of freedom and the coupling of thermal and flow components. The material properties and boundary conditions can easily be handled by user routines.

There are several feasible transient events, which are possible during the operation of the machine like e.g. plasma disruption, safety discharge, power supply fault, cryogenic system failure etc. In order to investigate the performance of the TF feeder in transient events, some of the typical transient cases are discussed here:

- spontaneous quench of the feeder and consecutive quench propagation
- Analysis of the loss of helium flow in the feeder and no safety discharge of the magnet system
- Analysis of a quench during loss of helium flow with a following safety discharge

Before these transient events are analyzed the results of the steady state model described in section 6.3 have been repeated to verify it.

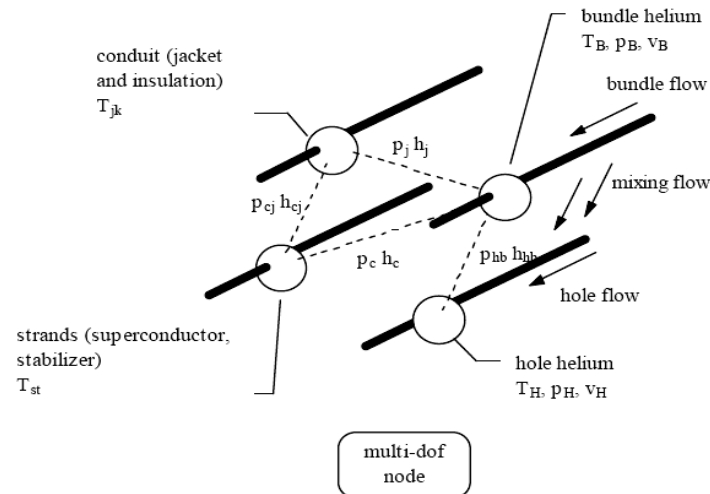
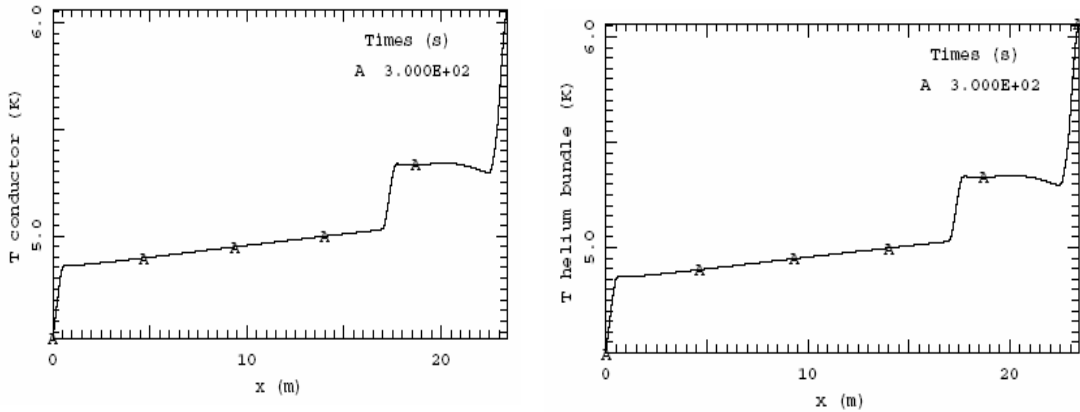


Figure 6.12 Basic finite element used in Gandalf, showing the degrees of freedom and the coupling of the thermal and flow components

6.4.1 Verification of the single channel steady state model

The different sources of steady state heat flux including radiation, residual gas conduction, and thermal conduction due to spacers and vacuum barrier and resistive losses in the joints have been imposed on the jacket and the actual magnetic field profile was modeled for the TF feeder. No external heat acting as quench initiation energy was given to the conductor. The optimization of the helium mass flow rates have been carried out for the duration of 300 seconds to be comparable to steady state. All the relevant critical parameters e.g. temperatures of the conductor and the helium, temperature margin and critical current density margin along with mass flow distribution of helium in the bundle and the hole region have been studied in terms of space and time history. As an example, the temperature profile is obtained for a helium mass flow rate of 5.0 g/s. The helium mass flow rate distribution between the bundle and the central spiral channel is found to be 70:30%.

The results show that there is an efficient heat transfer process taking place between the sc strands and the helium in the bundle, in the central channel (hole), and the jacket. As already predicted in the steady state analysis, the outlet of the sc feeder is the critical location (see Figure 6.13).



**Figure 6.13 Temperature profile for the conductor and the bundle
(With helium mass flow rate of 5.0 g/s)**

For example, the temperature margin of the feeder is plotted along the length with a helium mass flow rate of 5.0 g/s as shown in Figure 6.14. The result also shows that the outlet (location at $x = 25.0$) of the feeder is critical, where the temperature margin is lower.

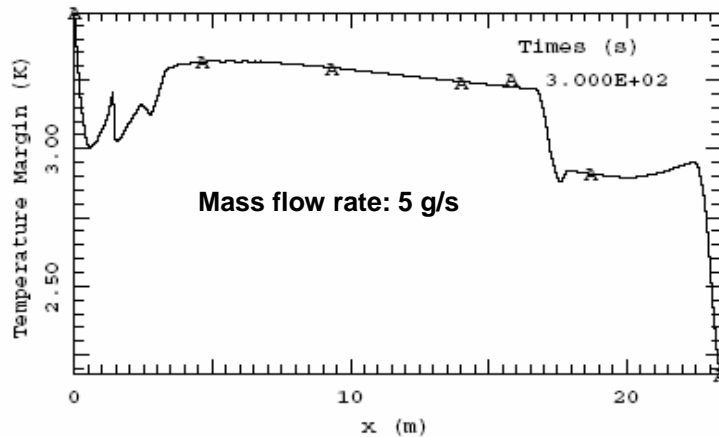


**Figure 6.14 Temperature margin along the length of the TF feeder
(With 5.0 g/s helium mass flow rate)**

1-D Gandalf analysis has also shown that a total helium mass flow of 5.0 g/s is required to obtain the temperature margin of 1.5 K. Looking at the distribution of mass flow rates between the bundle and the central channel, 3.6 g/s in the bundle region and of 1.4 g/s in the central channel is required. This is a similar number as computed in the steady state analysis. So, these results are almost similar to that of the results obtained in case of the steady state model where the bundle region mass flow rate was 3.4 g/s. It turned out that the central channel plays a role in the steady state process and will provide an additional margin as the bundle and central channel are hydraulically coupled.

6.4.2 Analysis of quench initiation and propagation

For simulating the initiation of a quench, a short time energy input it would be generated during a conductor movement. To simulate the typical external disturbance due to conductor movement, an external heat is imposed on the superconducting cable. In Gandalf code, this is done by putting an energy E/l for a time t along the conductor starting at $x_a = 11.65$ m and ending at $x_e = 11.75$ m. Here, the energy input as disturbance is given by external heat put into the center of the conductor at $x_o = 11.7$ m, as shown in Figure 6.15. A typical conductor movement is considered with a time scale of 1 ms and an effective disturbance length of 10 cm. The estimation of the minimum amount of disturbance energy density is needed to provoke a quench at $x_o = 11.7$ m as discussed below.

An external heat flux is given at the centre of the feeder $11.65 < x < 11.75$;

transient time of disturbance (t) = 1 ms, total time of integration = 1 s;

total cross-section area of the conductor = 758 mm^2 (including copper and sc);

The external minimum heat flux (Q_0 in W/m) required to quench the feeder is about **$2.0 \times 10^6 \text{ W/m}$**

From above details, the transient energy margin (EM) is estimated as following,

$$E M = (Q_0) (t) / (A_{\text{total}}) = (2.0 \times 10^6) (1 \times 10^{-3}) / (758 \times 10^{-6}) \text{ --- (in J/m}^3 \text{)} = \sim 2638 \text{ kJ/m}^3$$

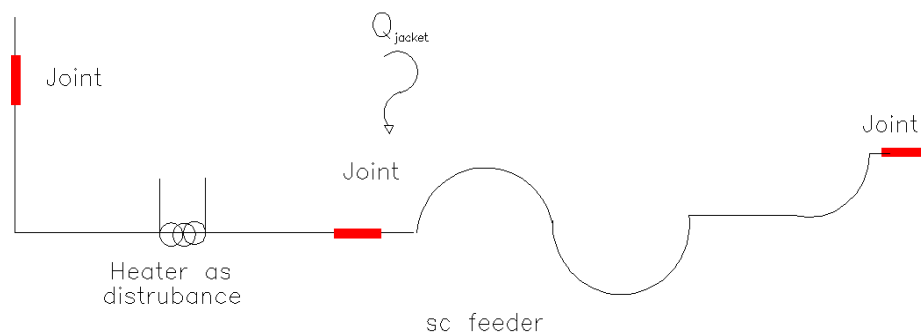


Figure 6.15 Simulation of a conductor disturbance by means of an external heater

The results are shown in Figures 6.16 (a) - 6.16 (f) respectively,

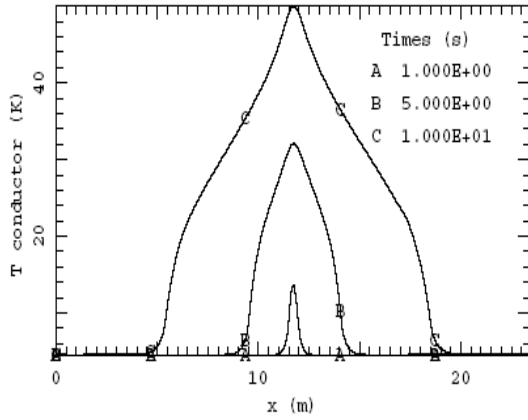


Figure 6.16 (a) Conductor temperature distribution

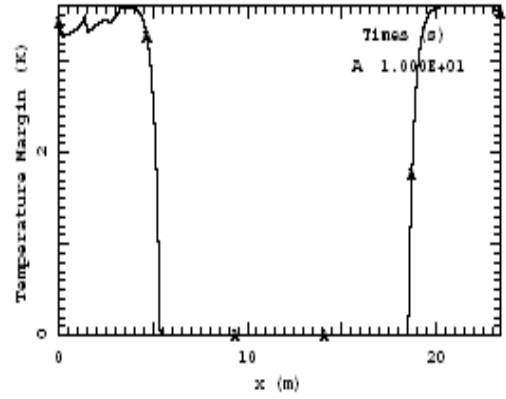


Figure 6.16 (b) Temperature margins along the length

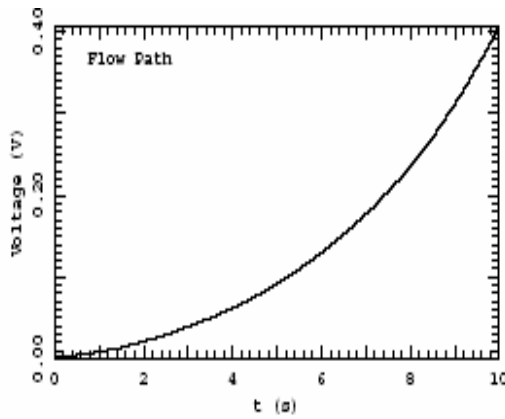


Figure 16 (c) Voltage rises with time

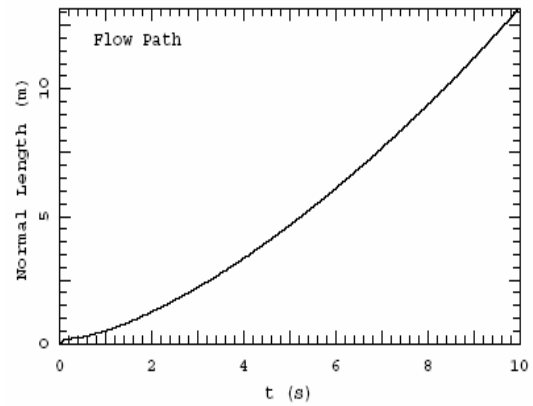


Figure 16 (d) Normal lengths with time

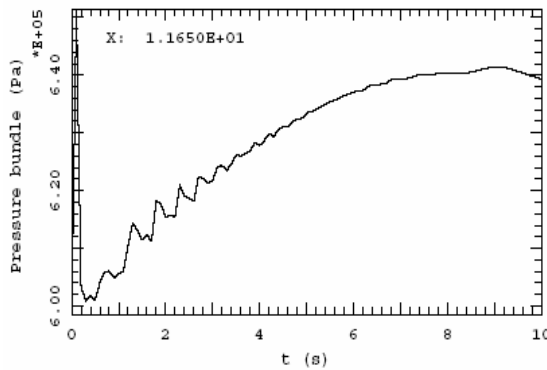


Figure 16 (e) Pressure in the bundle (x = 11.65 m)

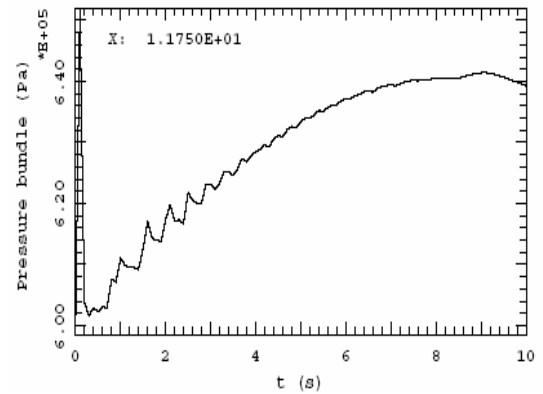


Figure 16 (f) Pressure in the bundle (x = 11.75 m)

From above results, it is clear that the quench evolution is more intense at the center of the conductor where actually the energy disturbance is applied. The temperature evolution with respect to time shows homogenous propagation. The voltage rise and normal zone propagation length show that the quench propagation process is quite slower than that of the magnets. Only 1 – 2 m normal zone length is developed for the voltage of 50 mV. Also the pressure rise within the heated zone is only 0.6 bar initially and then it gets stabilized over the time to an average pressure rise of 0.4 bar.

6.4.3 Analysis of the loss of helium flow in the feeder

Sudden cryogenic failure, as helium supply to the magnet, current lead and feeder stops, are known as loss of flow accident (LOFA). In this situation, tokamak control will immediately impose the machine to a fast discharge condition. Here, particularly in case of the TF feeder, a LOFA event is studied without and with fast discharge.

6.4.3.1 Analysis of a LOFA and a no safety discharge of the magnet

Considered is a LOFA event at maximum current in the TF feeder and no initiation of a safety discharge of the magnet. The temperature along the feeder will rise due to the external heat deposition and resistive heat generation of the joints. Since the temperature margin is lowest at the current lead end while cooling from the magnet side, the feeder will start quenching from the current lead side.

The results show that the quench propagation is much slower than in the coils. After 38 s the current sharing temperature is reached at the outlet of the feeder. After the quench has started, about 10 further seconds are needed to reach a detectable voltage level of ~40 mV and a length of the normal zone about 1.5 m. This is shown in Figures 6.17 (a) and 6.17 (b) respectively,

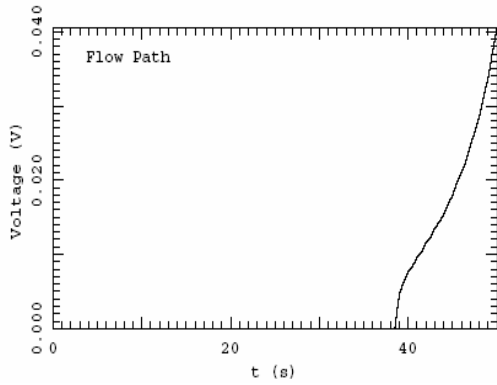


Figure 6.17 (a) Voltage develops only at 38 s

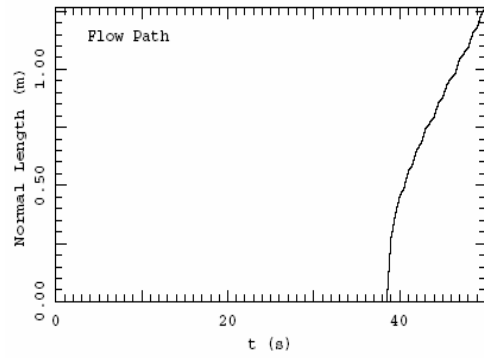


Figure 6.17 (b) Normal zone length with time

6.4.3.2 Analysis of a LOFA and a consecutive safety discharge of the magnet

Here, consider a LOFA event followed by a safety discharge of the magnet. This event is less severe than the one described above and should only evaluate the time needed to reach the critical temperature. The parameters used in the analysis are a quench detection time of 1 s, a delay time of 1 s (needed for switch and breaker operation) and an exponential discharge time of 12 s. The results show that the TF feeder is safe and stable up to 90 s after the LOFA has been started; the temperature margin along the feeder length is shown in Figure 6.18. After 90 s, there will not be a current in the feeder due to the discharge, so the feeder will not quench even after 90s because the conductor temperature remains lower than the critical temperature. So, for the TF feeder it will be easy to handle the situation after a LOFA with following a safety discharge.

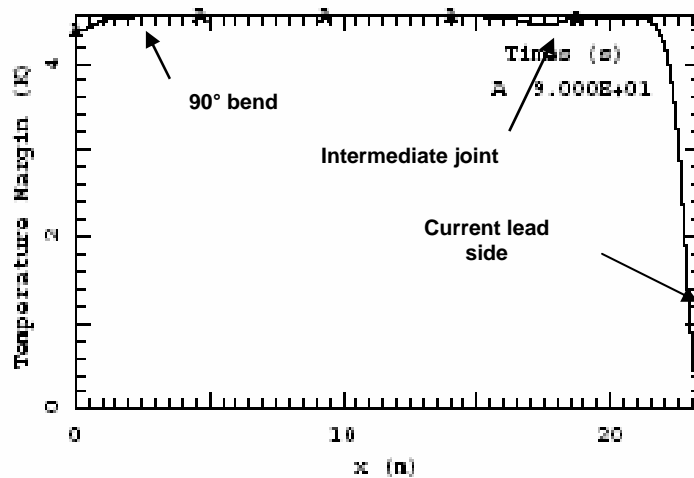


Figure 6.18 LOFA event followed by a magnet dump with steady state heat load

6.4.4 Effect of higher heat loads: Experience from the TOSKA facility

During the TFMC experiment performed with 80 kA conventional current lead in the TOSKA facility of FZK, a very high background steady state heat flux of 213 W/m imposed to each of the bus bar systems was found [81]. The calculation is carried out that how much higher mass flow rate of helium is required for the TF feeder to operate safely with such higher heat loads.

The steady state thermo-hydraulic calculation has shown that a helium mass flow rate of 16 g/s is required to operate the TF feeder. The same results are also obtained using Gandalf code for verification.

6.5 Discussions on PF and CS LTS current feeder systems

Since the conductors for the PF and the CS LTS feeders are the same as for the TF feeders but operating at lower currents, they have a higher energy margin. Steady state thermo-hydraulic calculations have been done for the PF and CS feeders at maximum currents using Gandalf. They showed that the PF feeder requires a helium mass flow rate of 4.6 g/s and the CS feeder requires 4.2 g/s (inlet pressure and temperature of 6 bar and 4.5 K). Under the LOFA conditions, the PF and CS feeders are rather stable and safe for more than 90 s. The conductor does not quench under the safety discharge conditions.

When a superconducting cable sees a changing magnetic field, it will dissipate power in terms of AC loss. The AC loss can be split into two main origins, one is hysteresis loss in the filaments and the other ones are coupling losses within strands and among strands in a cable or composite. In case of the PF and CS feeders, the contribution of AC losses has to be estimated. The time averaged AC loss in (W/m) has been estimated over a full plasma cycle ($t_{\text{cycle}} = 1800$ s) for the ITER plasma current reference scenario (inductive operation, 15 MA) discussed in Appendix-1. As the net effective field of the feeder is not constant due to its self field and stray field of ITER magnets, an average value of AC loss should be considered. The total length of the feeder is 25 m and the maximum effect of stray field occurs for a short length of 2 m only. The peak-to-peak current value of ± 45 kA, the self field of 0.45 T and the maximum stray field of 1.13 T are considered over a full plasma cycle. The coupling time constant of the NbTi conductor is assumed 25 ms with $n = 2$ (Where, n is the demagnetization factor) as per ITER DDD design guideline report. The time averaged AC loss over a full plasma cycle is 1 mW/m, which is 140 times less than that of the steady state heat loss (which is about 1.4 W/m) as per standard coupling loss formula mentioned in the ITER design

guide line report [71]. The hysteresis contribution is 7.8×10^{-5} W/m. So, the net contribution of the AC loss in case of the PF and CS feeder systems is negligible. But as far as the stability of the feeder is concerned, the transient energy margin in a short energy pulse as a conductor movement disturbance should be considered as a part of transient energy margin or stability. Analysis shows that in case of 45 kA of pulsed current in the CS feeder with a 1 ms disturbance due to conductor movement, 3.8×10^6 W/m heat input is needed to provoke a quench. This means the CS feeder has a quite higher transient energy margin of ~ 5013 kJ/m³.

Input parameters

Helium Pressure = 6 bar, Helium temperature = 4.5 K at inlet

Mass flow rate = 5.0 g/s

I_{op} = Operating current = 45 kA

A_{sc} = Cross-section area of superconductor = 96 mm²

A_{cu} = Cross-section area of Copper = 662 mm²

A_{total} = Total cross-section area = $A_{sc} + A_{cu} = 758$ mm²

External heat flux is given at the centre of feeder $11.65 < X < 11.75$ m

Transient time of disturbance (t) = 1 ms

Total time of integration = 1 s

External minimum heat flux (Q_0 in W/m) required to quench the feeder is **3.8×10^6 W/m**

From above data, the transient energy margin (EM) is estimated as following,

$$E M = (Q_0) (t) / (A_{total}) = (3.8 \times 10^6) (1 \times 10^{-3}) / (758 \times 10^{-6}) \text{ --- (in J/m}^3 \text{)} = \sim 5013 \text{ kJ/m}^3$$

6.6 Quench detection and instrumentation

The LTS feeder system consists mainly of joints at different three locations, at the straight part of the feeder, the S-bend, and the vacuum barrier at the interface between the cryostat feed through and the CTB (refer Figure 1.1 of chapter 1). Single temperature, pressure and flow measurements should be carried out at the inlet and the outlet within the cryogenic supply and return header / piping distribution. These measurements are not essential for all feeders.

- During all the possible operations, vacuum monitoring of feeder duct and CTB is essential.

- The temperature of the thermal shield at least at one location of the feeder duct as well as the CTB should be measured particularly for cool-down and warm up phases.
 - During the normal and quench operations, the voltage drop between each joint within the current feeder system should be monitored.
 - In case of the LTS feeder system, as far as the quench detection is concerned, the pressure and flow measurements are not adequate. The 1-D thermo hydraulic estimation for the LTS feeder shows that during the quench or loss of flow accident (LOFA), these parameters have no significant changes because the feeder has a short length compared to that of the main magnet windings. So, the fastest detection is a direct measurement of the voltage drop along the feeder but may be a temperature measurement at the outlet would be the better choice.
- **Interface with Cryostat feed through and CTB**

Interfaces are a critical issue for any current feeder system of a fusion device because, these are the weak points from the temperature margin point of view, lead to failure and need more maintenance. In principle, one can separate the vacuum of individual sub - systems as it contains vacuum barriers. As the interface deals with cryogenic feeds, current feeders, and instrumentation cables, the design needs special attention from the point of view of thermal stress and electrical breakdown. Electrical insulation and vacuum monitoring systems are permanently required. The double insulation scheme is shown in Figure 6.19.

The overall quench detection and instrumentation requirement is summarized in Table 6-4. It is recommended that other than voltage taps or co-wound wires, one should have redundant quench detection scheme. The measurement of the helium temperature of the outlet would be the better option as an optional quench detection tool.

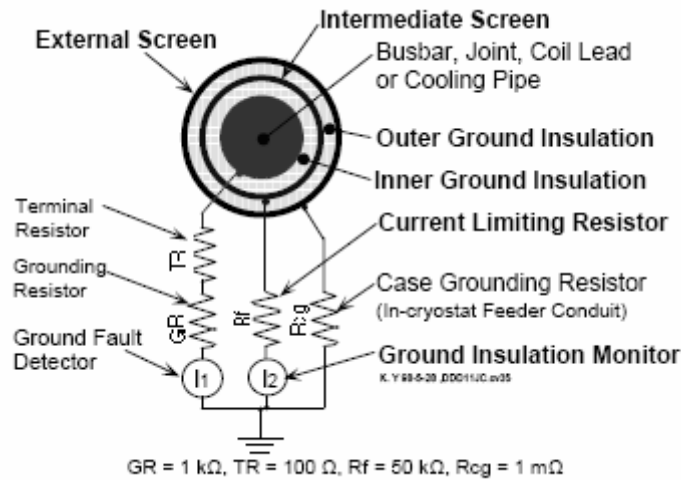


Figure 6.19 Insulation monitoring scheme for feeders, joints, leads and cooling pipes [2]

Table 6-4 Summary of instrumentation required for the LTS feeder system

Operation	Temperature (fluid)	Pressure (fluid)	Flow (fluid)	Voltage drop	Insulation monitor (Resist. measure)	Vacuum monitor
Cool-down	Yes Only at the outlet of each feeder	Not envisaged	Not envisaged	Not envisaged	Not envisaged	Yes within feeder duct and CTB
Warm up	Yes Only at the outlet of each feeder	Not envisaged	Not envisaged	Not envisaged	Not envisaged	Yes within feeder duct and CTB
Normal	Yes Only at the outlet of each feeder	Not envisaged	Not envisaged	Yes Co-wound wires along the feeder length	Yes for all feeders and leads	Yes within feeder duct and CTB
Quench	Yes Only at the outlet of each feeder	Not envisaged	Not envisaged	Yes Co-wound wires along the feeder length	Yes for all feeders and leads	Yes within feeder duct and CTB
Fault conditions	Yes Only at the outlet of each feeder	Not envisaged	Not envisaged	Yes Co-wound wires along the feeder	Yes for all feeders and leads	Yes within feeder duct and CTB

Chapter 7 – Comparative study of an ITER design with and without HTS current leads

In this chapter, a comparative study of an ITER design with and without HTS current leads has been worked out in order to demonstrate the advantage of the use of the HTS current leads for ITER. The detailed comparison of operation costs and capital costs has been carried out for the forced-flow conventional current leads and HTS current leads.

7.1 Introduction

ITER is planned to use 9 current lead (CL) pairs for the TF coils at 68 kA, 6 CL pairs for the CS coils at 45 kA and 6 CL pairs for the PF coils at 52 kA. The smaller CLs for the correction coils can be assumed to be of conventional type [3]. The main power consumption is caused by the helium refrigerator power which is necessary to cool the current leads. However, for an assessment of the overall costs only the average power consumption is useful. The CLs for the correction coils are not included in the comparison study as they are only of conventional type.

The ITER project needs a techno-economical assessment of its current lead system because the leads require about one third of the overall cryogenic power. Therefore the current lead plays a major role in order to minimize the overall cryogenic requirements. The main criteria for the ITER current lead design, beside the general operation requirements, are

- reliability during operation,
- serviceability in case of emergency,
- capital investment costs, and
- operating costs.

Since the ITER magnet system has a considerable stand-by time with idle current operation periods, it has a significant variation in the operation duty cycle of different magnets like e.g. for the TF system operation, the duty cycle is 32% whereas in case of the PF and CS systems it is only 6% per year of operation. So, one has to look for various design and cooling scenario options for the current lead system to provide a technically acceptable solution minimizing the total operating costs and keeping the reliability and serviceability in emergency cases. The various options are analyzed and compared in the following.

The performance assessment of the comparative study of the current leads is based on the test results of the conventional current leads given in the ITER DDD [3] and the HTS current lead performance is based on the test results of the EU 70 kA prototype HTS current lead [67-68] [82], discussed in chapter 5. The cost comparison study is done for the two cooling modes i.e. 50 K helium and 80 K helium for the HTS CLs with the conventional CLs at 4.5 K for ITER [69].

7.2 Cost Analysis for the operation

7.2.1 Definition of the duty cycle of the ITER magnet system

As a reference for the ITER operation, the inductive operation scenario II has been chosen. The total plasma pulse time is 1800 s and a similar time is required for the stabilization of the cryogenic system before the next plasma shot will start, i.e., one plasma cycle will last for 3600 s. For ITER, six plasma shots are planned per day. It is further assumed that there is no plasma operation during weekend and that there will be a stand-by time for maintenance etc. for 4 months per year.

Since the TF system is a steady state DC system, 6 shots à 3600 s result in six hours operation time and 18 hours stand-by time per day. Since there will be no discharge and re-charge of the TF coil system between each plasma cycle, it is assumed that it will be ramped up and down once per day, the flat top time being 14 h and the ramp up and down times 2 h each. This is because the TF system needs a long time to be energized and discharged. Therefore the TF magnets will be loaded with current in the early morning and discharged in the evening when all experiments of the day are done. This corresponds to a total duty cycle of

$16 \text{ hours}/24 \text{ hours} * 5 \text{ days}/7 \text{ days} * 8 \text{ months}/12 \text{ months} = 32\%$ current operation averaged over one year [69]. As the average power consumption of the leads is based on the assumption of the particular duty cycle, if one will change the duty cycle then there will be a change in overall power consumption of the leads like e.g. there might be a case for the TF coils with 2 weeks operation time and one week stand-by.

Similar, for the pulsed magnet systems like PF, CS and CC, the operation will result in three hours current time and 21 hours of stand-by time per day. This would correspond to a duty cycle of

$3 \text{ hours}/24 \text{ hours} * 5 \text{ days}/7 \text{ days} * 8 \text{ months}/12 \text{ months} = 6\%$ current operation averaged over one year.

As the current lead system is contributor to the major heat load for the cryogenic system of any fusion device, the machine duty cycle plays an essential role in order to size the

cryogenic capacity of the specific helium refrigerator / liquefier system with a large capacity helium reservoir. Here, the reservoir will act as additional storage. It will empty during the operation and it will be re-filled during the stand-by. Otherwise, the duty cycle is important for estimating the power consumption of the current leads.

The helium consumption for the each lead can be calculated by using the weighted average mass flow rate deduced in the following way:

$$\dot{m}_{ave} = \frac{\dot{m}_{lop} I_{op} t_{lop} + \dot{m}_{l_0} I_0 t_{l_0}}{t_{lop} + t_{l_0}} \quad (7.1)$$

Where \dot{m}_{lop} = Specific helium mass flow under operation (in g/s-kA),

\dot{m}_{l_0} = specific helium mass flow for idle current mode (in g/s-kA),

\dot{m}_{ave} = average specific helium mass flow (in g/s),

I_{op}, I_0 = operation and idle currents,

t_{lop} = time of current operation

t_{l_0} = time of idle current operation.

The average helium mass flow rates have to be calculated for each current lead type.

7.2.2 Calculations of the power consumption

For the evaluation of the operation costs, the efficiency of the specific refrigerator system plays a key role. The following approximation has been used to compare the operation costs of a HTS current lead with a conventional one.

The power consumption is calculated by adding the power loss present at the cold end of the leads and the loss removed by the helium mass flow rate at different inlet temperatures in the heat exchanger of the current lead. For example, in case of the conventional current leads the heat exchanger is working from 300 K to 4.5 K. Here, the helium mass flow rate at 4.5 K will be used to cool the heat exchanger as well as to remove the heat load at the cold end where as in case of the HTS current leads, the cold end heat load of the HTS module is removed by 4.5 K helium but the conventional heat exchanger will be cooled by either 50 K helium flow or 80 K helium flow. In both cases the cold end heat load will be removed by 4.5 K helium. The following general relation will be used to estimate the power consumption of the particular type of leads [43]:

$$P_g = \dot{m} \left(\frac{H_r}{e_1(T)} \right) + Q_k \left(\frac{P_e}{P_k} \right)_{refrigeration} = \dot{m} \left(\frac{H_r}{e_1(T)} \right) + Q_k \left(\frac{1}{\eta_c e_2} \right) \quad (7.2)$$

$$\eta_c = \left(\frac{T_c}{T_w - T_c} \right) \quad (7.3)$$

$$H_r = 300 (S_1 - S_2) - (h_1 - h_2) \quad (7.4)$$

P_g is the total power consumption (in Watts),

\dot{m} is the mass flow rate of coolant in (g/s),

Q_K is the conduction and resistive loss (for $I \neq 0$) at the 4.5 K level

η_c is the Carnot efficiency of the machine,

$e_1 = e_1(T)$ is the exergy efficiency at the different temperatures

e_2 is the thermodynamic efficiency at 4.5 K.

S_1 and S_2 are the entropies at 300 K and respective temperature

h_1 and h_2 are the enthalpies at 300 K and respective temperatures

The thermodynamic exergy efficiency $e_1(T)$ is calculated for different temperatures and the value of e_2 is related to the Watt to Watt ratio of the particular refrigerator and it is defined only at 4.5 K. It changes with the small-scale cryo plants to the large-scale cryo plants significantly. For example, the SST-1 He refrigerator (1.3 kW at 4.5 K) has a Watt to Watt ratio of 466, whereas a 18 kW at 4.5 K refrigerator module at LHC CERN has the Watt to Watt ratio of 233. The helium refrigerator system for the ITER will consist of four 18 kW modules at 4.5 K comparable to the LHC refrigerators [37].

As discussed earlier in Chapter 3, the data of thermodynamic efficiencies for world wide kW class helium refrigerators and an extrapolation for ITER refrigerator have been given. For 4.5 K, an e_2 value of 0.295 is taken. Table 7-1 summarizes the helium properties for the different temperature levels because these helium properties at different temperatures are essential for an estimate of the power consumption for the conventional as well as the HTS current leads. For different temperatures the derived values of e_1 , e_2 and H_r are summarized in the Table 7-2.

Table 7-1 Helium properties at different pressures and temperatures [79]

P_{in}/P_{out} [bar]	T_o [K]	T_1 [K]	T_2 [K]	S_1 [J/g-K]	S_2 [J/g-K]	h_1 [J/g]	h_2 [J/g]
4.0/ 3.6	300	290	5.0	28.78	4.025	1522	14.94
4.6/ 4.4	300	290	50.0	28.35	19.13	1523	275.5
4.6/ 4.4	300	290	80.0	27.40	20.52	1524	432.6

Table 7-2: Helium parameters at 4.4 bar / 4.6 bar

T_1 [K]	T_2 [K]	Carnot efficiency	W/W ratio	Exergetic Efficiency e_1	Efficiency at 4.5 K e_2	H_r
300	4.2	0.01426	237	0.295	0.295	5919
300	50	0.2	17.6	0.284	0.295	1521
300	80	0.364	11	0.25	0.295	973

(Here, 4.4 bar / 4.6 bar values corresponds to the pressure values at the outlet and inlet of the heat exchanger respectively)

7.2.2.1 Cooling power for forced flow conventional leads

As discussed earlier in chapter 6, for constant cross section conventional leads, the following input numbers are used [62 - 63]:

$$\dot{m}(I=0) = 0.04 \text{ g/s/kA/lead}$$

$$\dot{m}(I=I_{\max}) = 0.06 \text{ g/s/kA/lead}$$

$$Q_K(I=0) = \text{Conduction loss at cold end} = 0.1 \text{ W/kA/lead}$$

$$Q_K(I=I_{\max}) = 0.1 \text{ W/kA/lead} + Q_{\text{joule}} (I_{\max}^2 R_j) \text{ with } R_j = 1 \text{ n}\Omega$$

$$\text{Efficiency factor } e_1 = e_2 = 0.295 \text{ at } 4.5 \text{ K}$$

Here, the constant cross section current leads are assumed for all the current leads for ITER in the present study.

The Table 7-3 summarizes the computed values of helium mass flow rates and heat loads at cold ends, Table 7-4 gives the value of power consumption during operation and stand-by and Table 7-5 summarizes the computed numbers of consumption as per duty cycle for the conventional current leads for ITER.

Table 7-3 Helium mass flow rates and heat loads at cold end (at 4.5 K) for all leads

System	I_{\max}	Number of current leads	$\dot{m}(I=I_{\max})$ [g/s]	$\dot{m}(I=0)$ [g/s]	$Q_K(I=I_{\max})$ [Watts]	$Q_K(I=0)$ [Watts]
TF	68 kA	18	73.44	48.96	205.63	122.4
PF	52 kA	12	37.44	24.96	94.84	62.4
CS	45 kA	12	32.4	21.6	78.3	54
Total		42	143.28	95.52	378.77	238.8

Table 7-4 Power consumptions of the cooling system during operation and stand-by

System	mH_r/e_1 (at $I=I_{\max}$) (in MW)	mH_r/e_1 (at $I=0$) (in MW)	$Q_K(P_e/P_k)$ (at $I=I_{\max}$) (in kW)	$Q_K(P_e/P_k)$ (at $I=0$) (in kW)	P_g (at $I=I_{\max}$) (in MW)	P_g (at $I=0$) (in MW)
TF (68 kA) (18 nos.)	1.474	0.982	48.73	29.01	1.522	1.011
PF (52 kA) (12 nos.)	0.751	0.5	22.48	14.79	0.773	0.515
CS (45 kA) (12 nos.)	0.650	0.433	18.56	12.8	0.668	0.446

Table 7-5: Power consumption for the ITER duty cycle

System	Leads	ITER duty cycle	P _g (in MW)
TF	18	0.32	1.175
PF	12	0.06	0.530
CS	12	0.06	0.459
Total			2.164

For the ITER duty cycle, the power consumption averaged over a year for cooling the current leads system is 2.164 MW.

7.2.2.2 Cooling power for HTS current leads

As described, an HTS current lead basically consists of an HTS part and a copper section which act as a heat exchanger. There will be a joint between the HTS part and copper part which could influence the temperature of the warm end of the HTS part.

Mainly two cooling modes of the HTS current lead have been considered. Two case studies have been carried out, i.e., using a helium temperature of 50 K and 80 K at the inlet of the heat exchanger. For 50 K helium cooling, two options have been used, i.e., fixing the upper end temperature of the HTS part, $T_{HTS,top}$, to 65 K for current operation, and optionally to 65 K or 105 K for idle current operation. The 65 K option is applicable for short time zero current operation, e.g., during and between plasma cycles, whereas the second option is possible during stand by operation. For the 80 K helium cooling, $T_{HTS,top}$ is fixed to 85 K for current operation, and to 105 K for idle current operation. As a reference, the test results of the EU 70 kA HTS current lead are used in order to calculate the power consumption of the HTS current leads for the different options.

Case 1 50 K helium operation ($T_{HTS,top} = 65$ K)

$$\dot{m}(I=0) = 0.032 \text{ g/s/kA/lead } (T_{HTS,top} = 65 \text{ K})$$

$$\dot{m}(I=I_{max}) = 0.069 \text{ g/s/kA/lead } (T_{HTS,top} = 65 \text{ K})$$

$$Q_K(I=0) = \text{Conduction loss at cold end} = 0.198 \text{ W/kA/lead } (T_{HTS,top} = 65 \text{ K})$$

$$Q_K(I=I_{max}) = 0.198 \text{ W/kA/lead} + Q_{joule} (I_{max}^2 R_j) \text{ with } R_j = 3.7 \text{ n}\Omega$$

Case 2 50 K helium operation ($T_{HTS,top} = 65$ K / 105 K)

$$\dot{m}(I=0) = 0.0147 \text{ g/s/kA/lead } (T_{HTS,top} = 105 \text{ K})$$

$$\dot{m}(I=I_{max}) = 0.069 \text{ g/s/kA/lead } (T_{HTS,top} = 65 \text{ K})$$

$$Q_K(I=0) = \text{Conduction loss at cold end} = 0.3529 \text{ W/kA/lead } (T_{HTS,top} = 105 \text{ K})$$

$$Q_K(I=I_{max}) = 0.198 \text{ W/kA/lead} + Q_{joule} (I_{max}^2 R_j) \text{ with } R_j = 3.7 \text{ n}\Omega$$

Case 3 80 K helium operation ($T_{\text{HTS,top}} = 85 \text{ K} / 105 \text{ K}$)

$$\dot{m}(I=0) = 0.022 \text{ g/s/kA/lead } (T_{\text{HTS,top}} = 105 \text{ K})$$

$$\dot{m}(I=I_{\text{max}}) = 0.22 \text{ g/s/kA/lead } (T_{\text{HTS,top}} = 85 \text{ K})$$

$$Q_K(I=0) = \text{Conduction loss at cold end} = 0.3529 \text{ W/kA/lead } (T_{\text{HTS,top}} = 105 \text{ K})$$

$$Q_K(I=I_{\text{max}}) = 0.2779 \text{ W/kA/lead} + Q_{\text{joule}} (I_{\text{max}}^2 R_j) \text{ with } R_j = 3.7 \text{ n}\Omega$$

Table 7-6 shows the cooling requirements for all HTS current leads in ITER for 50 K and 80 K helium cooling operation. It should be also noted that the helium mass flow rates given for 80 K operation are not optimized numbers because they were extrapolated using the 80 K measurement data of the Forschungszentrum Karlsruhe 70 kA HTS current lead which was designed for 50 K operation and not for 80 K. So in case of an optimized current leads design the actual mass flow rates will be lower with an optimized heat exchanger (better heat transfer and lower contact resistance), the cooling power could be reduced by roughly 30% [70]. At higher operating temperature the higher helium mass flow rate is required due to the following two reasons,

- (i) Temperature difference between the helium at the inlet of the heat exchanger and the top part of the HTS module.
- (ii) Heat load at the joint due to Joule heating

At the higher operating temperature, the difference between the HTS top part and helium inlet is decreased as well as Joule heating is increasing as we are reaching towards the current sharing temperature of the HTS module. Here, also it should be noted that the higher operation temperature ($T_{\text{HTS,top}} = 105 \text{ K}$) is kept during the longer stand by i.e. during night time. The short stand-by during off-plasma condition i.e. the time between two consequent plasma shots, one cannot keep the leads at $T_{\text{HTS,top}} = 105 \text{ K}$ the cool-down time would be too long.

In Tables 7-7 to 7-9, the cooling power consumption of the HTS currents in ITER are calculated. The final reduction factors for HTS current lead operation compared to conventional current leads are given in Table 7-10.

Table 7-6: Cooling requirements for HTS current leads

50 K He operation				
$T_{HTS,top} = 65$ K for both the stand by and the I_{max} operation				
Coil	Stand by operation		I_{max} operation	
	Heat input at 4.5 K	He mass flow rate	Heat input at 4.5 K	He mass flow rate
TF	242 W	39 g/s	550 W	84.5 g/s
CS	107 W	17.3 g/s	197 W	37.3 g/s
PF	124W	20 g/s	243W	43 g/s
Total	473 W	76.3 g/s	990 W	164.8 g/s
50 K He operation				
$T_{HTS,top} = 105$ K for the stand by and $T_{HTS,top} = 65$ K for the I_{max} operation				
TF	432 W	18 g/s	550 W	84.5 g/s
CS	191 W	7.9 g/s	197 W	37.3 g/s
PF	220 W	9.2 g/s	243 W	43 g/s
Total	843 W	35.1 g/s	990 W	164.8 g/s
80 K He operation				
$T_{HTS,top} = 105$ K for the stand by and $T_{HTS,top} = 85$ K for the I_{max} operation				
TF	432 W	27 g/s	587 W	269.3 g/s
CS	191 W	11.9 g/s	213 W	118.8 g/s
PF	220 W	13.7 g/s	262 W	137.3 g/s
Total	843 W	52.6 g/s	1062 W	525.4 g/s

Table 7-7: Results of power consumption derived from 50 K He HTS leads

	Standby ($T_{HTS,top} = 65$ K) (in MW)	Standby ($T_{HTS,top} = 105$ K) (in MW)	I_{max} Operation (in MW)	ITER duty cycle ($T_{HTS,top} =$ 65 K) (in MW)	ITER duty cycle ($T_{HTS,top} =$ 105 K) (in MW)
TF	0.267	0.198	0.582	0.368	0.321
PF	0.136	0.101	0.288	0.145	0.112
CS	0.117	0.087	0.246	0.125	0.097
Total	0.520	0.386	1.116	0.638	0.530

Table 7-8: Results of power consumption derived from 80 K He HTS leads

System	Standby (in MW)	I_{max} Operation (in MW)	ITER duty cycle (in MW)
TF	0.207	1.202	0.525
PF	0.105	0.603	0.135
CS	0.091	0.519	0.117
Total	0.403	2.324	0.777

Table 7-9: Results of power consumption derived from 80 K He HTS leads neglecting the 80 K He mass flow rate

System	Standby (in MW)	I_{max} Operation (in MW)	ITER duty cycle (in MW)
TF	0.102	0.153	0.118
PF	0.052	0.069	0.053
CS	0.045	0.056	0.046
Total	0.199	0.278	0.217

Table 7-10: Reduction factors of HTS current leads compare to conventional current leads

	HTS CL operation with			
	50K He ($T_{HTS,top} = 65\text{ K}$)	50 K He ($T_{HTS,top} = 105/65\text{ K}$)	80 K He ($T_{HTS,top} = 105/85\text{ K}$)	with 80 K He (neglecting 80 K mass flow rate(*))
Standby	3.79	5.11	4.89	9.91
Operation	2.66	2.66	1.27	10.66
For ITER duty cycle	3.39	4.08	2.79	9.97

(* - As in ITER, plenty of 80 K cooling capacity is already available for the cryostat shield cooling and the current lead cooling requirement at 80 K is negligible compared to the shield cooling, one can neglect the 80 K helium flow rate)

Comparing both options for HTS current leads cooling i.e. 50 K helium and 80 K helium, it seems that 50 K helium is more reliable and economic because in case of 50 K helium cooling, the temperature margin is rather high whereas in case of 80 K it is just neat to the limit. The 80 K helium option would be very expensive from the capital cost point of view because at 80 K the critical current of Bi-2223/Ag/AgAu tapes is much lower at 50 K. So, a large amount of superconductor is needed in case of 80 K operation. Also at 80 K the exergy efficiency of the helium refrigerator is less compared to 50 K helium. However, the 80 K helium option will be beneficial when plenty of 80 K helium is already available like e.g. in case of ITER cryostat cooling, where a cooling power of about 1 MW at 80 K is required [38]. In such a case, the current lead cooling requirement will be negligible.

7.2.2.3 Liquid nitrogen (LN₂) operation for HTS current leads

An alternate option for HTS current leads is to cool the current lead heat exchanger with liquid nitrogen instead of helium. This requires the need of a LN₂ reservoir and of a sub-cooler (in case of using pressurized nitrogen).

Due to the very successful results from the previous test campaigns of the 70 kA HTS current lead, the proposal was to test this current lead also with LN₂ cooling at atmospheric and sub-atmospheric pressure. Such an operation with LN₂ cooling would be also very interesting for ITER because LN₂ is available at the ITER site in any case. The advantages are as follows:

- The distribution is much simpler and the available time for discharging the coils after a LOFA is not critical because it depends only on the dimensions of the LN₂ reservoir in the HEX.

- The LN₂ reservoir could be designed in such a way that a cooling capacity is available, which is large enough to fulfil the ITER requirements more easily.
- The cooling of the current leads is independent of the cooling of the magnets and current feeders.
- Due to better heat transfer to the nitrogen bath and a more constant temperature of the interface region between the HTS part and the heat exchanger, the temperature difference between the HTS and the LN₂ bath would be smaller than in case of 80 K He cooling which results in a bigger temperature margin of the HTS elements.
- In addition a large amount of cooling power can be saved if the HTS current leads are cooled with LN₂. The HTS current lead test with ($T_{\text{HTS, top}} = 75 \text{ K}$, $T_{\text{op}} = 70 \text{ K}$) has shown that almost the same time margin of 5.5 min for a LOFA. was achieved as in the 50 K helium option.

The disadvantages are as follows:

- The specific heat as well as the enthalpy of nitrogen gas at 1 - 2 bar pressure and 65 – 80 K temperatures is much lower than that of helium at 4 bar and 50 – 80 K. This means that the heat exchanger is more efficient in case of helium than of nitrogen cooling.
- The LN₂ bath located at the intermediate region of HTS current leads could increase the lateral lead dimensions because the additional heat exchanger requires more space for installation.
- The temperature margin of the HTS current lead with LN₂ cooling is similar to 80 K helium cooling, but much smaller than with 50 K helium cooling.
- The LN₂ inlet temperature depends on the pressure drop inside the heat exchanger. A low pressure drop is recommended which reduced the heat exchanger efficiency.
- The use of sub-atmospheric pressurized LN₂ to reduce the inlet temperature requires the installation of a pump in the exhaust line of the current lead at room temperature. Any failure of the pump will immediately lead to an increase of the LN₂ temperature and a drastic reduction of the temperature margin of the HTS current lead. A redundancy of the pump is indispensable.

The following Table 7-11 shows the power consumption and a comparison of the reduction factors for 80 K and sub-cooled LN₂ operation at atmospheric and sub-atmospheric pressures for all ITER current leads. In LN₂ operations, the inlet temperature of the heat exchanger is considered as 77 K, and the T_{HTS, top} is different depending upon the particular operations like e.g. in case of atmospheric pressure condition, the temperature of the top of the HTS part was 83 K during operation whereas in stand by it was kept at 77 K. In the sub-atmospheric case, T_{HTS, top} = 70 K during stand by and in operation it was 80 K. In the calculation of the power consumption, 30% of Carnot efficiency is assumed in case of LN₂ cooling which is possible to achieve in practical cases [68].

Table 7-11 Comparison of 80 K helium with LN₂ cooling for the ITER HTS leads

Operation	Current	Power consumption (in MW)	Reduction factor
80 K operation	I = 0	0.403	3.15
	I = I _{max}	2.324	1.67
LN ₂ operation (atmospheric)	I = 0	0.483	2.63
	I = I _{max}	1.002	3.9
LN ₂ operation (Sub-atmospheric)	I = 0	0.446	2.84
	I = I _{max}	1.445	2.69

7.3 Capital Cost Analysis for HTS current leads for ITER

To estimate the real price of the conventional current leads for ITER is not an easy task, because it depends on many factors, for example on the heat exchanger design, the type of superconductor insert at the bottom of the lead (as already discussed in Chapter 5), the high voltage isolation requirements etc. If one looks for an optimized design of a heat exchanger and a Nb₃Sn type insert [64] then the current lead would cost much more compared to a simpler wire bundle or tube bundle heat exchanger and NbTi type sc wires at the cold end (at 4.5 K) of the conventional lead. To avoid discussions about cost to design relations, only the capital cost analysis for the HTS modules needed for the ITER current leads are assessed.

In the following cost assessment, only the current leads needed for the TF, CS and PF coils are considered; the CC current leads are not taken into account as discussed earlier. A detailed cost analysis of the HTS part has been performed using two different companies who have an infrastructure to manufacture the required HTS tapes and have the capability to carry out the processing of tapes to stacks.

American Superconductor Corporation (AMSC) and European Advanced Superconductors (EAS) are well known manufacturers of Bi-2223 based HTS tapes and stacks as per customer requirements. In order to compute the capital costs for the HTS current leads it is assumed that the difference to the conventional current leads is mainly due to the costs of the HTS part i.e. HTS module. This is because a conventional heat exchanger is needed for the both types of leads and the HTS lead requires small heat exchanger compared to the conventional one. So, the small savings in case of smaller heat exchanger will be balanced for the additional efforts to integrate the HTS module.

The basis of the capital cost estimations is the fabrication of a 70 kA HTS current lead. Using the data from the two suppliers (AMSC and EAS) the final capital costs for the HTS module for all ITER current leads are estimated.

To simplify the design, the number of panels and the number of stacks/panel are kept constant and only the number of tapes/stack are adjusted to obtain the current capacity for the specific maximum current of the TF, CS and PF coil systems. This is possible for case 1 (AMSC reference) but not for case 2 (EAS reference) because the lower critical current of the EAS tapes require more tapes. The resultant stacks would consist of up to 16 tapes which may cause manufacturing problems. Here, all leads are scaled to their specific maximum current.

7.3.1 Basic assumptions to the HTS current lead capital cost analysis

There are many numbers of leads required for ITER with different operating currents but nevertheless the concept of the design remains the same. After the construction of one prototype, we can neglect the design costs for the other leads.

The material costs are just directly proportional to the total length of required tapes. The AMSC reference costs for material came from the fact that twice the amounts of stacks were fabricated than needed at AMSC. So in the capital cost analysis for case 1 an overall series production reduction factor of 1.6 was assumed which includes 25% higher stack production than required for all leads. The EAS reference costs for material comes from series production estimation by the manufacturer. So in the capital cost analysis for case 2 there is no overall series production reduction factor.

For a large numbers of leads, the construction and assembly costs scale with the total number of units using an overall reduction factor of 2. This is the results of experience.

The testing costs at the company mainly depend on number of stacks and panels to be tested and in series testing the resultant value might be reduced by a factor of 2.

7.3.2 Results of the capital cost analysis for HTS current leads modules

Case 1 (AMSC reference)

From the 70 kA HTS current lead task, the AMSC Bi-2223 tape cost is deduced to be 128 € / meter including stack manufacturing. The quality inspection cost of the AMSC tapes per panel is 1.33 k€. Using the AMSC tapes critical current performance; with each tape I_c (77K, self-field) is 100 A. The total AMSC tapes requirements for the ITER current leads are given in the following Table 7-12.

As the critical current of tapes is a function of the field and the temperature, there are two components of the field which have to be considered, i.e. parallel and perpendicular component.

For the 70 kA HTS current lead, the maximum parallel component of B ~178 mT at 70 kA gives the critical current (I_c) of 40 A and the maximum perpendicular component of B ~119 mT at 70 kA gives (I_c) of 120 A.

One can get an average value of the effective I_c at 70 K as 80 A for our application.

Table 7-12: HTS Bi-2223 tape length requirements for ITER (AMSC reference)

System	Tapes /stack	Stacks /panel	Panels /lead	Total number of tapes / lead	Total number of panels for all leads	Total length of tapes for all leads (with same unit length)
TF	13	7	12	1092	216	13760 m
PF	10	7	12	840	144	7056 m
CS	9	7	12	756	144	6350 m
Total	-	-	-	-	504	27166 m

In Table 7-13, the cost break down for the ITER HTS modules using the AMSC reference is summarized.

Table 7-13 Cost break down for ITER HTS modules (AMSC reference)

	Single piece cost	Series production cost
HTS part		
Design cost	25 k€	25 k€
Material cost	83 k€	2.179 M€
Fabrication and assembly cost	53 k€	1.113 M€
Testing cost at the manufacturer	16 k€	0.336 M€
Total cost	177 k€	3.653 M€
Specific cost	3.11 k€/kA/lead	1.53 k€/kA/lead

Case 2 (EAS reference):

The EAS Bi-2223 tape costs are quoted to be 60 € / meter but with a lower critical current (I_c) compared to AMSC and also without stack manufacturing. EAS also offers stack manufacturing in the mean time (the tapes will be soldered instead of sintered) but the cost is not known.

The quality assurance cost per panel is assumed to be the same as for the AMSC reference, i.e., 1.33 k€. Since the EAS does not provide panels, the cost of testing might be different in case of EAS. As per EAS tapes, I_c at 70 K is 70 - 75 A for our application, the ITER current lead requirements are estimated and given in Table 7-14.

Table 7-14 HTS Bi-2223 tape length requirements for ITER (EAS reference)

System	Tapes /stack	Stacks /panel	Panels /lead	Total number of tapes / lead	Total number of panels for all leads	Total length of tapes for all leads
TF	12	9	12	1296	216	16330 m
PF	11	8	12	968	144	8131 m
CS	10	7	12	840	144	7056 m
Total	-	-	-	-	504	31517 m

In Table 7-15 the cost break down for the ITER HTS modules using the EAS reference are summarized. Here, it should be noted that the critical current of a tape is higher in case of AMSC compared to EAS, but the cost of the AMSC tape per meter is almost twice higher for AMSC. That is why one gets the overall cost lower in case of EAS compared to AMSC assuming other costs are same.

Table 7-15 Cost break down for ITER HTS modules (EAS reference)

	Single piece cost	Series production cost
HTS part		
Design cost	25 k€	25 k€
Material cost	45 k€	1.891 M€
Fabrication and assembly cost	83 k€	1.743 M€
Testing cost	16 k€	0.336 M€
Total cost	169 k€	3.995 M€
Specific cost	2.96 k€/kA/lead	1.67 k€/kA/lead

The difference between the cost estimations of AMSC and EAS references is about 10% which is within the error of uncertainty of such estimations.

To conclude, the HTS current lead modules require about 3.9 M€ which is the average between the AMSC and the EAS reference costs.

7.4 Summary of an ITER design with and without HTS current leads

The application of HTS current leads will provide a techno-economical solution for future fusion machines which use a superconducting magnet system consisting of low temperature superconductors (LTS) conductors. The operation costs analysis has shown the following cooling power per year for an ITER duty cycle:

Conventional current leads	2.164 MW
HTS current leads	
50 K He cooling ($T_{\text{HTS,top}} = 65 \text{ K}$)	0.638 MW
50 K He cooling ($T_{\text{HTS,top}} = 105/65 \text{ K}$)	0.53 MW
80 K He cooling	0.777 MW

Using electricity costs of 5 cents/kWh, one gets for the yearly costs

Conventional current leads	0.948 M€
HTS current leads	
50 K He cooling ($T_{\text{HTS,top}} = 65 \text{ K}$)	0.279 M€
50 K He cooling ($T_{\text{HTS,top}} = 105/65 \text{ K}$)	0.232 M€
80 K He cooling	0.340 M€

Depending on the cooling mode, the cost reduction is 0.716 M€ (50 K) to 0.608 M€ (80 K).

Concerning the HTS modules required for ITER, about 3.9 M€ are needed. To this number, design and development costs as well as costs for the fabrication and test of a prototype HTS current lead has to be added. Also the costs for the tests of the series current leads have to be taken into account.

The higher investment costs for the HTS current leads are more than compensated by the cost saving for the 4.5 K refrigerator plant. If looking to the maximum liquefaction capacity required for cooling all ITER leads, 130 g/s would be needed at 4.5 K which is equivalent to about 22 kW refrigeration capacity [38].

A 22 kW cryo plant unit will require much higher investment cost than the costs required for the HTS parts of the current leads [83]. Cost estimations for a 18 kW cryo plant unit result in about 10 M€ [37].

To conclude, the favoured operation options for the ITER HTS CLs would be either 50 K helium or 70 K LN₂-cooling (with sub-atmospheric pressure), both allowing a safe and stable operation even in case of LOFA. The cooling power consumption of 50 K helium and 70 K sub-atmospheric LN₂ are more or less same. The 80 K helium is less optimal with respect to the cooling power consumption. It also provides less temperature and time margin in case of LOFA. However, this option may be attractive for a device where plenty of 80 K cooling power is already available for the radiation shield cooling.

Chapter 8 – Conceptual design of a HTS current feeder system for ITER

The present HTS technology has reached the maturity that HTS conductors are applicable for a high current capacity feeder system as required in ITER. It is therefore interesting to investigate the substitution of the water cooled high current aluminum feeders by high temperature superconductor (HTS) feeders. In this chapter, the different design options of Bi-2223/AgMg/Ag based feeders as demonstrator unit modules for ITER are discussed. The performance of different cooling schemes for HTS feeders is studied and the design related critical issues e.g. bending of the feeder, thermal losses including steady state and pulsed (AC) losses, different cooling schemes, the bus bar termination (metallic transition to room temperature) and finally techno-economical aspects for ITER are investigated.

8.1 Introduction

In the ITER project, a techno-economic feasible solution of its current feeder system is envisaged in order to eliminate the Joule heating of the water-cooled Aluminium feeders and to reduce the overall space for the installation. As part of a task collaboration of CRPP and the Forschungszentrum Karlsruhe, the possibility to replace the part of high current water-cooled Al feeders by HTS feeders has been investigated. Because the ITER magnet system has a considerable varying duty cycle of operation i.e. 32% for the TF and 6% for the PF and CS systems, it is essential to optimize the operational costs of the current feeder system by taking into consideration both, the maximum and the idle currents [2]. In this chapter, the conceptual design of the HTS feeders for the TF (at maximum conductor current of 68 kA), PF (at maximum conductor current of 52 kA) (in the backup mode) and CS (at maximum conductor current of 45 kA) coils of ITER is described. A maximum discharge / test voltage of 17.5 / 36 kV for these feeders is envisaged. The design is based on the availability of 50 K helium or 70 K sub-cooled LN₂ and a maximum temperature of the HTS feeders of 65 K or 75 K, respectively. In addition, the economic aspects related to the replacement of the conventional current leads and the Al feeders by HTS feeders are discussed [84]. Figure 8.1 shows the conceptual scheme of a HTS current feeder system for the ITER TF coils in case of the 50 K helium cooling. As described in chapter 4, the route layout of the Al bus bars is not clearly defined so far [59]. So the conceptual design of a 12 m long unit module of a HTS feeder is investigated.

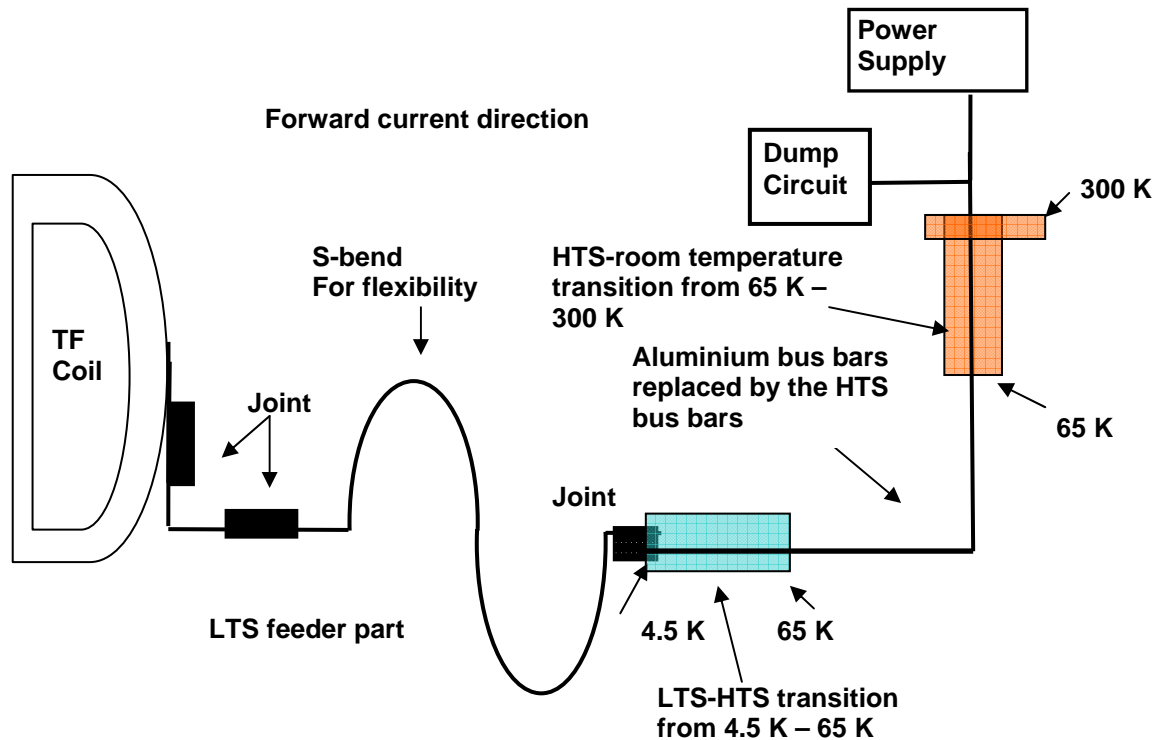


Figure 8.1 Conceptual layout of the TF current feeder system with a combined LTS / HTS bus bar system in case of 50 K helium cooling

8.2. Design concept of the HTS feeders for ITER

8.2.1 Design Drivers

The HTS feeders have to fulfill the following requirements:

- (i) The HTS feeders should be designed for the minimum steady state heat loads of 1-2 W/m except joint and vacuum barrier losses.
- (ii) As the PF and CS feeders are operating under pulsed current conditions leading to AC losses, the designed bus bars should have minimum AC losses as per average plasma current with full ITER plasma cycle of 1800 s for different current operation reference scenarios discussed in APPENDIX-I [2].
- (iii) Use of the warm dielectric insulation scheme should be preferred.
- (iv) The HTS tapes within the conductor area as well as the central channel (former) should be actively cooled.
- (v) A temperature margin of at least 15 K should be maintained at the maximum current operation.
- (vi) The bus bar and its metallic transition to room temperature should be Paschen tight.
- (vii) Smooth bending and flexibility to fulfill the space requirements are mandatory.

8.2.2 HTS feeder design concept

Many design and development activities for HTS cables are reported for power applications [85 - 87]. There exist two concepts, one with a stacked layout and another based on power transmission cable design. The stacked layout of the HTS feeder is not desirable for long lengths, as it needs a long furnace for preparing the stacks and also bending of the stacks is not permitted. The power transmission cable concept is suited for long lengths with a flexible cryostat. Here, for the ITER HTS feeders, the main focus is given on the power transmission cable concept. The conductor is housed in a flexible evacuated steel cryostat with thermal and electrical insulation. The superconducting tapes (Bi-2223/AgMg/Ag) are wound onto a flexible stainless steel former. The vacuum and an optimum number of superinsulation layers, so-called MLI, are used as thermal insulation and as electrical insulation; a warm dielectric insulation is preferred for protection against high voltage and simplicity of the design. Finally, a steel shield will be wrapped around the warm dielectric for mechanical protection.

Active forced-flow cooling of the HTS tapes, alternatively in the bundle and in the central flexible pipe, is considered with two possible different cooling schemes, i.e., 50 K helium and 70 K sub-cooled LN₂ as discussed in detail in section 8.4. Because of the constant number of Bi-2223 tapes in the different layers there exists a small gap between adjacent tapes in the outermost layers for the coolant flow. If the coolant space is not sufficient then additional spacers may be introduced. A sketch of a superconducting power transmission cable with a warm (room temperature) dielectric insulation is shown in Figure 8.2. For the DC operation of the TF feeders, the current distribution among the layers is determined by the contact resistances whereas in the case of the pulsed operation of the PF and CS feeders, the mutual inductances are also of importance. In the development of superconducting power transmission cables it was found that for a constant twist pitch and alternating coiling direction most of the AC current flows in the outermost layers of the cable. This behaviour is a consequence of the variation of the self and the mutual inductances of the different layers. A uniform current distribution among the layers can be achieved by variation of the twist pitches of the individual layers as a consequence the winding angle increases continuously from a negative minimum to a positive maximum value [88 - 89]. A power transmission cable is designed for 50 Hz application which is different from the pulsed operation. The AC losses are connected to the time integral of a square of time derivative of the field, frequency, winding pitch and conductor geometry.

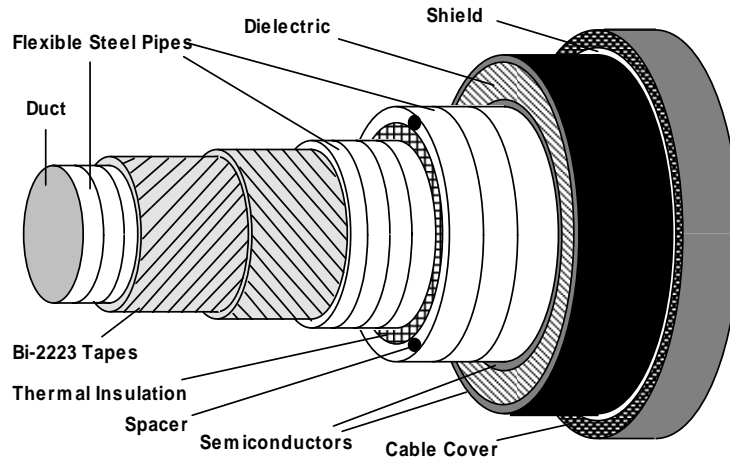


Figure 8.2 Illustration of a single-phase warm dielectric power transmission cable [84]

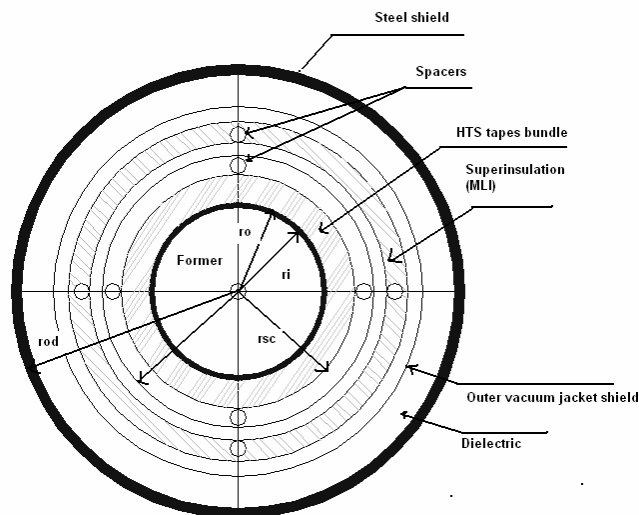


Figure 8.3 Cross-section of an HTS power cable showing the main dimensions

The main dimensions of the HTS feeder are defined in Figure 8.3. The superconducting Bi-2223/AgMg/Ag tapes (4 mm width x 0.22 mm thickness) from EAS are wound on to a commercially available flexible corrugated steel tube (from Flexwell™ tubes) with an inner radius of r_i and outer radius of r_o respectively. Due to the twist of the tapes within the feeder, the actual width of the tape w is enlarged by a factor of cosine of the twisting angle φ with respect to the axial direction given by,

$$W_{eff} = \frac{W}{\cos \varphi} \quad (8.1)$$

The actual number of tapes per layer is given by, n as mentioned below,

$$n = \left(\frac{2\pi r_0}{w_{\text{eff}}} \right) \quad (8.2)$$

Where n is an integer number. The detailed optimization between the total numbers of tapes with respect to the critical current of particular HTS feeders for ITER is discussed in section 8.3.

The thermal insulation of the HTS feeders is provided by a vacuum space within the MLI (superinsulation) between the two flexible corrugated tubes as shown in Figure 8.3.

The electrical insulation of a HTS feeder is provided by a dielectric (e.g. Teflon) which surrounds the outer flexible stainless steel pipe of the thermal insulation. The maximum electric field in the dielectric is

$$E_m = \frac{1}{r_{\text{id}}} \frac{U}{\ln(r_{\text{od}}/r_{\text{id}})} \quad (8.3)$$

Where U is the voltage, r_{id} the inner and r_{od} the outer radius of the dielectric.

8.3 Design optimization of the HTS feeders

To reach high critical current densities in cuprate superconductors, a network of low-angle grain boundaries is required. In Bi-2223 tapes, a c -axis texture is sufficient to reach high critical current densities. This means that the crystallographic c axis of the superconducting filaments is perpendicular to the broad face of the tapes. Because of their layered structures the cuprate superconductors are characterized by highly anisotropic physical properties. Therefore, the field dependence of the critical current of the textured Bi-2223 tapes depends on the direction of the applied magnetic field with respect to the crystallographic c direction. The decrease of the critical current is more pronounced for magnetic fields parallel to the crystallographic c axis, i.e. perpendicular to the broad face of the tapes. In the proposed feeder design, the maximum magnetic field at the outermost Bi-2223 layer is parallel to the broad face of the tapes, which is the favourable field direction. Magnetic fields in the unfavorable field direction occur at conductor bends and are also generated by the return conductor.

In the HTS power transmission cable design, the magnetic field component parallel to the broad face of the tape, B_{parallel} , is always larger than that of the perpendicular component, $B_{\text{perpendicular}}$, because the tapes are wound in a layered form on a thin conductive tube. The illustration for a single tape is shown in Figure 8.4. This assumption depends strongly on the real distance between adjacent tapes and also on

the distance between the different layers. For example the insertion of a spacer would increase the perpendicular component generated by the stray field of the other layers.

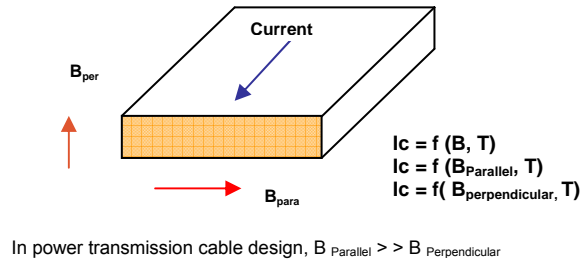


Figure 8.4 Illustration of current carrying single HTS tape

The critical current of a single tape as a function of the parallel and perpendicular components of the magnetic field and the operating temperature are discussed in the following description. Figure 8.5 shows the critical current of a single Bi-2223/Ag/AgMg tape as a function of $B_{parallel}$ for the different operating temperatures. The data are based on the I_c values of Bi-2223/Ag/AgMg tapes from European Advanced Superconductors (EAS).

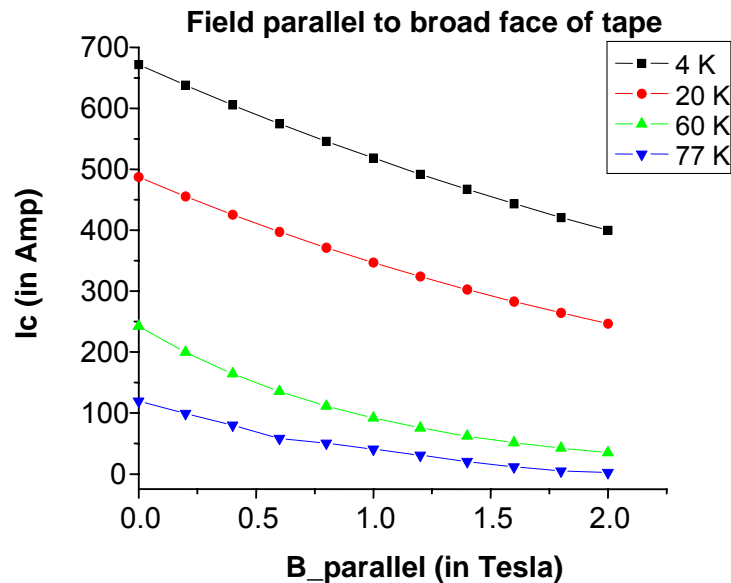


Figure 8.5 Critical current characteristics of a single Bi-2223/Ag/AgMg tape

The temperature dependence of the critical current of cuprate superconductors at zero applied magnetic fields can typically be well represented by the scaling law [84] [90].

$$I_c = I_{c0} \left(1 - \frac{T}{T_c} \right)^\alpha \quad (8.4)$$

Where I_{c0} is the critical current at zero temperature, T_c the critical temperature and α is a scaling exponent. The values of the scaling parameters are:

$$I_{c0} = 728.9 \text{ A}, T_c = 111.8 \text{ K}, \text{ and } \alpha = 1.54$$

For a given operating temperature, scaling laws are obtained for the critical current as a function of the scaling of the magnetic field and the temperature, separated in the low field regions [90]. Figure 8.5 shows the critical current of the Bi-2223 tapes as a function of the magnetic field applied parallel to the broad face of the tapes. The critical current decreases nearly exponentially with increasing applied field in the low and the high field region. The reciprocal values of the slopes of the straight lines can be considered as scaling of the fields. Generally, the scaling of fields for the low field region is considerably smaller than those for the high field region. In the present design, the maximum self-field of the HTS feeder is below 1 T for 70 kA. Thus, the main focus is given on the low field scaling law.

Low field scaling law:

$$I_c(B, T) = I_c(T, 0) \exp\left(-\frac{B}{B_{sc}}\right) \quad (8.5)$$

$$B_{sc}(T) = B_{sc0} - bT \quad (8.6)$$

Here, $I_{c0} = 728.9 \text{ A}$, $T_c = 111.8 \text{ K}$, and $\alpha = 1.54$

Here, B_{sc0} and b are known as the scaling parameters. They are used to describe the critical current of the Bi-2223 tapes in the low field region.

For particular temperature, let us say $T_{hts} = 65 \text{ K}$, the critical current of a Bi-2223/Ag/AgMg tape is plotted in Figure 8.6. Table 8-1 summarizes the low field scaling parameters.

Table 8-1 Scaling parameters for the critical current of the Bi-2223 tapes in the low field region for magnetic fields applied to the broad face of the tapes.

Scaling Parameter	Parallel Field	Perpendicular Field
$B_{sc0} \text{ (T)}$	3.15	0.574
$b \text{ (T/K)}$	0.0351	0.0062

The scaling laws are applicable for the estimation of the critical current of a single tape within an accuracy of 10 – 30%. The amount of superconductor optimization study has been carried out with different former sizes as commercially available flexible corrugate steel tubes from Flexwell™.

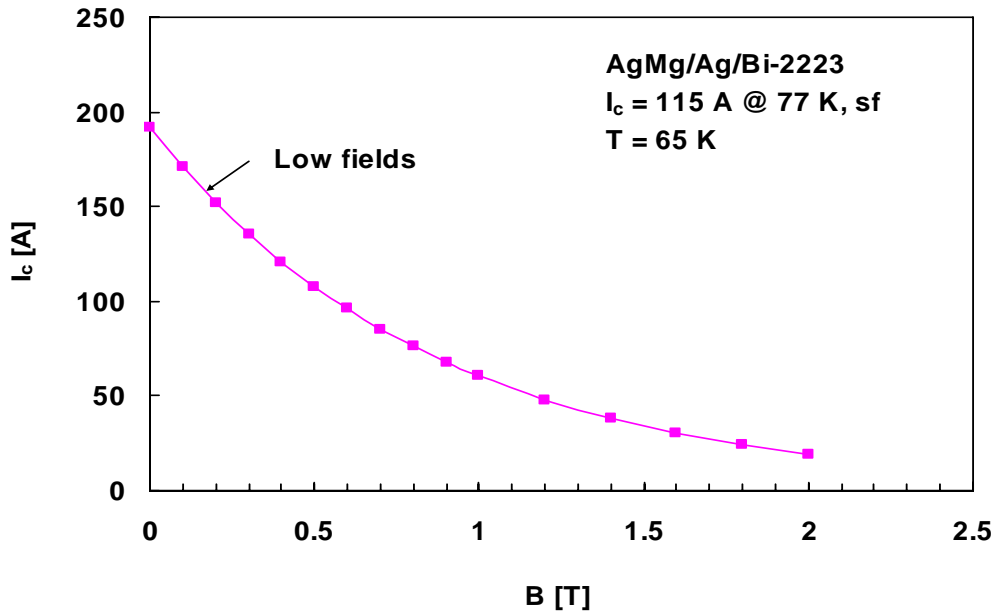


Figure 8.6 Critical current of Bi-2223/Ag/AgMg tapes as a function of the magnetic field applied along the broad face of the tapes at 65 K

In order to gain in the bus bar cross-section at least by a factor of 2-3 compared to water-cooled Al bus bars, three different diameters of the formers have been analyzed in the present study.

The critical current of the feeder has been determined for three different flexible steel formers sizes with outer radius r_o values of 26.5, 34.0 and 42.25 mm. The corresponding number of tapes in a single layer is 35, 46 and 57 for a tape winding angle of 20° . Here, an effective width of the tape of 4.7 mm is considered instead of actual width of the tape of 4.4 mm.

The magnetic self-field in parallel direction generated by the multi-layer cable conductor is given by [84],

$$B_s = \frac{\mu_0 n N I}{2\pi(r_o + N t)} \quad (8.7)$$

Where n is the number of Bi-2223 tapes per layer, N the number of layers, I the average current carried by a single tape, r_o the outer radius of the stainless steel former and $t = 0.22 \text{ mm}$ the thickness of a single Bi-2223 tape.

The critical current of the tape $I_c(B_s)$ and the critical current of the feeder I_c^{bb} are defined as following,

$$I_c(B_s) = \left(\frac{2\pi(r_0 + Nt)B_s}{\mu_0 Nn} \right) \quad (8.8)$$

$$I_c^{bb} = NnI_c(B_s) \quad (8.9)$$

As mentioned in equations 8.8 and 8.9, it is clear that the critical current of the feeder increases with the number of layers whereas the critical current of the single tape decreases for a fixed number of tapes per layer. This is because as the number of layers increases the self-field of the feeder increases and the effective I_c for a single tape is decreasing.

The nominal operating current of the TF feeders is 68 kA. To limit the ratio of the operating to the critical current I_{op}/I_c to a value of 0.8, the basis for this factor is to maintain at least 15 K temperature margin. For that the minimum required critical current of the TF feeders is 85 kA. The nominal operating current of the PF and CS feeders is 45 kA. In the case of the PF feeders a back-up mode with a conductor current of 52 kA is foreseen. To limit the value of I_{op}/I_c in the back-up mode to 0.8 a feeder critical current in excess of 65 kA is needed. To avoid the necessity of a third bus bar design identical layouts will be used for the PF and CS feeders.

In the following, the different layouts are described for the two cooling options investigated, i.e., the 50 K helium and 70 K sub-cooled LN₂ cooling.

8.3.1 50 K helium design

The 50K helium design is worked out for three different diameters of the former i.e. 53 mm, 68 mm, and 84.5 mm respectively. The design is based on availability of the 50 K helium and the warm end temperature of an HTS feeder is at 65 K considered. As an example, the design optimization for the former diameter of 84.5 mm is shown in detail. In Figure 8.7, the average current of a single tape in the bus bar is plotted as a function of the maximum magnetic self-field (so called single tape load line) for different number of layers as resulted from equ.8.7. The number of tapes per layer has been fixed to 57 for the former outer diameter of 84.5 mm. The intersections of the $I_c(B,T)$ line and the straight lines, describing the relation between the self-field and the tape current, provides the critical currents of the tapes in the different multi-layer bus bars for an operating temperature of 65 K. The straight lines describe the relation between the critical currents of the tapes and the magnetic self-field at the outermost layer. Similar type of load lines of I_c can be generated for all other considered former diameters. The

critical current of the feeder as a function of the number of Bi-2223 layers and the operating temperature has been determined for all the former diameters and is shown in Figures 8.8, 8.9, and 8.10 respectively.

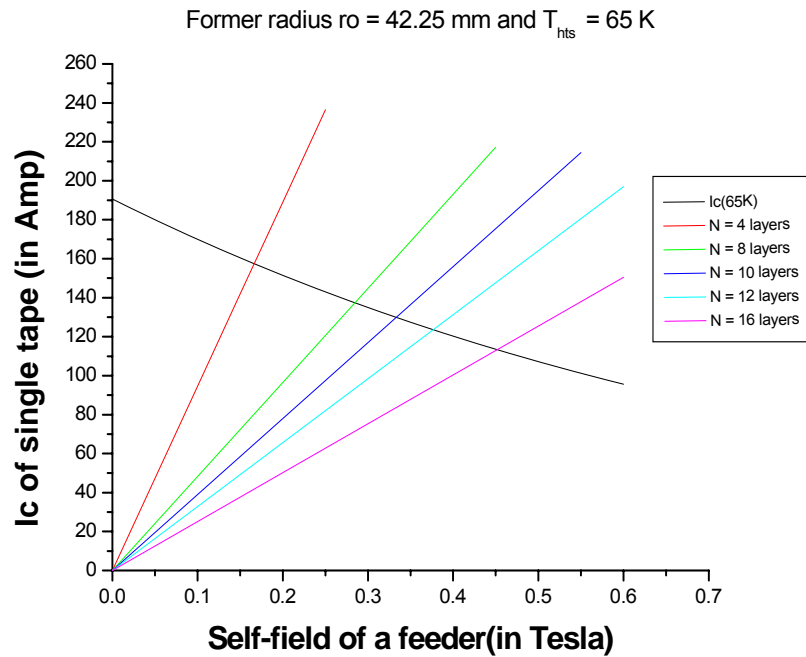


Figure 8.7 Determination of the critical current of Bi-2223 tapes in the multilayer feeder at 65 K.

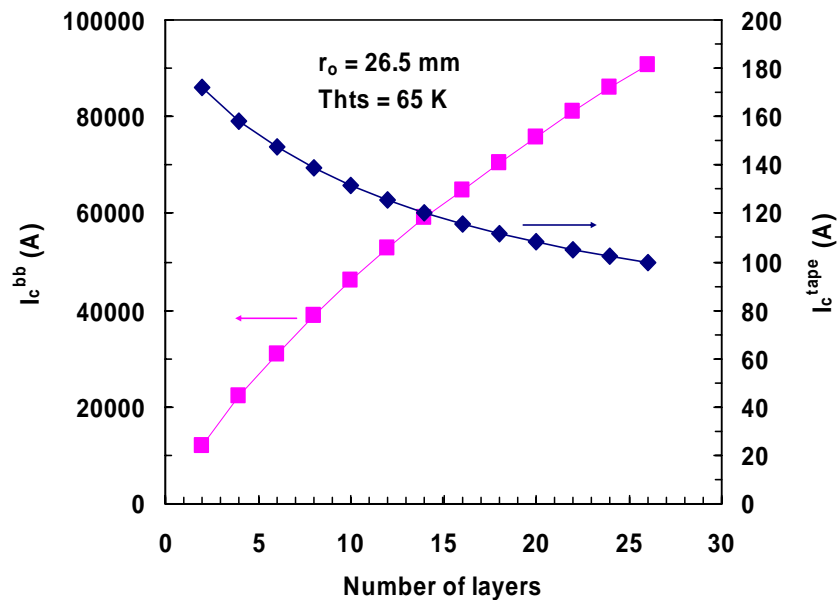


Figure 8.8 Critical currents of the feeder and the tape at 65 K as a function of the number of Bi-2223 layers wound onto a flexible stainless steel pipe of 26.5 mm outer radius

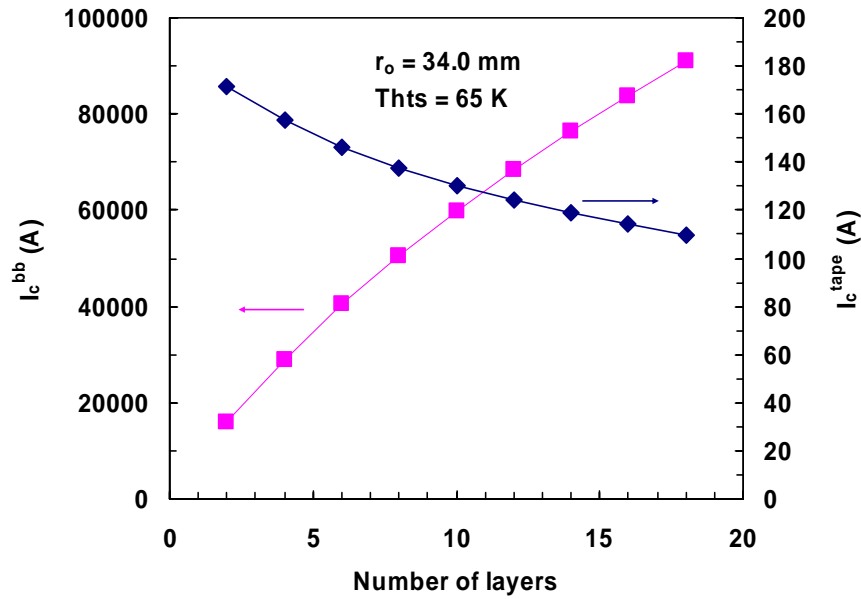


Figure 8.9 Critical currents of the feeder and the tape at 65 K as a function of the number of Bi-2223 layers wound onto a flexible stainless steel pipe of 34.0 mm outer radius

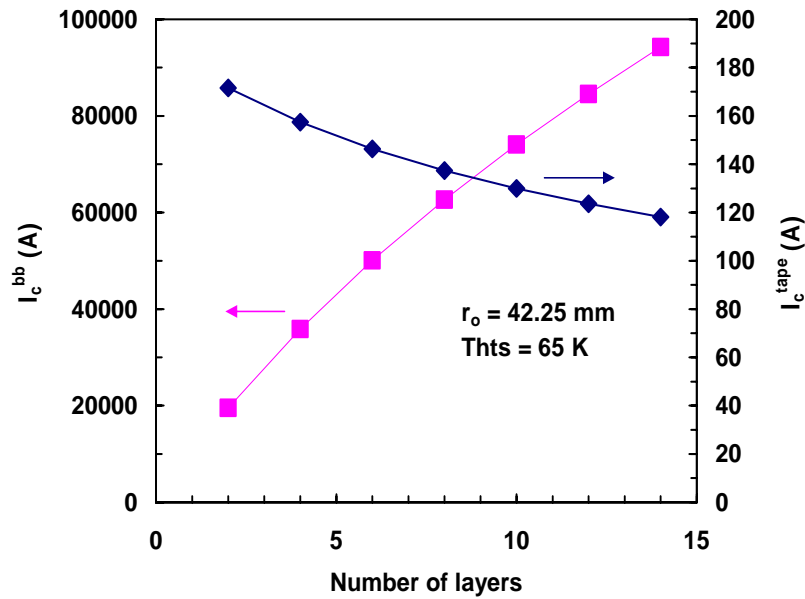


Figure 8.10 Critical currents of the feeder and the tape at 65 K as a function of the number of Bi-2223 layers wound onto a flexible stainless steel pipe of 42.25 mm outer radius

The results show that the critical current of a single tape decreases as the number of layers is increased but the overall critical current of the feeder is increasing. The actual optimized number of layers should be determined from the feeder critical current requirement using an intersection value of the $I_c(B,T)$ corresponding to the self-field of the feeder.

From the Figures 8.8, 8.9, and 8.10, it is clear that in order to achieve the critical current of 85 kA for the TF HTS bus bar,

- (i) 35 tapes per layer and 24 layers are required for the former outer diameter of 53 mm
- (ii) 46 tapes per layer and 16 layers are required for the former outer diameter of 68 mm
- (iii) 57 tapes per layer and 12 layers are required for the former outer diameter of 84.5 mm

Similarly, in case of the PF and CS HTS feeders, the total number of tapes and layers can easily be deduced for different former sizes from above figures. The choice of the particular former size depends upon the amount of superconductor used, heat loads, and the space for installation. Here, the main focus is given on the minimization of an amount of the superconductor in the feeder due to its higher cost implications. It seems that the former diameter of 84.5 mm with 12 numbers of layers would be appropriate to achieve the TF feeder critical current of 85 kA. Similarly, for the PF and CS HTS feeders, the former diameter of 84.5 mm with 8 numbers of layers would be sufficient to achieve the critical current of 65 kA. So, hereafter the main study will focus on the former diameter of 84.5 mm only. Other former diameters will be neglected for further discussions.

8.3.2 70 K sub-cooled LN₂ design

If the operating temperature is increased, the critical current of the single tape is reduced and a large number of tapes are necessary to meet the requirement, which in turn increases the total number of layers as well as space requirements. As the 70 K sub-cooled LN₂ operation is concerned, the feeder design is carried out also with the former (diameter of 84.5 mm) and the operating temperature is 70 K and corresponding the HTS tape temperature of 75 K are considered in the following analysis.

In Figure 8.11, the average current of a single tape in the bus bar is plotted as a function of the maximum magnetic self-field (so called single tape load line) at 75 K for different number of layers as resulted from equ.8.7. The feeder critical current as a function of the number of Bi-2223 layers is shown in Figure 8.12.

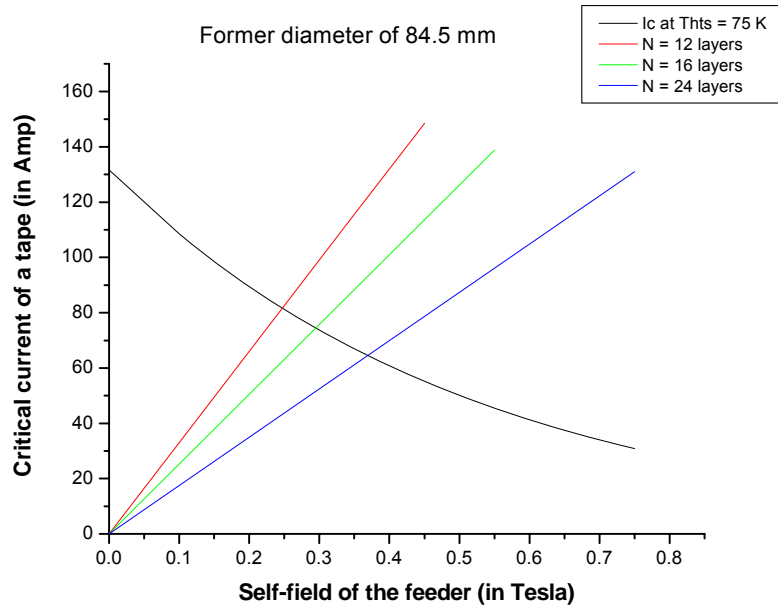


Figure 8.11 Determination of the critical current of Bi-2223 tapes in multilayer feeder at 75 K.

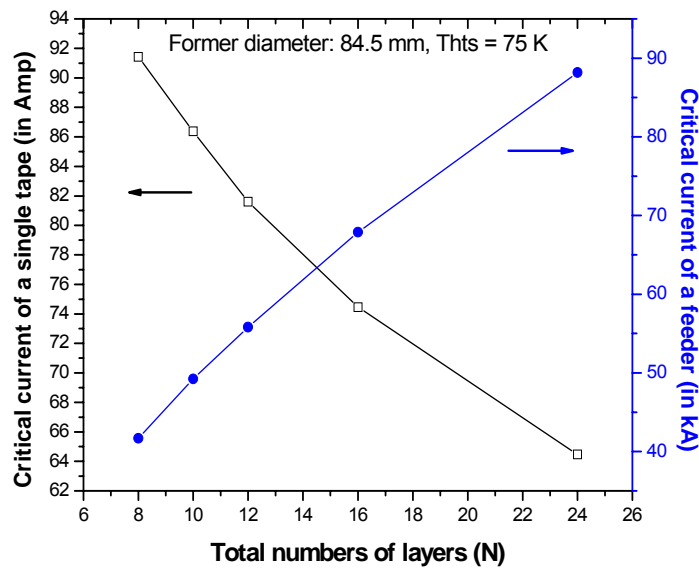


Figure 8.12 Feeder and tape critical currents at 75 K as a function of the number of Bi-2223 layers wound onto a flexible stainless steel pipe with a former diameter of 84.5 mm

From Figure 8.12, it is clear that the total numbers of 23 layers are sufficient to achieve the critical of 84.5 kA for the TF feeder and 18 layers are sufficient to achieve the critical current of 65 kA for the PF and CS HTS feeders with a former diameter of 84.5 mm and operating temperature of 75 K.

8.3.3 Comments on 80 K helium design

The thermal shields of ITER will be cooled by helium gas of 80 K inlet temperature [38]. Therefore, it would be desirable to use this helium gas also to cool the HTS bus bars at 80 K helium. In the meantime, the operation of the 70 kA EU HTS current lead with 80 K helium cooling has been experimentally demonstrated that the 80 K helium cooling is possible [67– 69]. For this reason the operation of the HTS bus bars with warm end temperatures between 80 and 85 K has been considered. The results of these estimations are described in [89]. The main result of this estimation is that for a former diameter of 68 mm diameter, 38 layers of Bi-2223/AgMg/Ag tapes would be required for an operating temperature of 80 K, resulting in a total number of tapes of ~ 1725 . It seems to be not feasible to wind such a large number of layers onto a cable former. In addition, severe problems in the current distribution among the layers may occur. Also the required amount of superconductor is enormous. Operating temperatures of 80 K or above would lead to unreasonably high superconductor costs for the HTS bus bars.

8.3.4 Effect of an external magnetic field and of the bending on the HTS feeder performance

In the region of a bend the magnetic field is enhanced as compared to a straight conductor. In addition, field components perpendicular to the broad face of the Bi-2223 tapes are generated. The magnetic field for a bend of 1000 mm radius has been estimated for the TF feeder design with a former diameter of 84.5 mm. A sketch of the conductor arrangement is shown in Figure 8.13. In the calculation of the magnetic field the bus bar is represented by a single current line in the centre. The procedure is to use the race track EFFI model similar to that described in [91]. The detailed results of the field calculations are presented in [84].

The magnetic field at the surface of the outermost superconducting layer of a straight TF feeder, based on the design with a former diameter of 84.5 mm, is 303 mT at the nominal current of 68 kA. The results indicate that for a bend of 1000 mm radius the maximum field perpendicular to the broad face of the tapes is approximately 21 mT at a current of 68 kA. The maximum magnetic field is reached in the centre of the bend region. The maximum parallel field reaches a value of ≈ 331 mT at a current of 68 kA. The critical current in the bend region at a temperature of 65 K is limited by the enhanced parallel field and not by the additional field component perpendicular to the broad face of the tapes. The reduction of the tape critical current due to the enhanced tangential field is less than 5%.

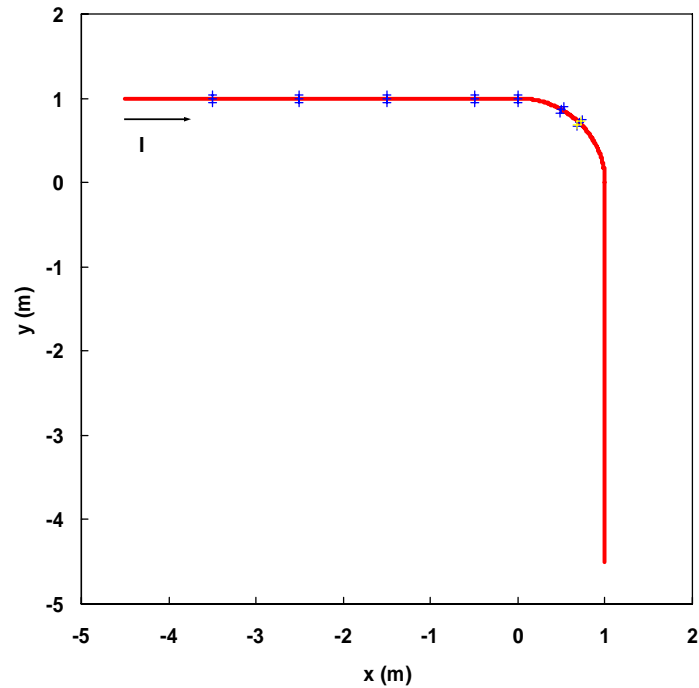


Figure 8.13 Conductor arrangement used for the estimation of the magnetic field at the positions marked by the crosses.

- **Magnetic Field of the Return Conductor**

For a power cable type bus bar with a conductive former, the self-field is always parallel to the broad face of the tape surface. Taking into consideration the return conductor, it creates a stray field which has field components parallel and perpendicular to the broad face of the tapes.

In the case of the TF feeder design with a former diameter of 84.5 mm, the outer radius of the superconducting layers is 44.89 mm. The self-field generated by a single conductor at the nominal current is 0.303 T. The outer diameter of the bus bar is approximately 170 mm. Taking into consideration the return conductor, its stray field has field components parallel and perpendicular to the broad face of the tapes. Assuming, that the distance of the return conductor is 300 mm, the contribution of the return conductor to the maximum magnetic field parallel to the broad face of the Bi-2223 tapes is 0.053 T. The resulting maximum tangential magnetic field is 0.356 T. The maximum magnetic field perpendicular to the broad face of the tapes is 0.0464 T. The critical current of the tape at 65 K in tangential magnetic fields of 0.303 and 0.356 T are 134.5 and 126.6 A, respectively. On the other hand, the critical current of the tape at 65 K for a magnetic field of 0.0464 T, perpendicular to the broad face of the tape, is 145 A. Thus,

the critical current is not limited by the small field perpendicular to the broad face of the tapes generated by the return conductor. The critical current of the feeder at 65 K is reduced from 84.5 to 80.3 kA. Thus, the enhancement of the parallel magnetic fields leads only to a 5% reduction of the critical current of the feeder.

8.4 Description of the HTS feeder cooling schemes

There exist two possible cooling methods for the HTS feeders as mentioned below.

- (i) Active cooling of the HTS tapes bundle along with the former (central channel)
- (ii) Only the former (central channel) is cooled and the HTS tapes within the bundle are cooled by conduction

The second method is only applicable for 1- 4 kA class HTS power cables where only less number of HTS tapes and layers are required compared to the high current HTS feeders of ITER.

The first method gives the assurance of safe and reliable cooling because all the HTS tapes within the bundle region are actively cooled for a feeder and the central channel so called former is also cooled via the return path as shown in Figure 8.14. In this method, first the fresh helium or sub-cooled LN₂ passes through the HTS tape bundle area and return back to the former.

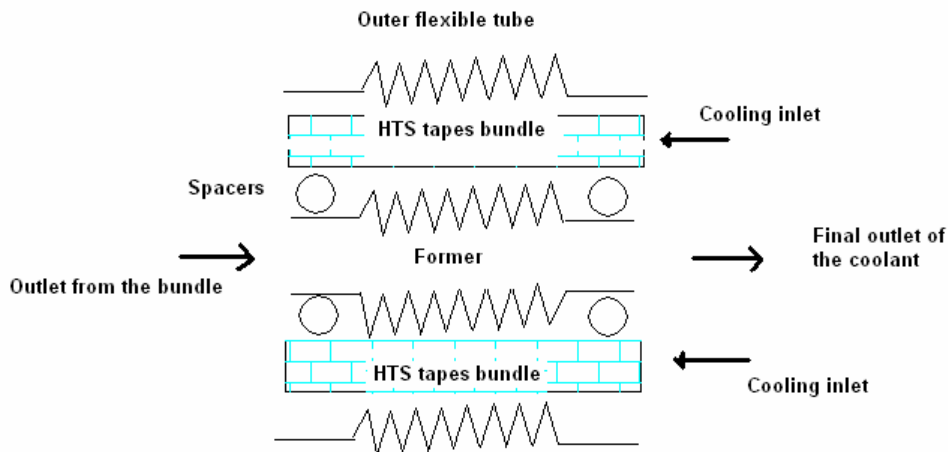


Figure 8.14 Cooling scheme of the HTS feeders for ITER

Following above concept, it is possible to cool the HTS feeder using either forced flow 50 K helium or sub-cooled LN₂ at 70 K. The forced flow cooling of 1-3 kA class HTS power cable with sub-cooled liquid nitrogen (LN₂) at 70 K has been discussed in the literature [92].

8.4.1 Cooling scheme with 50 K helium

The 50 K helium cooling of the HTS feeder system is done by a closed helium cycle as shown in Figure 8.15, in which the room temperature helium flow at a pressure of 20 bar passes through the purifier and a 80 K helium cold box with an efficient pre-cooler working with LN₂. Here, the main stream of the 80 K helium is distributed to the ITER thermal shield cooling circuit but a part of the flow will be diverged from this circuit for the cooling of the LTS/ HTS transition region and HTS feeder respectively. The bottom part of the HTS module is cooled in series with the LTS bus bar with the separate forced flow 4.5 K Helium cooling branch. In this scheme, the turbine generates the 50 K helium stream with an isentropic expansion of 80 K Helium gas at 8 – 9 bar. The 50 K helium stream is produced and used to cool the HTS feeder as shown in Figure 8.15. The stream cools the HTS bus bar and the conventional transition heat exchanger in a series cooling mode. Finally, the return stream comes out at room temperature and fed back to the main compressor to close the loop.

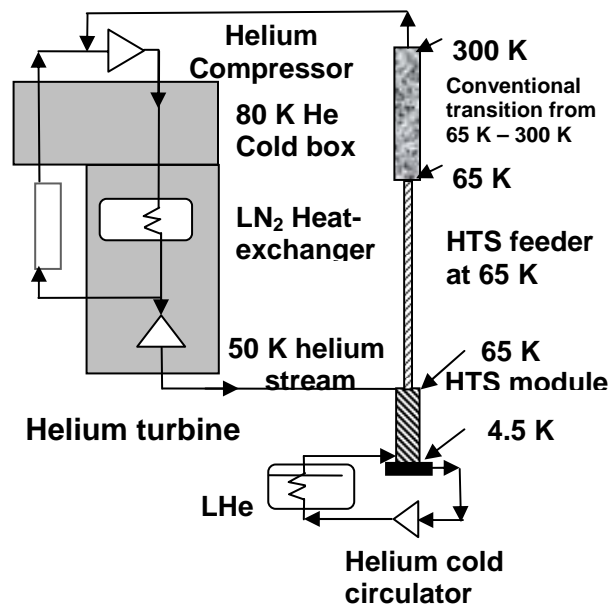


Figure 8.15 50 K helium cooling scheme for the HTS feeder system [93]

8.4.2 Cooling scheme with sub-cooled LN₂

As a second option, it is also possible to cool the HTS feeder with forced flow sub-cooled liquid nitrogen at 70 K. The cooling flow scheme is shown in Figure 8.16. The sub-cooled liquid nitrogen (secondary loop) is produced with the help of a specially designed sub-cooler dewar. It consists of an efficient heat exchanger, a vacuum pump

and a LN₂ bath (primary loop) at 70 K. The temperature of 70 K is obtained by reducing the pressure in the primary loop. The liquid nitrogen level in the secondary loop will be maintained by continuous filling from the main LN₂ storage tank, which is kept at a pressure of 2.5 bar which corresponds to a saturation temperature of around 86 K. This high pressure LN₂ stream will be used to cool the HTS feeder. The feeder termination which serves also as the transition to room temperature is also part of this cooling scheme. Finally, the nitrogen gas is released at the outlet of the termination and vents directly to the atmosphere with a control valve.

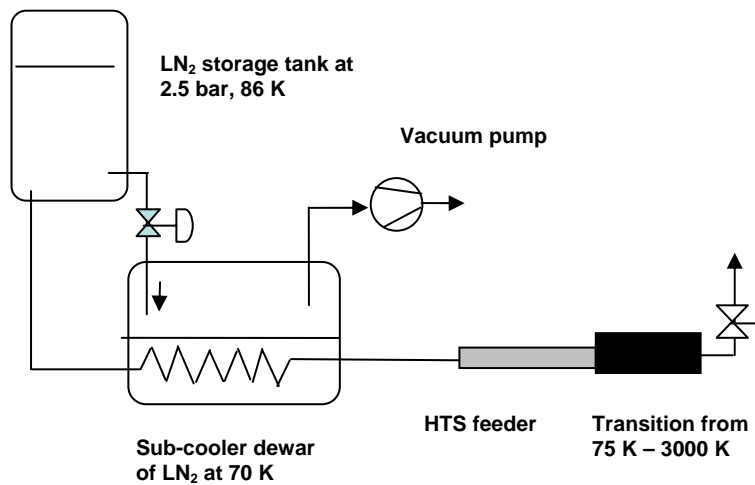


Figure 8.16 Sub-cooled LN₂ cooling for the HTS bus bar and its transition at 75 K [93]

8.5 Thermal analysis of the HTS feeders

8.5.1 Steady state and pulsed heat losses analysis

Several steady state heat loads are acting on the HTS feeder including radiation, conduction, usual end connection losses like e.g. Joint losses and contributions from power supply ripples. In case of pulsed operating feeders like e.g. for the PF and CS HTS feeders one will have additional pulsed losses so-called AC losses.

The heat leak through the superinsulation is given by [84],

$$Q_c = \left(\frac{2\pi K(T_2 - T_1)}{\ln\left(\frac{r_{10th}}{r_{2th}}\right)} \right) \quad (8.10)$$

Here, K is the thermal conductivity of the superinsulation (in W/m-K), T_1 and T_2 are the temperatures of the cold and warm surfaces respectively, r_{10th} and r_{2ith} are the radii space between the superinsulation is occupied within the feeder.

The thermal conductivity of the superinsulation is 2×10^{-4} W/m-K for 50 – 70 K operations. The values of r_{10th} and r_{2ith} are considered as 54.6 mm and 73.5 mm for the former diameter of 84.5 mm in case of all the HTS feeders. The basic formulae for radiation power loss (in Watt) is given by,

$$Q_{rad} = \left(\frac{\sigma A_1 (T_2^4 - T_1^4)}{\left(\frac{1}{\epsilon_1} \right) + \left(\frac{A_1}{A_2} \right) \left(\frac{1}{\epsilon_2} - 1 \right)} \right) \quad (8.11)$$

Where, T_1 and T_2 are the temperature of the cold and warm surfaces respectively, σ = Stefan Boltzmann constant = 5.67×10^{-8} (Watt/m²-K⁴), A_1 and A_2 are the surfaces areas of the cold and warm surfaces. The ϵ_1 and ϵ_2 are the emissivities of the cold and warm surfaces. Here, $\epsilon_1=0.08$ and $\epsilon_2 = 0.2$ have been considered for the present analysis and could possible to be reduced by providing 20 layers of superinsulation.

Joule heating is generated at both ends of the HTS feeder, from the 70 kA HTS current lead experience, it is possible to achieve an overall contact resistance of 20 nOhm at both sides for temperature range of 50 – 70 K.

A vacuum barrier of steel (SS 304 L / SS 316 LN) with an optimized length of 300 mm and 160 mm outer diameter contributes to the conduction loss with 5.0 Watt.

During the test of the 70 kA HTS current lead the voltage measurements were affected by the 600 Hz ripple of the power supply. The question arises, if the 600 Hz ripple of the power supply causes ripple losses in the HTS feeders. In the case of the PF and CS coils the AC losses due to the pulsed operation are expected to be much larger than the 600 Hz ripple losses. The ripple current is $\Delta I = V_L/R_L = 28.7 \text{ V} / 66.7 \text{ k}\Omega = 0.43 \text{ mA}$. Consequently the ripple current is only of the order 10^{-8} of the transport current of 68 kA. Based on this estimation it can be expected that the AC losses caused by the 600 Hz ripple of the power supply would be negligible in the ITER HTS feeders.

As the PF and CS feeders for ITER are operated in pulsed mode, there will be the AC losses acting on these feeders. The AC losses include different sources like e.g. hysteresis losses, transport current losses, magnetization losses, eddy current losses in the former and coupling losses due to different twists and layered structures within the cable.

It is possible to minimize the eddy current losses in the former by using braided corrugated structural material e.g. steel. The coupling losses could possibly be overcome by using optimized twisting techniques. A uniform current distribution among the layers can be achieved by a variation of the twist pitches of the individual layers as consequence of the winding angle which increases continuously from a negative minimum to a positive maximum value [88 - 89]. In the present case, the transport current (hysteresis) losses will be estimated for the ITER PF and CS HTS feeders. By using the standard Norris formulae with the mono block model, an upper limit of the transport current loss could be calculated. In a hollow cylinder the transport current loss per cycle is given by [94],

$$Q_{AC} = \frac{\mu_0 I_{c0}^2}{\pi t_{cycle}} \left[(1 - \Gamma) \ln(1 - \Gamma) + \Gamma - \frac{\Gamma^2}{2} \right] \quad (8.12)$$

Where,

$$\Gamma = \frac{I_p}{I_{c0}} \quad (8.13)$$

Here, μ_0 is the permeability of the free space; I_p and I_{c0} are the peak current and fictitious critical current. The fictitious critical current (I_{c0}) is defined as,

$$I_{c0} = \pi r_{sc}^2 j_{ov} \quad (8.14)$$

Where r_{sc} is the outer most radius of superconducting layer and j_{ov} is overall critical current density. The AC losses in the PF and CS bus bars have been estimated for the reference operating scenario described in ITER DDD [2]. The conductor currents required in the CS and PF coils during the reference scenario are listed in Appendix-I. The biggest variation in the currents (+39.9 kA to -45 kA) is foreseen for the CS coil units CS1U and CS1L. In the estimation of the transport current AC losses averaged over a full cycle of 1800 s length a peak current of ± 45 kA were used. For all considered PF/CS bus bar designs the AC losses averaged over a full cycle of 1800 s are lower than 0.004 W/m, which is much smaller than the thermal losses.

The heat loss is not varying much in the temperature range of 50 K - 70 K from the ambient (300 K). At 70 K operation, the contact resistance is 10% higher than the 50 K operation so the Joule heating will slightly increase at 70 K. Tables 8-2 and 8-3 show the summary of heat loads at 50 K and 70 K respectively with the former diameter of 84.5 mm for all the HTS feeders. The heat loads are summarized for a unit module length of 12-m for all the HTS feeders

Table 8-2 Summary of heat loads at 50 K operation

Source	TF feeder	PF / CS feeder
Thermal conduction due to superinsulation	12 W	12 W
Radiation	9.3 W	9.3 W
Joule heating for Joint-1 (towards HTS module side)	9.25 W	5.4 W
Joule heating for Joint-2 (towards transition side)	9.25 W	5.4 W
Vacuum barrier	5.0 W	5.0 W
Ripple loss due to power supply	0.012 W	-
AC losses	-	0.048 W
Total	~ 45 W	~ 37 W

Table 8-3 Summary of heat loads at 70 K operation

Source	TF feeder	PF / CS feeder
Thermal conduction due to superinsulation	11.6 W	11.6 W
Radiation	10.2 W	10.2 W
Joule heating for Joint-1 (towards HTS module side)	10.1 W	6.0 W
Joule heating for Joint-2 (towards transition side)	10.1 W	6.0 W
Vacuum barrier	4.8 W	4.8 W
Ripple loss due to power supply	0.014 W	-
AC losses	-	0.005 W
Total	~ 47 W	~ 38.6 W

So, from above results it is clear that there is no significant variation in the total heat loads within the 50 – 70 K range for a particular HTS feeder. For simplicity a generalized unique heat load of 47 W at 50 – 70 K for the TF HTS feeders and 39 W at 50 – 70 K for the PF / CS HTS feeders are reasonable to be considered as upper limits for the heat loads.

8.5.2 Hydraulic analysis

The one dimensional (1-D) hydraulic model of the TF HTS feeder is developed as shown in Figure 8.17, as it has maximum operating current among other feeders. The hydraulic study includes the analysis of optimization of coolant requirements, the pressure drop and the coolant inlet/outlet conditions. The analysis has been carried out for the two cooling options i.e. 50 K Helium and sub-cooled LN₂ at 70 K.

The estimation of the pressure drop and the heat transfer coefficient in case of 50 K helium is carried out as single channel steady state helium analysis, already discussed in chapter 6. The hydraulic analysis related to sub-cooled LN₂ at 70 K of a flexible corrugated pipe is done by using the models described in [92].

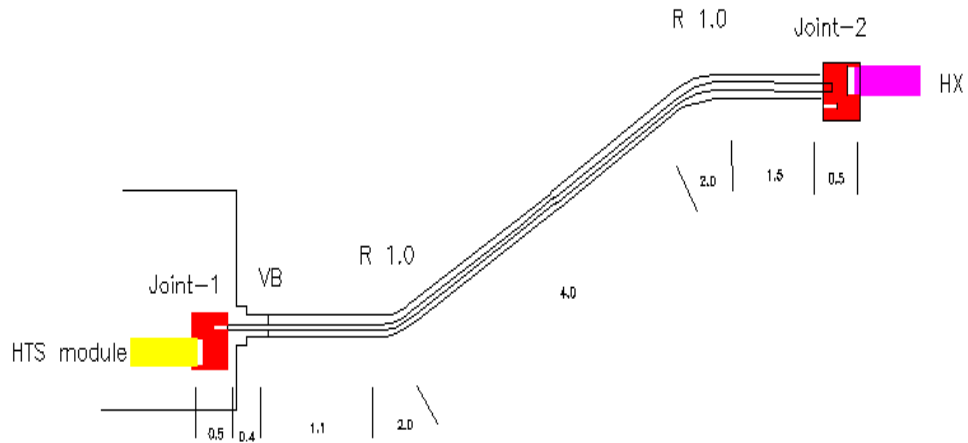


Figure 8.17 Model of an HTS bus bar with two bends

Table 8-4 Results of 1-D hydraulic analysis for the TF bus bar

Parameters	50 K helium cooling	70 K (LN ₂ sub-cooling)
Flow length	12 m	12 m
Inner diameter of the bundle	84.5 mm	84.5 mm
Free gap within the bundle	4.5 mm	2.0 mm
Void fraction within the bundle region	67.8%	37.5%
Cooled perimeter within the bundle	4.734 m	8.789 m
Flow area	1000 mm ²	760.7 mm ²
Inlet pressure	6.0 bar	2.6 bar
Inlet temperature	50 K	70 K
Total mass flow rate	5 g/s	12 g/s + 2.2 g/s for sub-cooler
Pressure drop	0.027 bar	0.15 bar
Total heat load	47 W	47 W
Available heat transfer coefficient	355 W/m ² K	300 W/m ² K
$\Delta T = T_{out} - T_{in}$ in the bus bar	1.79 K	~2.05 K
Refrigeration plant efficiency	0.284	0.30
Power consumption	~ 24 kW	~27 kW + 5 kW LN ₂ for sub-cooler

As the 50 K helium option needs less number of layers compared to 70 K sub-cooled LN₂, for the fixed dimension of the former and cryostat, the void fraction is higher in case of 50 K helium. Due to a higher flow area of the coolant smaller pressure drop is obtained in case of 50 K helium compared to 70 K cooling.

Here it is important to note that the power consumption of 50 K helium is lower than that of 70 K sub-cooled LN₂ because an additional cooling power is required for continuous filling of the sub-cooler with LN₂ in order to absorb the heat load of the heat exchanger which is dipped in the bath of sub-cooled LN₂ at 70 K. The heat load of 384 W is expected for the heat exchanger. The latent heat of vaporization for single phase sub-cooled LN₂ is 176 J/gm at 2.5 bar pressure, which leads to a steady state evaporation of 2.2 g/s from the sub-cooler dewar. For the above mentioned values of heat loads, the sub-cooled LN₂ stays within the single phase region and can be confirmed by the pressure – enthalpy (p-H) diagram of sub-cooled LN₂ with above mentioned operating conditions because here the pressure drop of 0.15 bar will have nearly isenthalpic expansion with negative J-T effect so there will be a little temperature rise. Thus, it will not cause any two-phase choking problem for 12 m length.

It is interesting to note that in case of ITER, when the actual length of the HTS feeder will be more than 12 m, the situation might be different. Because as the length of the HTS feeder is increasing, the heat loads as well as the pressure drop are also increasing. So corresponding the temperature margin might reduce and there might be a chance of generation of two-phase flow. Also, the inlet supply pressure of the storage supply dewar is limited to 2.5 bar maximum. Thus, for a longer length of the HTS feeder the cooling with sub-cooled LN₂ at 70 K will not be possible compared to 50 K helium cooling. The 50 K helium will be attractive due to the lower power consumption and it also provides a higher temperature margin and a lower amount of superconductor compared to sub-cooled LN₂ option. Finally, Table 8-5 summarizes the main parameters of the HTS feeders at 50 K helium operation for ITER.

Table 8-5 Summaries of the main parameters of HTS feeders (at 50 K helium) for ITER

	TF HTS feeders	PF /CS HTS feeders
Operating current	68 kA	45 (52) kA
Critical current	85 kA	66 kA
Discharge /test voltage	17.5 / 36 kV	17.5 / 36 kV
HTS tape	Bi-2223/AgMg/Ag	Bi-2223/AgMg/Ag
Tape dimensions	4.4 mm x 0.22 mm	4.4 mm x 0.22 mm
Former dimensions	(ID / OD) (80 / 84.5 mm)	(ID / OD) (80 / 84.5 mm)
No. of tapes per layer	57	57
No. of layers	12	8
Electrical insulation	(ID / OD) (162.5 / 181 mm)	(ID / OD) (162.5 / 181 mm)
Feeder outer diameter	(ID/ OD) (164.5 / 185 mm)	(ID/ OD) (164.5 / 185 mm)

8.6 Feeder termination (metallic transition to room temperature)

The function of the bus bar termination is to connect the HTS feeder located at lower temperature, i.e., around 65 K – 70 K, to the bus bar located at room temperature for the connection to the discharge network and to the power supply. The Paschen tight design of such a transition and the HTS feeder is essential. The design of the termination can be similar to that of a conventional heat exchanger part used in current leads. This design requires attention for material selection and geometrical dimensions in order to minimize the losses i.e. an optimization has to balance conductive and resistive losses as well as cooling. A typical termination is similar to the heat exchanger of the 70 kA HTS current lead developed at the Forschungszentrum Karlsruhe for the high current capacity current leads [63] which can be used for the transition from 65 K – 300 K is shown in Figure 8.15. In Table 8-6 the main results of the conventional transition (65 K – 300 K) pieces in case of 50 K helium cooling are summarized. These parameters are scaled from the experiments carried out for a 70 kA HTS current lead as demonstrator for ITER [67] [68].



Figure 8.15 Photograph of the conventional heat exchanger of the 70 kA HTS current lead [63]

**Table 8-6 Main results of the conventional heat exchanger for the HTS bus bar transition
(50 K helium cooling)**

Parameter	TF transition	PF transition	CS transition
Maximum operation current	68 kA	52 kA	45 kA
Critical current	85 kA	65 kA	>56 kA
Current operation	Steady state	Pulsed	Pulsed
Material	E-copper	E-copper	E-copper
RRR	50	50	50
Length	700 mm	700 mm	700 mm
Cu-cross section	6368 mm ²	4139 mm ²	3582 mm ²
Top/bottom temperature	290 K / 65 K	290 K / 65 K	290 K / 65 K
Helium inlet temperature	50 K	50 K	50 K
Mass flow rate (I=0)	2.17 g/s	1.66 g/s	1.44 g/s
Mass flow rate (I=I _{max})	4.7 g/s	3.58 g/s	3.1 g/s
Q _k (I = 0)	13.46 W	10.29 W	8.91 W
Q _k (I = I _{max})	30.57 W	20.29 W	16.4 W

8.7 Techno-economical comparison study with the conventional bus bars

Finally, the operation and capital investment costs of the Al bus bars and the HTS feeders for 50 K helium operation have been estimated and compared. The capital cost of the HTS feeders is mainly governed by the cost of an amount of superconductor needed. Here, each type of HTS feeders i.e. the TF, PF and CS with single length of 12 m is considered for the costs comparative analysis. All the HTS feeders are considered with the former diameter of 84.5 mm.

- **Capital cost estimation for the amount of superconductor used**

The capital cost of the HTS feeders is based on the availability of Bi-2223 / AgMg / Ag tapes from EAS at the rate of 60 € /m. The actual required length of the tape is larger by a factor $1/\cos\phi$ than the length of the feeder because of the twist pitch. In the present cost estimation, a twist angle of 20° is used. In principle, the required length of the tapes is further increased because some material is needed for the forerun in the winding process. Table 8-7 summarizes the total capital investments cost for the HTS tapes for each type of single HTS feeders in ITER.

Table 8-7 Summary of the total capital investment costs for HTS tapes for each type of single HTS feeders in ITER

Feeder	n	N	Total number of tapes for unit length	Total number of tapes for 12 m	Effective length using twist	Cost @ 60 € /m
TF	57	12	684	8208	8734	525 k€
PF	57	8	456	5472	5823	350 k€
CS	57	8	456	5472	5823	350 k€

(Here, n is total numbers of tapes per layer and N is total numbers of layers)

So, the total capital cost of the HTS tapes is 1225 k€

- **Capital and operation costs for the water-cooled Al bus bars for ITER**

It seems to be reasonable to assume that the costs for the ITER TF bus bars would be comparable to those for the 80 kA bus bars installed for the 70 kA HTS current lead test at the Forschungszentrum Karlsruhe. The numbers are as follows [95]:

Engineering design, drawings etc. 42.0 k€

Material, fabrication including water cooling,

Assembly, leak and insulation tests 6.40 k€/m

It is also assumed that the engineering design costs would be valid for the single feeder only; other feeders could be made by the same design layout. The costs for the material and fabrication including tests are linearly scaled for all the feeders depending upon the design current requirements. Table 8-8 summarizes the capital investment costs of the each type of water-cooled Al bus bars in ITER.

Table 8-8 Capital investment costs for the water-cooled Al bus bars in ITER

Bus bar	Design cost	Material, fabrication and test costs for unit length	Material, fabrication and test costs for 12 m
TF (68 kA)	42.0 k€	6.4 k€ /m	76.8 k€
PF (52 /45 kA)	-	4.3 k€ /m	51.6 k€
CS (45 kA)	-	4.3 k€ /m	51.6 k€

So, the total costs of the each type of single 12 m long water-cooled Al feeders is around 225 k€.

It is clear that the total cost of the HTS material is 5-6 times higher than the capital cost of water cooled Al bus bars. But as the water-cooled bus bars are of conventional type,

they generate Joule heating in terms of electrical power loss and comparable water cooling charges depending on the operation duty cycle of the machine. In case of ITER, the operation duty cycle of the TF system is 32% average over a year and of the PF /CS systems its 6%. By considering the total operation hours of 8760 hrs per year, the TF system would be under operation for 2803 hrs whereas the PF / CS systems will be operating for 525 hrs respectively,

If one assumes an electricity cost for 1 kW-hr of 0.05 € then the power consumption cost for 1 year of operation would lead to around 7.5 k€ for each type of single bus bars as basic electrical load discussed in chapter 4. Similar cost is also applied for water cooling charges. Finally, the total operation cost of each type of single water cooled Al bus bars is around 15 k€ per year. The accumulated operation cost for 20 years then comes out to be 300 k€, it seems that there is not sufficient saving using the HTS feeders due to their higher capital costs. But in future, superior performance of the HTS tapes at rather lower cost would be available in the market by which the amount of superconductor as well as capital cost for the superconductor would reduce reasonably. Of course, looking at the present design, one could save in the space for their installation. The present ITER TF water cooled Al bus bars have dimensions of 236 x 217 mm², leading to a cross-section area of 51212 mm² whereas in case of TF HTS feeders an outer diameter of 180 mm is required, leading to 25434 mm², so at least one can save on the cross-section by a factor of 2 using the HTS feeders.

Chapter 9 - Conclusions and future prospects

9.1 Conclusions

A detailed conceptual design and analysis of a LTS feeder system for ITER has been carried out. A steady state model of the TF feeder has been worked out taking into account the magnetic field, i.e., self field of the feeder, stray field from the ITER torus and stray field of the return conductor. The different cooling modes have been analysed and compared to judge the best performance of the feeder. Despite of any types of cooling mode, the outlet of the feeder has the lowest temperature margin. So in turn a feeder cooling providing the inlet at the coil side and the outlet at the current lead side is the favoured solution. To obtain a temperature margin of 1.5 K, a minimum mass flow rate of forced flow supercritical helium of 3.4 g/s in the bundle region is required for a safe and reliable operation of the TF feeder under normal conditions.

A detailed one dimensional transient thermo-hydraulic analysis has been carried out for the TF, PF and CS feeders in order to evaluate the helium mass flow rate taking into account the central cooling channel of the bus bar conductor and to study the performance under fault conditions, i.e., loss of helium mass flow rate (LOFA) and quench. The analysis showed that under normal operating conditions, the TF feeder requires a total helium mass flow rate of 5 g/s, the PF feeder requires 4.6 g/s and the CS feeder requires 4.2 g/s in order to provide a safe and reliable operation. The estimation has shown that the time averaged AC loss in (W/m) is negligible over a full plasma cycle ($t_{\text{cycle}} = 1800$ s) for the ITER plasma current reference scenario (inductive operation, 15 MA).

The quench initiation and propagation in the TF feeder was studied by simulating short time energy input which would be generated during a conductor movement. To simulate the typical external disturbance due to conductor movement, an external heat is imposed on the superconducting cable at the center location. The results show that a minimum heat energy density of 2638 kJ/m^3 was required to provoke a quench in the conductor. The quench evolution is more intense at the center of the conductor where actually the energy disturbance is applied. The temperature evolution with respect to time shows homogenous propagation. The voltage rise and normal zone propagation length show that the quench propagation speed is quite slower than that of the magnets. Only 1 – 2 m normal zone length is developed for a detectable voltage level of 50 mV and the maximum conductor temperature of ~ 25 K is estimated. Also the pressure rise within the heated zone is only 0.6 bar initially and then it gets stabilized over time to 0.4 bar as an average pressure rise compared to the inlet pressure of 6 bar.

In case of a LOFA event at rated current in the TF feeder and no initiation of a safety discharge of the magnet the temperature along the feeder will rise due to the external heat deposition and resistive heat generation of the joints. Since the temperature margin is lowest at the current lead end while cooling from the magnet side, the feeder will start quenching from the current lead side. The results show that the quench propagation is much slower than in the coils. After 38 s the current sharing temperature is reached at the outlet of the feeder. After the quench has started, about 10 further seconds are needed to reach a detectable voltage level of ~40 mV and the length of the normal zone of about 1.5 m. In case of the PF and CS coils, the feeders are even more stable; it took more than 90 s to reach current sharing temperature.

In case of a LOFA event and following a safety discharge of the magnet (dump time of 12 s, detection time of 1 s and delay time of 1 s), the results show that the TF feeder is safe and stable up to 90 s after the LOFA started; since after 90 s, there will be no current in the feeder as it was discharged, the feeder will not quench. The conductor temperature remains lower than the critical temperature. So, it will be easy to handle a LOFA even with following a safety discharge in case of the TF feeder.

The application of HTS current leads will provide a techno-economical solution for ITER. The cooling power required for the current leads can be considerably reduced if HTS current leads will be used. The operation cost analysis has shown that the cooling power per year for an ITER duty cycle can be reduced by a factor of 4 – 12 depending on the cooling modes for the HTS current leads, i.e., either 50 K helium, or 80 K helium. In turn, the cost reduction is 0.716 M€ for 50 K helium cooling and 0.608 M€ for 80 K helium cooling for one year operation assuming electricity costs of 0.05€/kWh. The 80 K helium operation is less optimal with respect to the cooling power consumption. However, it may be attractive if enough 80 K cooling power is already available for radiation shield cooling.

A sub-atmospheric liquid nitrogen (LN₂) operation at 70 K would require more HTS material than the 50 K helium operation but would save a substantial amount of HTS material compared to 80 K operation. Such an operation would be possible with reliability and redundancy of the vacuum pump which generates the sub-atmospheric pressure. An attention should be given for the design of the heat exchanger because the temperature of LN₂ is limited by the pressure drop in the heat exchanger as well as on the sizing of a proper liquid nitrogen inventory for safe operation.

Concerning investment costs required for the HTS modules for the ITER current leads, about 3.8 M€ are required. To this number, design and development costs as well as costs for the cold test of the HTS current leads have to be added.

The higher investment costs for the HTS current leads are more than compensated by the cost saving for the 4.5 K refrigerator plant. If looking to the maximum liquefaction capacity required for cooling all ITER leads, 130 g/s would be needed at 4.5 K which is equivalent to about 22 kW refrigeration capacity. A 22 kW cryoplant unit will require higher investment cost than the costs required for the HTS parts of the current leads. An estimated cost for the cryoplant unit is about 10 M€.

The conceptual design, the optimization and the main parameters of a HTS feeder model for ITER have been investigated, which is similar to that used for HTS power transmission cables. To reach a reasonably small number of layers it is necessary to operate the bus bars at temperatures of 65 K – 75 K.

For such a high current HTS feeders design, the operation temperature is one of the main control parameters. The optimization between the amount of superconductors needed and the operation cost of the cryogenic system is essential. Both the 50 K helium and the 70 K sub-cooled LN₂ cooling are possible options for the ITER HTS feeders. The 50 K helium option looks more economic because less amount of superconductor is needed compared to 70 K sub-cooled LN₂ and 80 K helium cooling. Sub-cooled LN₂ cooling consumes more power and gives less temperature margin compared to 50 K helium cooling but the LN₂ cooling system is much simpler compared to the helium cooling scheme. But for a longer length of HTS feeders, the LN₂ cooling scheme may not be desirable due to higher pressure drop, larger heat loads and limited input pressure from the main LN₂ storage dewar.

A thermal heat load of the order of 2-3 W/m has been found in case of the TF HTS feeder for an optimized diameter of the former of 84.5 mm. The AC losses in the PF and CS bus bars averaged over a full plasma cycle have been found to be negligible compared to the thermal losses. The cooling power required for a combination of the HTS feeder and its termination is expected to be not significantly larger than that necessary to cool only the HTS current lead. Based on the present Bi-2223 performance and conductor prices, the total cost of the HTS tapes is 1225 k€ and the capital cost of each type (TF, PF, and CS) of single water-cooled Al bus bar is 225 k€ both calculated for a length of 12 m. Finally, the total operation costs is 300 k€ for 20 years of operation. It seems that there is not sufficient savings using the HTS feeders due to their higher capital costs. But in future, the superior performance of HTS tapes at rather lower cost would be available in the market so that the capital costs and the size of HTS current feeders would be reduced.

The main advantage of the use of HTS feeders instead of water-cooled aluminium bus bars could be the reduction of the required space. Using flexible stainless steel pipes of optimized dimensions, the cross-section of the HTS feeders may be reduced at least by

a factor of 2 as compared to the water-cooled Al bus bars. For the use of HTS feeders it would be desirable to have a small number of bends with a sufficiently large bending radius. As the HTS feeders are far away from the main magnet systems of ITER, there is no influence of any external magnetic field on the feeder except the return feeder. The optimization of the amount of superconductor, the design of the transition part, and economic and reliable cooling schemes are the key issues for the HTS feeder design.

9.2 Future prospects

In order to promote the applications of HTS materials in ITER and beyond, several future prospects may be drawn from this present work.

The conceptual design and thermo hydraulic analysis of the LTS feeder system for ITER provides a baseline for the actual optimization. The helium mass flow rate optimization is essential to ensure a safe and reliable operation. The one dimensional thermo-hydraulic analysis using Gandalf code is an appropriate computational tool for the estimations of the quench and stability parameters as it is valid for dual channel CICC.

The use of HTS current leads provides a techno-economical solution for ITER. The successful test of a 70 kA HTS current lead demonstrator developed in the EU fusion program has already shown that the HTS materials have reached their maturity and benefits could be achieved. The 70 kA HTS current lead prototype for the TF feeder system should be made according to this line. In case of the PF and CS pulsed magnet systems, the conductor currents required in the CS and PF coils during the reference scenario are listed in Appendix-I. The biggest variation in the currents (+39.9 kA to -45 kA) is foreseen for the CS coil as well as PF coils. Thus, the current lead heat exchanger should be designed for the average current of the various operation scenarios whereas the HTS modules have to be designed for the maximum operation currents. Finally, the series HTS current leads for ITER can be manufactured after successful fabrication and test of the prototype.

Here, the design of the HTS feeder system is worked out as a unit module of 12 m length because in the present ITER design the room temperature routing of the feeders is not clearly defined. The test results of the prototype HTS feeder will verify the conceptual design, operation parameters and the performance of cooling schemes. This R & D activity is necessary to acquire the knowledge required for a later serial fabrication. Finally one general remark is given which is beyond the scope of the thesis: For fusion machines towards DEMO and commercial reactors, the development of a HTS fusion conductor will be the key to operate the magnet system at higher temperatures, or higher magnetic fields. The high temperature superconductors provide

plasma volume and/or the toroidal magnetic field need to be enhanced. Thus the favourable physical properties of the high temperature superconductors may be used to increase either the operation temperature of the magnet system or the toroidal magnetic field. The operation of the magnet system at liquid nitrogen would increase the thermodynamic efficiency while an increase of the toroidal magnetic field would allow in principle a more compact design of a fusion reactor. Presently the use of Bi-2212, Bi-2223 and YBCO conductor material is under investigation in the long term program within the fusion community. But there are several challenges to overcome like e.g. cabling and bundling techniques, and large-scale winding techniques, large electromagnetic forces and stresses, higher heat loads including steady state and AC losses, and neutron flux influence.

As soon as HTS magnets in the temperature region of ≥ 65 K would become applicable, this would eliminate the use of any type of current leads because the HTS magnet may be connected to the power supply being at the room temperature via HTS feeders (at 65 K – 75 K) and a conventional transition part (from 65 K – 300 K).

**Appendix-1: Current operation reference scenario in ITER
(Inductive operation, 15 MA)**

Table 1 Currents in the CS conductors during the reference operating scenario in ITER.

Magnet	CS3U	CS2U	CS1U	CS1L	CS2L	CS3L
Time (s)	I (kA)					
0	39.9	39.9	39.9	39.9	39.9	39.9
1.6	35.9	34.7	35.7	35.7	32.4	35.9
4.61	33.2	31	25.8	25.8	29.1	34.6
7.82	30.8	27.6	20.8	20.8	26.2	33.3
11.38	28.4	24.2	16	16	23.2	32.1
15.24	26	20.8	11.7	11.7	20.3	30.8
19.52	23.6	17.4	7.4	7.4	17.3	29.6
24.17	21.2	14	3.3	3.3	14.4	28.3
29.37	18.9	10.6	-1.2	-1.2	11.4	27.1
35.25	13.6	8.9	-6.4	-6.4	8.4	24.9
42.12	8.4	7.2	-11.3	-11.3	4.7	22.6
49.26	6.7	5.5	-17.1	-17.1	2.9	20.4
56.21	4.6	2.6	-22.1	-22.1	0.5	18.2
63.22	3.5	-1.8	-26.5	-26.5	-3.3	17.3
72.55	1.7	-6.1	-31.5	-31.5	-6.8	15.4
100	-2.1	-16	-40.4	-40.4	-15.6	10.3
105	-2.3	-16.5	-39	-39	-15.7	9
110	-2.4	-16.8	-38.1	-38.1	-15.8	8.1
115	-2.4	-17	-37.5	-37.5	-15.9	7.4
120	-2.5	-17.2	-37.1	-37.1	-16.1	6.9
125	-2.5	-17.2	-37	-37	-16.2	6.6
130	-2.6	-17.3	-37.1	-37.1	-16.4	6.5
530	-3	-35	-44.9	-44.9	-32.1	1
546	-0.8	-36.8	-43.8	-43.8	-32.5	0.6
564	2.4	-38.9	-42.3	-42.3	-32.9	0.3
580	5.8	-40.8	-40.8	-40.8	-33.3	0.2
590	6.8	-42.6	-43.2	-43.2	-34.6	2.2
616.6	1.6	-41.4	-39.5	-39.5	-33.6	-1.4
647.4	-4.6	-37.7	-32.9	-32.9	-30.7	-5.4
668.3	-8.7	-33.9	-27.4	-27.4	-28.4	-8.1
689.1	-12.9	-26.6	-23.6	-23.6	-24.3	-10.9
710	-17	-17.8	-17.8	-17.8	-17.8	-13.6
720	-19.1	-18.2	-18.2	-18.2	-18.2	-16.4
900	0	0	0	0	0	0
1490	0	0	0	0	0	0
1790	39.9	39.9	39.9	39.9	39.9	39.9
1800	39.9	39.9	39.9	39.9	39.9	39.9

Table 2 Currents in the PF conductors during the reference operating scenario in ITER.

Magnet	PF1	PF2	PF3	PF4	PF5	PF6
Time (s)	I (kA)					
0	38.2	5.9	2.6	2.2	3.5	19.9
1.6	32.8	2.5	1.8	1.2	0.4	19.3
4.61	34	-9.9	1.5	1.8	-8.4	21.8
7.82	35.2	-17.9	4	-5.1	-7.5	24
11.38	36.4	-20.4	3	-8.4	-8.7	26.2
15.24	37.5	-21.9	1.2	-10.9	-10.9	28.4
19.52	38.7	-21	-2.8	-10.3	-15	30.6
24.17	39.9	-21.8	-5.9	-10.3	-19.3	32.8
29.37	41	-21.3	-9.8	-10.8	-23.1	35
35.25	39.8	-21.3	-12.5	-12.5	-25.4	36.5
42.12	38.6	-22.1	-15.2	-13.7	-27.8	38
49.26	35	-22.5	-17.7	-15.6	-29.1	38.6
56.21	33.3	-24.3	-19.5	-17.8	-30.2	39.1
63.22	31.5	-25.5	-21.8	-19.8	-31.6	39.7
72.55	29	-26.4	-24.1	-21.6	-33	40.1
100	21.6	-25.5	-29.3	-22.8	-37	41
105	21.6	-23.5	-31	-24.8	-35.9	40.7
110	21.7	-22.2	-32.2	-26	-35.1	40.6
115	21.7	-21.3	-33.1	-27	-34.6	40.4
120	21.7	-20.9	-33.7	-27.6	-34.2	40.4
125	21.7	-20.9	-34.1	-27.8	-34.1	40.3
130	21.7	-21.2	-34.2	-28	-34.1	40.3
530	6.9	-18.5	-35.9	-28.5	-34.6	34.9
546	6.9	-19.8	-32.8	-28.1	-33.9	33.6
564	7	-22.6	-28.6	-27.7	-33	32.1
580	7	-25.9	-24.5	-27.5	-32.2	30.8
590	9.6	-32.9	-20.2	-26	-33.2	30.5
616.6	2.9	-27.1	-16.8	-22.4	-25	20.5
647.4	-5.2	-20.1	-12	-17.7	-15.7	8.5
668.3	-10.6	-17.1	-8.8	-11.5	-12.9	0.5
689.1	-16	-11.6	-5.7	-7	-7.1	-7.5
710	-21.4	-3.7	-2.7	-2.7	-0.5	-15.5
720	-23.8	-3.7	-2.1	-2.3	0	-16.4
900	0	0	0	0	0	0
1490	0	0	0	0	0	0
1790	38.2	5.9	2.6	2.2	3.5	19.9
1800	38.2	5.9	2.6	2.2	3.5	19.9

Bibliography

- [1] R. Aymar et al, ITER design, Plasma Phys. Control Fusion, Vol. 44, 2002, pp. 519-562
- [2] ITER N11 DDD 142 01-07-12R 0.1, Magnet Engineering Description, pp.1-97
- [3] ITER N 11 DDD 120 01-07-10 R0.1, Feeder design, pp.1-18
- [4] T. Mito et al, Development and test of a flexible superconducting bus-lines for LHD, IEEE Transactions on Magnetics, Vol. 30, No. 4, Part 2, 1994, pp. 2090-2093
- [5] Y.M. Park et al, Development for SC Bus-line for the KSTAR magnet system, Proceedings of LINAC 2002 conference, Gyeongju, Korea, 2002, pp. 491-493
- [6] J.M. Lock, Cryogenics, Vol. 9, 1969, pp. 438-442
- [7] M.N. Wilson, Superconducting Magnet Design, Oxford University Press, Ch.11, pp.379
- [8] T. Ando et al, Design of a 60 kA HTS current lead for fusion magnets, IEEE Transactions on Applied Superconductivity, Vol. 11, No.1, March 2001, pp. 2335-2338
- [9] R. Heller et al, Design and fabrication of current lead using Bi-2223/Ag Au demonstrator for ITER TF coil, IEEE Transactions on Applied Superconductivity, Vol. 14, No. 2, June 2004, pp. 1774-1777
- [10] H.K. Onnes, Commun. Phys. Lab. Vol. 12, 1911, pp. 120
- [11] W. Meissner and R. Ochsenfeld, Naturwiss. Vol. 21, 1933, pp. 787
- [12] Werner Buckel and Rinhold Kleiner, Superconductivity: Fundamentals and Applications, a text book, Wiely – VCH publication, 2nd edition, May 2004.
- [13] J.G. Bednorz and K.A. Mueller, Z. Phys. Vol. B 64, 1986, pp.189
- [14] P. Chaddah, Critical current densities in superconducting materials, Sadhana, Vol.28, Parts1 &2, February/April 2003, pp. 273-282
- [15] S. W. Van Sciver, Helium Cryogenics, Plenum Press, 1986, pp. 42-46.
- [16] P. Komarek, Hochstromanwendung der Supraleitung, B.G. Teubner Publications, Stuttgart, 1995, pp. 23-33.
- [17] K.-H. Mess, P. Schmueser, and S. Wolf, Superconducting Accelerator Magnets, World Scientific Publications, March 1996, pp. 7-26
- [18] K. Funaki et al, Recent activities in Japan about the HTS transformers, Superconductor Science and Technology, Vol. 13, 2000, pp. 60-67
- [19] P. J. Lee, Engineering Superconductivity, Wiley–Inter science Publications, 2001, pp. 200 – 270

- [20] E. Barzi et al, Heat treatment optimization of Internal tin Nb₃Sn strands, IEEE Transactions on Applied Superconductivity, Vo. 11, No. 1, March 2001, pp. 3573-3576
- [21] Cava R.J., Status and Current Directions in New Materials Research in High Temperature Superconductivity, in Banod, Y. Yamaguchi, Advances in Superconductivity V., New York, Springer 1993, 3-8
- [22] A product literature of European Advanced superconductors, link http://www.advancedsupercon.com/pdf/eas_hts.pdf
- [23] J.R. Hull, Applications of high-temperature superconductivity in power technology, Reports on Progress in Physics, Vol. 66, 2003, 1865-1886
- [24] Jodi Reeves, Micro structural investigation of current barriers in HTS materials, Ph.D. Thesis, University of Wisconsin Madison, 2001, pp.18
- [25] P. Komarek, Advances in large-scale applications of superconductors, Superconductor Science and Technology, Vol. 13, 2000, pp. 456-459
- [26] D. P. Ivanov, Overview of superconducting technology for fusion devices, Nuclear Fusion, Vol. 40, No.6, 2000, pp. 1245-1250
- [27] T. Satow et al, Achieved capability of the superconducting magnet system for the Large Helical Device (LHD), Nuclear Fusion, Vol.41, No.6, 2001, pp. 731-737
- [28] T. Ando et al, design of a 60 kA HTS current lead for Fusion magnets and its R & D, IEEE Transactions on Applied Superconductivity, Vol. 11, No.1, March 2001, pp. 2535-2538
- [29] A. Ballarino et al, High temperature superconductor current leads for the Large Hadron Collider, IEEE Transactions on Applied Superconductivity, Vol.9, No.2, 1999
- [30] R. F. Barron, Cryogenic systems, Second Edition, Oxford Science Publication, 1985
- [31] H. Lierl, Technology of cryogenics for storage rings, Accelerator conference at CERN 1998
- [32] Pierluigi Bruzzone, Superconductors for fusion magnets: realization, prototypes, and running projects, Superconductivity Science and Technology, Vol. 10, 1997, pp.919-923
- [33] M. Akiyama, Design Technology of Fusion Reactors, World Scientific Publishing Co, 1991, pp. 288-304
- [34] B. Sarkar et al, Integrated fluid flow distribution and cooling scheme with LHe liquefier/refrigerator for SST-1 magnet system, IEEE Transactions on Applied superconductivity, Vol. 14, No. 2, June 2004, pp. 1700-1703
- [35] B. Sarkar et al, 1 kW class helium Refrigerator/Liquefier system for SST-1, 18th International Conference on Cryogenic Engineering (ICEC-18) proceedings, 2000, pp. 123-126

- [36] N. Mitchell et al, Design of the ITER magnets to provide plasma operational flexibility, presented at IAEA 2004 meeting for ITER, IT/1-4
- [37] S. Claudet et al, Economics of large helium cryogenic systems: Experience from recent projects at CERN, paper presented at 1999 Cryogenic Engineering Conference (CEC/ICMC), July 1999, Montreal, Canada
- [38] ITER Design Description Document DDD 34, Cryo plant and cryo distribution no. (N 34 DDD 8 R 0.2)
- [39] R. Heller et al, Report on the comparison of ITER design with and without HTS current leads, EFDA No. TW4-TMSF-HTSCOMP Deliverable 1, June 2005
- [40] Hans Quack, Cryogenics for large systems, IEEE Transactions on Applied Superconductivity, Vol. 12, No. 1, March 2002, pp. 1355-1359
- [41] C. H. Rode et al, Operation of large cryogenic systems, IEEE Transactions on Nuclear Science, Vol. 32, NS-32, No. 5, October 1985, pp. 3557-3561
- [42] Claudet S. et al, Specifications of four new large helium refrigeration systems at 4.5 K for the LHC, Advances in Cryogenic Engineering, Vol. 45, 1999. pp. 1269-1276
- [43] T. Ando et al, Fabrication and test of a 60 kA HTS current lead for fusion magnet system, Advances in Cryogenic Engineering, Vol. 49 A, CEC-2003 Proceedings, 2004, pp. 929-936
- [44] V. Kalinin, Naka JWS, Presentation on 3rd Cryoplant Interface Meetings, 15-16 Dec.2005, Impact of HTS-CLs on ITER cryoplant
- [45] P.D. Weng et al, The modifications of conductor design for HT-7U TF magnets, IEEE Transactions on Applied Superconductivity, Vol. 10, No.1 , March 2000, pp. 1078-1081
- [46] M.A. Green, Induction Linac sc solenoids and two-phase cooling, Engineering note, LBNL-45288, SCMAG-17, pp. 1-15
- [47] John Wesson, Tokamaks, a book published by Oxford University Press, 3rd Edition, January 2004
- [48] ITER web site <http://www.iter.org>
- [49] Y. Shimomura et al, ITER-FEAT operation, Nuclear Fusion, 2001, pp. 309
- [50] M. Huguet et al, The ITER magnets: preparation for full size construction based on the results of the model coil programme, Nuclear Fusion, Vol. 43, 2003, pp. 352-357
- [51] T. Mito, S. Yamada et al, Conceptual design and development of Superconducting Bus-line for the LHD –Fusion Engineering and Design, Vol. 20 (1993), pp. 113-120
- [52] S. Yamada, T. Mito et al, Superconducting current feeder system for the Large Helical Device- IEEE Transactions on Magnetics, Vol. 32 (1996), pp. 2422-2425

- [53] D. Slack et al, Conceptual Design Review of TPX, Internal Publication Report no. 72-930319-LLNL/D.Slack-01, 1993
- [54] Y. S. Kim et al, Current Feeder System for the KSTAR Device- IEEE Transactions on Applied superconductivity, Vol.12, No. 1, 2002, pp. 571-573
- [55] V. L. Tanna, N.C. Gupta et al, Design and analysis of superconducting Bus-line for SST-1- Proceedings of 18th International Cryogenic Engineering Conference at Mumbai, India (2000), pp. 83-86
- [56] V.L. Tanna, B. Sarkar et al, Superconducting current feeder system with associated test results for SST-1 Tokamak Proceedings of 18th International Conference on Magnet Technology at Morioka, Japan (2003)
- [57] R. Heller et al, Development of forced flow cooled current leads for fusion magnets, Cryogenics, Vol.41, pp. 201-211, 2001
- [58] ITER DDD 4.1, Pulsed Power Supplies, Appendix-A, N 41 DDD 18 01-07-06 R 0.3, pp. 35-37
- [59] ITER Plant Description Document, G A0 FDR 1 01 – 07-13 R 0.1, Chapter 3.4, pp. 1-23
- [60] C. P. Dhard et al, Liquid nitrogen distribution system for SST-1, presented in ICEC 18 at Mumbai (India) during February 2000
- [61] R. Heller et al, Loss of He mass flow experiment with the 80 kA conventional current lead, internal report, in preparation
- [62] Y. Takahashi et al, Experimental Results and design of 50-kA current leads for Fusion devices, ICEC 16, Kitakushu, Japan during May 1996, pp. 795-798
- [63] R. Heller et al, Construction and operation of 80 kA current leads used for the ITER TFMC in the TOSKA facility, IEEE Trans. On Applied Superconductivity, 13, no.2, June 2003, 1918-1921
- [64] G. Friesinger, R. Heller, Use of Nb₃Sn inserts in a forced flow cooled 30 kA current lead, Applied Superconductivity, Vol.2, No.1, pp.21-27, 1994
- [65] A. V. Gavrilin, V. Keilin et al, Overloaded current leads, 15th Magnet Technology Conference Proceedings, Beijing, China, 1997, pp.1254-1257
- [66] Y.J. Lee et al, R & D progress on the KSTAR current leads, IEEE Transactions on Applied Superconductivity, Vol.14, No.2, pp. 1790-1793
- [67] R. Heller et al, Experimental Results of a 70 kA High Temperature Superconductor Current Lead Demonstrator for the ITER Magnet System, IEEE Transactions on Applied Superconductivity 15(2) Part 2, June 2005, pp.1496 - 1499
- [68] G. Zahn, W. H. Fietz, R. Heller, R. Lietzow, and V.L.Tanna, Cryogenic benefits of a 70 kA HTS current lead, Presented in CEC/ICMC-2005) during August – September 2005

- [69] W.H. Fietz, R. Heller, R. Lietzow, V.L.Tanna, G. Zahn, R. Wesche, E. Salpietro, A. Vostner, HTS current leads proposal for ITER, 21st International Symposium on Fusion Engineering (IEEE/NPSS) (SOFE 2005), September 2005 at Jacksonville, Florida USA
- [70] R. Heller, 70 kA HTS current lead operation at 80 K- the economic strategy for ITER?, - paper presented in 19th International Conference on Magnet Technology (MT-19) at Genova, Italy during September 2005
- [71] ITER superconducting Magnet and Electrical design guideline level 1, N11 FDR 1201-07-02 R 0.1, July 2001, pp. 1-75
- [72] R.P. Redd, A.F. Clark, Materials at low temperatures, American society for metals, 1983
- [73] S.J. Sackett, EFFI - a code for calculating the electromagnetic field, force, and inductances in the coil systems of arbitrary geometry, LLNL, Livermore, California, UCID-17621, 1997
- [74] M.S. Lubell, Empirical Scaling Formulas for Critical Current and Critical Field for commercial NbTi, IEEE Transactions on Magnetics 19, p. 754, 1983
- [75] HESS code, a computer program for steady state analysis of helium cooled conductors, developed by L. Bottura and NET team, NET/IN/87-62, 1987
- [76] S. Nicollet et al, Calculations of pressure drop and mass flow distribution in the TFMC of the ITER project, Cryogenics, Vol. 40, 2000, pp. 569-575
- [77] H. Katheder et al, Optimum thermo hydraulic operation regime for CICC, ICEC 15, Genova, Italy, 1994, pp. 595-598
- [78] Van Sceiver SW, Helium cryogenics, New York, Plenum Press, 1986, pp. 230 – 250
- [79] HEPAK (© copyright [Cryodata Inc.](#)) is a computer program for calculating the thermo physical properties of helium, Horizon Technology, version 3.4, Colorado, USA
- [80] Gandalf code, A computer code for quench analysis of dual flow CICC, L. Bottura, Cryosoft, version 2.2, January 2001
- [81] R. Heller et al, First Evaluation of the operation results of the forced flow cooled 80 kA current lead used for the TFMC experiment in the TOSKA facility, Forschungszentrum Karlsruhe, Internal report FE.5130.0016. 0012/B
- [82] R. Heller, S.M. Darweschad, G. Dittrich, W.H. Fietz, S. Fink, W. Herz, A. Lingor, A. Kienzler, I. Meyer, G. Nöther, M. Süsser, V.L. Tanna, R. Wesche, F. Wüchner and G. Zahn, Final Report on the Test of the 70 kA HTS Current Lead in the TOSKA Facility Contract No. FU05 CT 2003-00023 (EFDA No. 02-1013) Deliverable 4.2., Forschungszentrum Karlsruhe Internal Report FE.5130.0061.0012/A, Oct 2004
- [83] F. Millet, LHC-CERN, Switzerland, private communication

- [84] R. Wesche et al., EFDA No. TW4-TMSF-HTSCOM-Deliverable-2, CRPP Internal Report LRP 805/05, July 2005, unpublished
- [85] S. Mukoyama et al, IEEE Trans. On Applied Superconductivity, Vol.13, No.2, June 2003, pp. 1926
- [86] Bo Hue et al, Development of 4 m HTS power cable, Superconductivity Science and Technology, Vol. 17, 2004, pp. 415-417
- [87] Ying Xin et al, China's 30 m, 35 kV/2 kA rms HTS power cable project, Superconductor Science and Technology, Vol. 17, 2004, pp. 332-335
- [88] J. Rieger et al., Supercond. Science and Technology, Vol. 11, 1998, pp. 902-908
- [89] R. Wesche, Internal Report, Conceptual Design of HTS Bus Bars for ITER, Centre de Recherché en Physique des Plasmas, March 29, 2005
- [90] R. Wesche, Physica C 246 (1995) 186-194
- [91] R. Wesche, Internal Report, Calculation of the Stray Magnetic Field at the Hall Probes of the HTS Current Lead Module, Centre de Recherché en Physique des Plasmas, November 5, 2003
- [92] Deukyong Koh et al, IEEE Trans. on Appl. Superconductivity, Vol. 14(2), June 2004, pp. 1746- 1750
- [93] V.L. Tanna et al, Conceptual design of a HTS bus bar for ITER, paper presented in EUCAS 2005 at Vienna during 11-15 September 2005
- [94] W.T. Norris, J. Phys. D 3 (1970) 489-507
- [95] M.S. Darweschad, Institute for Technical Physics, Forschungszentrum Karlsruhe, private communication

